

MRes in Railway Systems Integration

College of Engineering, School of Engineering

University of Birmingham



**Control System Design Using Fuzzy Gain
Scheduling of PD with Kalman Filter for
Railway Automatic Train Operation**

Author: Reza Dwi Utomo

Supervisors: Dr Lei Chen & Prof Clive Roberts

Date: 05/04/2018

A thesis submitted in partial fulfilment of the requirements for the
award of MRes in Railway Systems Integration

UNIVERSITY OF
BIRMINGHAM

University of Birmingham Research Archive

e-theses repository

This unpublished thesis/dissertation is copyright of the author and/or third parties. The intellectual property rights of the author or third parties in respect of this work are as defined by The Copyright Designs and Patents Act 1988 or as modified by any successor legislation.

Any use made of information contained in this thesis/dissertation must be in accordance with that legislation and must be properly acknowledged. Further distribution or reproduction in any format is prohibited without the permission of the copyright holder.

Executive Summary

The development of train control systems has progressed towards following the rapid growth of railway transport demands. To further increase the capacity of railway systems, Automatic Train Operation (ATO) systems have been widely adopted in metros and gradually applied to mainline railways to replace drivers in controlling the movement of trains with optimised running trajectories for punctuality and energy saving. Many controller design methods have been studied and applied in ATO systems. However, most researchers paid less attention to measurement noise in the development of ATO control system, whereas such noise indeed exists in every single instrumentation device and disturbs the process output of ATO. Thus, this thesis attempts to address such issues.

In order to overcome measurement error, the author develops Fuzzy gain scheduling of PD (proportional and derivative) control assisted by a Kalman filter that is able to maintain the train speed within the specified trajectory and stability criteria in normal and noisy conditions due to measurement noise. Docklands Light Railway (DLR) in London is selected as a case study to implement the proposed idea. The MRes project work is summarised as follows: (1) analysing literature review, (2) modelling the train dynamics mathematically, (3) designing PD controller and Fuzzy gain scheduling, (4) adding a Gaussian white noise as measurement error, (5) implementing a Kalman filter to improve the controllers, (6) examining the entire system in an artificial trajectory and a real case study, i.e. the DLR, and (7) evaluating all based on strict objectives, i.e. a $\pm 3\%$ allowable error limit, a punctuality limit of no later and no earlier than 30 seconds, Integrated Absolute Error (IAE) and Integrated Squared Error (ISE) performances.

The results show that Fuzzy gain scheduling of PD control can cope well with the examinations in normal situations. However, such discovery is not found in noisy conditions. Nevertheless, after the introduction to Kalman filter, all control objectives are then satisfied in not only normal but also noisy conditions. The case study implemented using DLR data including on the route from Stratford International to Woolwich Arsenal indicates a satisfactory performance of the designed controller for ATO systems.

Acknowledgements

In the name of God, the Most Gracious, the Most Merciful.

*So truly where there is hardship there is also ease; truly where there is
hardship there is also ease. The moment you are freed [of one task]
work on, and turn to your Lord for everything. (Qur'an 94:5-8)*

It was common for me to think "is MRes study this hard?" or "am I this stupid?" I often got stuck, especially when I found my program in MATLAB not fitting the hypotheses. The monthly meeting with my supervisor also sometimes made me feel overwhelmed. However, the verses above always became my inspiration and aroused me that every difficulty must have its solution. I thought again: even the PhD study is much harder; I have walked so far so I must finish soon; I also should be grateful that my supervisor always monitored my study through the monthly meeting. I could not imagine how the life of some of my PhD friends who only meet their supervisors twice or three times a year.

I am very grateful to my lead supervisor, Dr Lei Chen. He was often available every time I asked to arrange a meeting every month, sometimes even twice a month. His comments, suggestions and criticisms became my inspiration, increased my curiosity to read more reading materials and discovering new things. He also helped me in lobbying for the extension of my study funding and allowed me to take an authorised absence due to the birth of my first child. Many thanks to him.

Further, although I only met my co-supervisor, Professor Clive Roberts, twice, at the beginning of my study and during the poster session, since he is extremely rushed chiefly as the Director of BCRRE (Birmingham Centre for Railway Research and Education), he provided me with valuable insights. He also suggested me to take LMR33 Railway Traction Systems Design module which was very useful in completing this thesis.

Exclusive gratitude is for Indonesia Endowment Fund for Education (LPDP) for funding my study and living expenses in the UK. I am gratefully indebted to them, including Government of Indonesia, for their support to me. I also thank Transport for London for providing valuable data for the case study of this thesis. And I acknowledge Cambridge Proofreading LLC in copy-editing this thesis for conventions of language, grammar and spelling.

Besides, I would also like to thank my friends and colleagues at BCRRE. Marco and Hongsin gave me beneficial lectures and suggestions. They always responded to every email I sent regarding MRes study promptly. Edward taught me new technical knowledge during the Lab session. It was useful knowledge. Joy and Aakeefa always happily helped my problems

in administrations. That was helpful. Nadeen provided me with a new hot-desk after my previous one had been occupied by another student. Thank you, Nadeen! I often shared my study progress with my MRes colleagues, especially Enshou and Huayu. They often told me valuable information. And for my Muslim friends, Yanuar, Haniff, Usman, Hassan, Aican, Hamad and Samra, I thank them all for providing me with helpful discussions. I highly appreciate Haniff for inviting my wife and me twice to his house, and Yanuar for becoming the only Indonesian student, besides me, at BCRRE whom I discussed extensively with.

My deepest gratitude goes to my beloved wife, Fitria Dewi Larassuci, who unweariedly encourage and hearten me. She always prays every day for my health, safety and success, and looks after our newborn baby. A sincere appreciation also goes to my parents, Bapak Sudiarmakno and Ibu Suchaeni, who have raised me with love and zeal and always brace me, and to my siblings, Mas Tomi, Rizky and Tasya, and my parents-in-law, Bapak Iwo and Ibu Ruswanti, who always support me. My thankfulness also goes to my housemates, Mbak Indriani and Mas Sujianto, who provided me with economical, warm and convenient accommodation.

Last but not least, I would like to thank all Indonesian people in Birmingham, especially Forum Jumat and LPDP awardees, and others not mentioned here.

Thank you very much.

May peace be upon you all.

Reza Dwi Utomo

March 2018

Table of Contents

| | | |
|----------|-----------------------------------------------------|------------|
| 1 | Introduction | 1 |
| 1.1 | Background | 1 |
| 1.2 | Aim and Objectives | 2 |
| 1.3 | Research Questions..... | 3 |
| 1.4 | Scope | 3 |
| 1.5 | Methodology..... | 5 |
| 1.6 | Thesis Structure | 5 |
| 2 | Literature Review | 6 |
| 2.1 | Recent Studies on ATO..... | 6 |
| 2.2 | Related Works in ATO Control Systems..... | 7 |
| 2.3 | Research Contribution | 10 |
| 3 | Introduction to Railway Control Systems..... | 11 |
| 3.1 | Protection Systems | 11 |
| 3.2 | Automatic Train Operation | 17 |
| 3.3 | Grades of Automation..... | 19 |
| 3.4 | Automatic Controller | 21 |
| 4 | Proposed Controller Design of Metro ATO..... | 37 |
| 4.1 | Train Modelling | 37 |
| 4.2 | Control Design..... | 41 |
| 4.3 | Noise Insertion and Improving the Controller | 49 |
| 4.4 | Analysis and Discussion..... | 53 |
| 5 | Case Study | 86 |
| 5.1 | Docklands Light Railway..... | 86 |
| 5.2 | Controller Design | 92 |
| 5.3 | Results and Discussion | 95 |
| 6 | Conclusions | 105 |
| 6.1 | Findings | 105 |
| 6.2 | Recommendations | 105 |

| | | |
|-----------|---------------------------------------------------------|------------|
| 7 | List of References..... | 107 |
| 8 | Appendix A – Table of Difference among GoAs..... | 117 |
| 9 | Appendix B – DLR Route Map..... | 118 |
| 10 | Appendix C – Gradient and Speed Limit..... | 119 |

List of Figures

| | |
|---------------------------------------------------------------------------------------------------------------------------------------------------|----|
| Figure 1 – Railway Systems (Schmid, 2015) | 11 |
| Figure 2 – An illustration of tripcock and trainstop (Connor, 2015) | 12 |
| Figure 3 – AWS scheme (Author, 2017) | 13 |
| Figure 4 – AWS indicators of the black indication (left side) and the yellow and black indication (right side) inside the cab (RSSB, 2015a) | 14 |
| Figure 5 – Layout of TPWS equipment (RSSB, 2015b)..... | 15 |
| Figure 6 – ATP speed supervision (IRSE, 1993)..... | 16 |
| Figure 7 – Inside a cab of Northern Line 1995 Stock assisted by ATO system (Connor, 2015) | 17 |
| Figure 8 – Diagram of control actions of ATO (Wang et al., 2016) | 18 |
| Figure 9 – The speed profiles of ATO and ATP system (Carvajal-Carreño, 2017) | 19 |
| Figure 10 – The structure of ATC system (Dong, Ning, et al., 2010) | 19 |
| Figure 11 – Grades of Automation (UITP, 2014) | 21 |
| Figure 12 – Block diagram of PID controller (Author, 2017) | 22 |
| Figure 13 – Example of integrator windup (Åström & Hägglund, 2006)..... | 23 |
| Figure 14 – Response from the controlled system (Ponton, 2007) | 25 |
| Figure 15 – Block diagram (top) and output and control signal responses (bottom) of relay feedback control (Yu, 2006) | 25 |
| Figure 16 – Block diagram of relay-feedback PID auto-tuning method..... | 26 |
| Figure 17 – Example of membership functions of (a) crisp sets and (b) Fuzzy sets (Mendel et al., 2014)..... | 27 |
| Figure 18 – Membership functions of (left) triangle, (middle) trapezoid and (right) Gaussian (Author, 2018) | 29 |
| Figure 19 – Architecture of Fuzzy logic controller (Mendel et al., 2014)..... | 30 |
| Figure 20 – Example of Fuzzy inference (Sivanandam et al., 2007) | 31 |
| Figure 21 – Simplified block diagram of Fuzzy gain scheduling based PID (Zhao et al., 1993) | 32 |
| Figure 22 – Probability density function of normal distribution (Author, 2018) | 33 |

| | |
|-----------------------------------------------------------------------------------------------------------------------------|----|
| Figure 23 – Illustration of the concept of Kalman filter (Ulusoy, 2017)..... | 34 |
| Figure 24 – Recursive procedures of Kalman filter (Author, 2018)..... | 36 |
| Figure 25 – Train modelling (Author, 2017) | 38 |
| Figure 26 – Gradient resistance (Author, 2017)..... | 40 |
| Figure 27 – Running resistance behaviour (Author, 2017) | 41 |
| Figure 28 – Block diagram of train modelling and the controllers (Author, 2017) | 42 |
| Figure 29 – Block diagram of proposed Fuzzy gain scheduling (Author, 2018) | 44 |
| Figure 30 – Block diagram of Fuzzy adaptation (Author, 2017)..... | 45 |
| Figure 31 – Membership function of error (Author, 2017)..... | 46 |
| Figure 32 – Membership function of delta error (Author, 2017)..... | 47 |
| Figure 33 – Membership function of h (Author, 2017) | 47 |
| Figure 34 - Probability density function of measurement noise with mean 0 and standard deviation 0.015 (Author, 2018) | 50 |
| Figure 35 – Block diagram of train modelling, controller and measurement errors (Author, 2017)..... | 51 |
| Figure 36 – Block diagram of the entire system with measurement errors and Kalman filter (Author, 2017) | 52 |
| Figure 37 – The system with simple controller (Author, 2017)..... | 55 |
| Figure 38 – Actual speed of the system with simple controller (traction part) (Author, 2017) | 55 |
| Figure 39 – Actual speed of the system with simple controller with settling time (traction part) (Author, 2018) | 56 |
| Figure 40 – Actual speed of the system with simple controller (braking part) (Author, 2017) | 57 |
| Figure 41 – Actual speed of the system with simple controller with settling times (braking part) (Author, 2017) | 57 |
| Figure 42 – Plot chart of control and output signals with respect to time (Author, 2018) | 58 |
| Figure 43 – Actual speed of PID (traction part) (Author, 2018) | 59 |
| Figure 44 – Actual speed of PID with settling time (traction part) (Author, 2018)..... | 59 |

| | |
|--------------------------------------------------------------------------------------------------------------------------|----|
| Figure 45 – Actual speed of PID (braking part) (Author, 2018) | 60 |
| Figure 46 – Actual speed of PID with settling time (braking part) (Author, 2018)..... | 61 |
| Figure 47 – Actual speed of PD (traction part) (Author, 2018) | 61 |
| Figure 48 – Actual speed of PD with settling time (traction part) (Author, 2018)..... | 62 |
| Figure 49 – Actual speed of PD (braking part) (Author, 2018) | 62 |
| Figure 50 – Actual speed of PD with settling time (braking part) (Author, 2018) | 63 |
| Figure 51 – Actual speed of Fuzzy-PD (traction part) (Author, 2018) | 64 |
| Figure 52 – Actual speed of Fuzzy-PD with settling time (traction part) (Author, 2018).... | 64 |
| Figure 53 – Actual speed of Fuzzy-PD (braking part) (Author, 2018)..... | 66 |
| Figure 54 – Actual speed of Fuzzy-PD with settling time (braking part) (Author, 2018) | 66 |
| Figure 55 – Comparison of simple control, PID, PD and Fuzzy-PD (traction part) (Author, 2018)..... | 67 |
| Figure 56 – Comparison of simple control, PID, PD and Fuzzy-PD (braking part) (Author, 2018)..... | 67 |
| Figure 57 – Speed limit for artificial train trajectory (Author, 2017) | 68 |
| Figure 58 – Altitude for artificial train trajectory (Author, 2017) | 69 |
| Figure 59 – Full-performance train trajectory (Author, 2017) | 70 |
| Figure 60 – Acceleration/Deceleration of full-performance train trajectory (Author, 2017) | 71 |
| Figure 61 – Train trajectory with coasting strategy (Author, 2017)..... | 72 |
| Figure 62 – Acceleration/Deceleration of train trajectory with coasting strategy (Author, 2017)..... | 73 |
| Figure 63 – Plot chart of control and output signals with respect to time (with gradient resistance) (Author, 2018)..... | 73 |
| Figure 64 – Error deviation of PD control in full-power trajectory (Author, 2018) | 75 |
| Figure 65 – Error deviation of PD control in trajectory with coasting (Author, 2018)..... | 75 |
| Figure 66 – Running time of PD control in full-power trajectory (Author, 2018) | 76 |
| Figure 67 – Running time of PD control in trajectory with coasting (Author, 2018) | 76 |
| Figure 68 – Error deviation of Fuzzy-PD in full-power trajectory (Author, 2018)..... | 77 |

| | |
|----------------------------------------------------------------------------------------------------------------|----|
| Figure 69 – Error deviation of Fuzzy-PD in trajectory with coasting (Author, 2018) | 78 |
| Figure 70 – Running time of Fuzzy-PD in full-power trajectory (Author, 2018)..... | 78 |
| Figure 71 – Running time of Fuzzy-PD in trajectory with coasting (Author, 2018)..... | 79 |
| Figure 72 – Error deviation of noisy Fuzzy-PD in full-power trajectory (Author, 2018) | 80 |
| Figure 73 – Error deviation of noisy Fuzzy-PD in trajectory with coasting (Author, 2018). | 80 |
| Figure 74 – Running time of noisy Fuzzy-PD in full-power trajectory (Author, 2018) | 81 |
| Figure 75 – Running time of noisy Fuzzy-PD in trajectory with coasting (Author, 2018) ... | 81 |
| Figure 76 – Error deviation of noisy Fuzzy-PD with KF in full-power trajectory (Author, 2018) | 82 |
| Figure 77 – Error deviation of noisy Fuzzy-PD with KF in trajectory with coasting (Author, 2018)..... | 84 |
| Figure 78 – Running time of noisy Fuzzy-PD with KF in full-power trajectory (Author, 2018) | 84 |
| Figure 79 – Running time of noisy Fuzzy-PD with KF in trajectory with coasting (Author, 2018)..... | 85 |
| Figure 80 – An on-board staff on DLR train (Author, 2017) | 86 |
| Figure 81 – DLR rolling stock (Author, 2017)..... | 87 |
| Figure 82 – B2007 rolling stock (Rail Technology Magazine, 2017) | 87 |
| Figure 83 – Traction curve and running resistance of DLR rolling stock (Kemp, 1987) | 88 |
| Figure 84 – Platform at Stratford International station (Author, 2017) | 89 |
| Figure 85 – Platform at Woolwich Arsenal station (Author, 2017)..... | 89 |
| Figure 86 – Map of the route from Stratford Int'l to Woolwich Arsenal (Google Inc., n.d.) | 90 |
| Figure 87 – Position of stations in the route from Stratford Int'l to Woolwich Arsenal (Author, 2017) | 90 |
| Figure 88 – Altitude of the route from Stratford International to Woolwich Arsenal (Author, 2017)..... | 91 |
| Figure 89 – Speed limit of the route from Stratford International to Woolwich Arsenal (Author, 2017) | 91 |
| Figure 90 – Block diagram of train modelling and modified controllers (Author, 2017).... | 93 |

| | |
|---------------------------------------------------------------------------------------------------------------------|-----|
| Figure 91 – Plot chart of control and output signals with respect to time – case study (Author, 2018) | 94 |
| Figure 92 – Full-performance train trajectory – case study (Author, 2018) | 95 |
| Figure 93 – Train trajectory with Coasting Strategy – case study (Author, 2018) | 96 |
| Figure 94 – Error deviation of Fuzzy-PD in full-power trajectory – case study (Author, 2018) | 97 |
| Figure 95 – Error deviation of Fuzzy-PD in trajectory with coasting – case study (Author, 2018)..... | 97 |
| Figure 96 – Running time of Fuzzy-PD in full-power trajectory – case study (Author, 2018) | 98 |
| Figure 97 - Running time of Fuzzy-PD in trajectory with coasting – case study (Author, 2018) | 98 |
| Figure 98 – Error deviation of noisy Fuzzy-PD in full-power trajectory – case study (Author, 2018)..... | 100 |
| Figure 99 – Error deviation of noisy Fuzzy-PD in trajectory with coasting – case study (Author, 2018) | 100 |
| Figure 100 – Error deviation of noisy Fuzzy-PD with KF in full-power trajectory – case study (Author, 2018) | 101 |
| Figure 101 - Error deviation of noisy Fuzzy-PD with KF in trajectory with coasting – case study (Author, 2018)..... | 101 |
| Figure 102 – Running time of noisy Fuzzy-PD in full-power trajectory – case study (Author, 2018)..... | 102 |
| Figure 103 – Running time of noisy Fuzzy-PD with KF in full-power trajectory – case study (Author, 2018) | 102 |
| Figure 104 – Running time of noisy Fuzzy-PD in trajectory with coasting – case study (Author, 2018) | 103 |
| Figure 105 – Running time of noisy Fuzzy-PD with KF in trajectory with coasting – case study (Author, 2018) | 103 |
| Figure 106 – Map of DLR routes (TfL, 2015a)..... | 118 |
| Figure 107 - Gradient of the route from Stratford International to Woolwich Arsenal (Author, 2017) | 119 |

Figure 108 – Speed limit of the route from Stratford International to Woolwich Arsenal
(Author, 2017) 120

List of Tables

| | |
|----------------------------------------------------------------------------------------------------|-----|
| Table 1 – Rule Base of Fuzzy adaptation | 48 |
| Table 2 – Comparison indices of constant speed reference test | 65 |
| Table 3 – Comparison indices of artificial trajectory test..... | 83 |
| Table 4 – B2007 Stock Information | 87 |
| Table 5 – Comparison indices of case study..... | 104 |
| Table 6 – Grades of Automation in more detail (Keevill, 2016). ‘Ops’ stands for operator. | 117 |

List of Equations

| | |
|-----------------------------------------------------------------------------|----|
| Equation 1 – PID Control Law | 22 |
| Equation 2 – Equivalent PID Control Law | 23 |
| Equation 3 – Rules for K_p , T_i and T_d | 24 |
| Equation 4 – The output of relay | 25 |
| Equation 5 – Interaction between relay and ultimate gain | 25 |
| Equation 6 – Interaction between critical period and frequency | 26 |
| Equation 7 – Fuzzy notations | 26 |
| Equation 8 – Operation of union | 27 |
| Equation 9 – Operation of intersection | 28 |
| Equation 10 – Operation of complement | 28 |
| Equation 11 – Triangular MF | 28 |
| Equation 12 – Trapezoidal MF | 28 |
| Equation 13 – Gaussian MF | 29 |
| Equation 14 – Example of Fuzzy rules | 30 |
| Equation 15 – Defuzzification methods of centroid and mean of maximum | 31 |
| Equation 16 – Probability density function of normal distribution | 33 |
| Equation 17 – Equation of mean | 33 |
| Equation 18 – Equations of variance and standard deviation | 33 |
| Equation 19 – Equation of covariance | 33 |
| Equation 20 – State space model | 34 |
| Equation 21 – Measurement model | 34 |
| Equation 22 – Prediction equations | 35 |
| Equation 23 – Estimate update equations | 35 |
| Equation 24 – Time-independent train modelling | 37 |
| Equation 25 – Transformations of derivative of speed | 37 |
| Equation 26 – Distance-independent train modelling | 37 |

| | |
|---------------------------------------------------------------------------------------|----|
| Equation 27 – Speed equation without predefined time value | 38 |
| Equation 28 – Difference of time | 38 |
| Equation 29 – Total running time..... | 39 |
| Equation 30 – Relation between traction and braking forces and its values..... | 39 |
| Equation 31 – Definition of gradient resistance..... | 39 |
| Equation 32 – Definition of running resistance..... | 40 |
| Equation 33 – The definition of tractive effort | 41 |
| Equation 34 –The definition of braking force..... | 41 |
| Equation 35 – Discrete-time PID control | 42 |
| Equation 36 – Discrete-time PD control..... | 43 |
| Equation 37 – Distance constant based discrete-time PD control..... | 43 |
| Equation 38 – The output value of relay | 43 |
| Equation 39 – Fuzzy sets of E and R..... | 44 |
| Equation 40 – Fuzzy sets of H..... | 45 |
| Equation 41 – Parameters of Fuzzy input E MFs..... | 45 |
| Equation 42 – Parameters of Fuzzy input R MFs | 46 |
| Equation 43 – Parameters of Fuzzy output H MFs..... | 48 |
| Equation 44 – Definition of alpha..... | 49 |
| Equation 45 – Relation among PID parameters, alpha and ultimate gain and period | 49 |
| Equation 46 – Train speed modelling..... | 51 |
| Equation 47 – Train speed modelling in matrix notation..... | 52 |
| Equation 48 – Measurement model of train speed | 52 |
| Equation 49 – Measurement model in matrix notation | 53 |
| Equation 50 – Initial conditions..... | 53 |
| Equation 51 – Covariance matrices of process and measurement noise | 53 |
| Equation 52 – Equations of IAE and ISE..... | 54 |
| Equation 53 – Coasting strategy..... | 72 |
| Equation 54 – Trajectory-based switch (first function)..... | 93 |

| | |
|---------------------------------------------------------------------------------------------|----|
| Equation 55 – Definitions of traction and braking weights..... | 94 |
| Equation 56 - K_p in Equation 45 with traction and braking weights (second function)..... | 94 |

Glossary of Terms / List of Abbreviations

| Term | Explanation / Meaning / Definition |
|---------------------|------------------------------------------------------------------------------------|
| F_t^T | Transpose of the matrix F_t |
| \ddot{x}_s | Acceleration at specified distance s (m/s ²) |
| \dot{x}_s | Actual speed at specified distance s (m/s) |
| \ddot{x}_{s-1} | Acceleration at specified distance $s - 1$ (m/s ²) |
| \dot{x}_{s-1} | Actual speed at specified distance $s - 1$ (m/s) |
| $\hat{x}_{t t}$ | Optimal state estimate at time t based on collected data until time t |
| $\hat{x}_{t t-1}$ | Predicted state estimate at time t based on collected data until time $t - 1$ |
| $\hat{x}_{t-1 t-1}$ | Initial state estimate at time $t - 1$ based on collected data until time $t - 1$ |
| $R_C(\cdot)$ | Curvature resistance (N) |
| $R_G(\cdot)$ | Gradient resistance (N) |
| $R_R(\cdot)$ | Running resistance (N) |
| $R_T(\cdot)$ | Tunnel resistance (N) |
| x_t | n -state-vector of the linear dynamical systems at time t |
| z_t | p -state-vector of measurements (or outputs) of the system at time t |
| F_t | $n \times n$ state transition matrix at time t |
| G_t | $n \times m$ state transition matrix at time t |
| H_t | $p \times n$ state transition measurement matrix at time t |
| K_d | Derivative gain |
| K_i | Integral gain |
| K_p | Proportional gain |
| K_t | Kalman gain at time t |
| K_u | Ultimate gain |
| $P_{t t}$ | Error covariance matrix at time t based on collected data until time t |
| $P_{t t-1}$ | Error covariance matrix at time t based on collected data until time $t - 1$ |
| $P_{t-1 t-1}$ | Error covariance matrix at time $t - 1$ based on collected data until time $t - 1$ |
| Q_t | Covariance matrix of v_t at time t |
| R_t | Covariance matrix of w_t at time t |
| T_d | Derivative time |
| T_i | Reset time |
| T_s | Settling time (s) |
| T_{total} | Total time required for a wave to travel (s) |

| Term | Explanation / Meaning / Definition |
|-------------------------|-----------------------------------------------------------------------------------------------------------|
| T_u | Ultimate period (s) |
| a_b | Backward acceleration (m/s ²) |
| a_f | Forward acceleration (m/s ²) |
| \dot{e} | Delta error |
| $e_{3\%}$ | Index of 3% error limit |
| e_{Time} | Index of time deviation |
| k_b | Control signal of relative braking force |
| k_t | Control signal of relative tractive effort |
| u_t | m -state-vector of the inputs of the system at time t |
| v_{actual} | Actual speed from the system (m/s) |
| v_{coast} | Coasting speed (m/s) |
| v_{noise} | Noisy speed after disturbed by measurement error (m/s) |
| v_{output} | Speed output after filtered by Kalman filter (m/s) |
| v_r or v_{ref} | Speed reference (m/s) |
| $v_{s,1}$ and $v_{s,2}$ | Gaussian process noise with zero mean and covariance matrix Q_s |
| v_t | n -state-vector of Gaussian random process noise with zero mean and covariance matrix Q_t at time t |
| w_B | Braking weight |
| w_T | Traction weight |
| w_s | Gaussian measurement errors with zero mean and covariance matrix R_s . |
| w_t | n -state-vector of Gaussian measurement noise with zero mean and covariance matrix R_t at time t |
| y_r | Set point value |
| y_s | Measured speed disrupted by Gaussian measurement errors (m/s) |
| z_{cog} | Centroid method |
| z_{mom} | Mean-of-maximum method |
| $\mu_A(x)$ | Membership function notation of Fuzzy set A for mapping element x |
| σ_x | Standard deviation of variable x |
| Δs | Distance difference constant with value 1 metre |
| $\Delta t(\cdot)$ | Time difference in seconds at every one metre displacement (s) |
| \cap | Intersection |
| \cup | Union |
| \neg | Complement |
| ANFIS | Adaptive Neuro-Fuzzy Inference System |

| Term | Explanation / Meaning / Definition |
|--------|------------------------------------------------------------------------------|
| ATC | Automatic Train Control |
| ATO | Automatic Train Operation |
| ATP | Automatic Train Protection |
| ATS | Automatic Train Supervision |
| AWS | Automatic Warning System |
| BR-ATP | British Rail Automatic Train Protection |
| CBTC | Communication Based Train Control |
| CIS | Customer Information Systems |
| DAS | Driver Advisory System |
| DLR | Docklands Light Railway |
| DTO | Driverless Train Operation |
| EMU | Electric Multiple Unit |
| ETCS | European Train Control System |
| FACT | Fully automatic control of trains |
| FLC | Fuzzy logic controller |
| GoA | Grades of Automation |
| h | Fuzzy control signal generated by Fuzzy scheme used to modify PID parameters |
| HST | High-speed train |
| IAE | Integrated Absolute Error |
| IEC | International Electrotechnical Commission |
| IEEE | Institute of Electrical and Electronics Engineers |
| IRSE | Institution of Railway Signal Engineers |
| ISE | Integrated Square Error |
| KF | Kalman filter |
| LMA | Limit of movement authority |
| MF | Membership function |
| n.d. | No date |
| OCC | Operation control centre |
| OMO | One-man operation |
| OSS | Overspeed sensor system |
| PD | Proportional Derivative |
| PDF | Probability density function |
| PID | Proportional Integral Derivative |

| Term | Explanation / Meaning / Definition |
|------------|-------------------------------------------------------------------------------------------------|
| PTC | Positive Train Control |
| RAIB | Rail Accident Investigation Branch |
| RSSB | Rail Safety and Standards Board |
| SPAD | Signal passed at danger |
| STO | Semi-Automatic Operation |
| TASC | Train Automatic Stop Control |
| TfL | Transport for London |
| TPWS | Train Protection and Warning System |
| TPWS-E | Train Protection and Warning System Eurobalise |
| TS | Takagi–Sugeno |
| TSS | Train stop system |
| UITP | Union Internationale des Transports Publics (The International Association of Public Transport) |
| UK | United Kingdom (Great Britain and Northern Ireland) |
| UTO | Unattended Train Operation |
| VCS | Vehicle Control Systems |
| A | Coefficient for mass-dependent resistance (N) |
| B | Coefficient for rolling stock resistance (Ns/m) |
| $B(\cdot)$ | Maximum available braking force (N) |
| C | coefficient for aerodynamic resistance (Ns^2/m^2) |
| E | Fuzzy set of error e |
| $F(\cdot)$ | Maximum available tractive effort (N) |
| H | Fuzzy set of h parameter |
| I | Identity matrix |
| N | Number of oscillations in a wave |
| NL | Negative large |
| NM | Negative medium |
| NS | Negative small |
| PL | Positive large |
| PM | Positive medium |
| PS | Positive small |
| R | Fuzzy set of delta error \dot{e} |
| S | Maximum distance (m) |

| Term | Explanation / Meaning / Definition |
|---------------------------|---------------------------------------------------------------------------------------------------------------|
| $T(\cdot)$ | Total running time from the beginning of the train starting, $i = 0$, until specified distance s (s) |
| $X \sim N(\mu, \sigma^2)$ | Normal distribution N of X with mean μ and standard deviation σ or variance σ^2 |
| ZE | Zero |
| $a(\cdot)$ | Acceleration (m/s ²) |
| $cov(x, y) = \sigma_{xy}$ | Covariance of variable x and y |
| d | Relay output amplitude when error e is greater than zero |
| $-d$ | Relay output amplitude when error e is less than zero |
| $-dec$ | Negative instantaneous deceleration from the system |
| $e(\cdot)$ | Error, i.e. the difference between set point value and the value of output of the system |
| f | Frequency (Hz) |
| $f(x)$ | Function of x |
| g | Gravitational acceleration constant, i.e. 9.81 m/s ² |
| m | Total train mass (kg) |
| $u(\cdot)$ | Control signal produced by the controller(s) |
| $v(\cdot)$ | Speed (m/s) |
| $var(x) = \sigma_x^2$ | Variance of variable x |
| y | Process value |
| α | Parameter for directly controlling PID parameters |
| γ | Positive constant with the interval [0.2, 0.6] implemented to adjust the convergence rate of α formula |
| $\theta(s)$ | Slope angle at certain distance s (°) |
| μ | Mean of the distribution |

1 Introduction

This introductory chapter details the fundamental background to this thesis, together with an overview of the research aim and objectives, research questions, scope, methodology and thesis structure.

1.1 Background

1.1.1 The Need for Railway Signalling and Automation

From the beginning of 18th century, the drastic technological advances resulting from the Industrial Revolution which changed humankind, railway transport evolved. It was Richard Trevithick who invented the world's first steam locomotive in 1804 and since then, steam locomotives began to be used as passenger transport (Gibbs, 2013). However, during World War II, steam power was gradually replaced by more reliable forms of energy: namely diesel and electric engines (Britannica Educational Publishing, 2012).

When trains became a form of public mass transport, their safety factor became an issue (Institution of Railway Signal Engineers [IRSE], 2009), and this led to the introduction of the signalling system, which is necessary to protect the trains from collisions and derailments. As defined by IRSE (1982), there are at least four key elements to the signalling system which are required for safety: a train detection system, such as track circuits and axle counters, interlockings, the indications to the drivers such as wayside light signals and cab signalling and the ability to stop the trains passing the signals in cases of danger. These are all based on train control systems. With the fast development of information and communication technology and underlined by the inevitability of human errors, in particular, those of the drivers, and the need to expand railway transport, the signalling system changed, resulting in the modern systems (IRSE, 1993), such as the Automatic Train Protection system (ATP), Automatic Train Operation system (ATO), Communication Based Train Control (CBTC), European Train Control System (ETCS) and Positive Train Control (PTC). These advanced systems take full advantage of automatic systems (Goddard, 2012).

1.1.2 The Need for a Reliable Controller

Today's most sophisticated signalling system on the urban railway, namely the CBTC system, exists in many modern cities around the world, for example, Heathrow Airport (Bombardier, 2017), Docklands Light Railway (DLR), Vancouver metro, Paris Metro (Line 14), Canarsie Line of the New York Subway (IRSE, 2009), Beijing's Line 2 (Alstom, 2012) etc. Since the CBTC system is a complex signalling system, its configurations require highly reliable controller

systems. Moreover, in order to drive the trains automatically from one stop to another using the CBTC system, an ATO system is compulsory (Institute of Electrical and Electronics Engineers [IEEE], 2004). Therefore, since such a control system plays a significant role, it is compulsory to provide a reliable controller system.

1.1.3 Following Optimised Train Trajectory regarding Error Deviation and Running Time

The control system of the ATO works by following the predetermined train trajectories as a guide. In most cases, the optimisation method is applied to those trajectories in order to produce better ones in terms of energy consumption and punctuality (Wang, Ning, Boom, & Schutter, 2016). Thus, the controller must obey these optimised paths taking into account speed inaccuracies of ± 3 km/h (IEEE, 2004). In addition, the ATO control system also must guarantee that the optimal punctuality is achieved so as to reduce the carbon footprint and optimise the running time.

1.1.4 The Need for Reducing Noise from Tracking Device

Furthermore, when the controller is applied as an ATO system on a train, one has to bear in mind that it is the nature of any electronic device, in particular in this case a sensor that is used to track the train's actual location and speed, is subject to high frequency noise, called measurement noise or error (Åström & Murray, 2008). This causes system disruption, so that the controller strives to follow the trajectory, and as a result, the IEEE (2004) standardised such a phenomenon of system disruption in order to implement CBTC systems. Consequently, the control system of the ATO must be able to reduce such noise.

1.2 Aim and Objectives

The study aims to develop a control design of an ATO able to maintain the train speed within the specified trajectory and stability in normal conditions and noisy situations. Such noisy circumstances are defined as conditions where the actual speed is corrupted due to measurement errors. Subsequently, in order to meet this aim, the author has determined that the following objectives are necessary:

- Defining a mathematical model of the train dynamics.
- Developing a control design for the ATO which can meet the following criteria:
 - a. Following a predefined trajectory.
 - b. Satisfying a speed tracking error of less than $\pm 3\%$.
 - c. Complying with punctuality to within no more than 30 seconds early and no more than 30 seconds late from the trajectory running time.

d. Showing superior IAE (Integrated Absolute Error) and ISE (Integrated Square Error) performance compared to conventional controllers.

- Applying a 5% Gaussian white noise. as the measurement error in the system.
- Improving control design to cope with a noisy speed profile.
- Implementing the entire system in the context of a real case study.

1.3 Research Questions

The author has defined the following research questions which underlie the study, namely:

- Is a PD (proportional and derivative) controller assisted by Fuzzy system able to cope with the specified objectives of the control design not only in normal conditions but also in noisy situations?
- How can the controller be designed and improved to work not only in standard circumstances but also in noisy conditions so that it can achieve the specified criteria of the control design?
- Is the Kalman filter method capable of assisting the controller in tackling noisy conditions for an actual speed profile?
- What scenario best represents real train environments in order to assess the control design?

1.4 Scope

The author has also determined the limitations of this thesis which are essential to define the study constraints before it is conducted. Those are the following:

- The train dynamics modelling is assumed to be able to represent the real train behaviours.
- In the model, it is the value of the distance difference that is assigned as constant, namely every 1 metre.
- The value of the output signal from the controller is bounded between 1 (full traction) and -1 (full braking).
- The train is assumed to be unable to apply traction and braking concurrently.
- Tunnel and curvature resistances are not considered as they are small and can be therefore be neglected (Rochard & Schmid, 2000).

- Artificial trajectory and its features, i.e. speed reference, speed limit and gradient, are assumed to be sufficient to determine the accuracy of the controller methods.
- All trajectories used are considered to have the optimal speed profile the train controller can follow.
- Energy consumption and passenger comfort are not considered to be objectives.
- As the train automatic stop control (TASC) of the ATO, which determines when the train stops at a station platform in minor stopping errors (especially important for the platform screen doors) is not considered, it is assumed that when the controller is about to approach a station stop, the train terminates in the exact position required, i.e. with zero error.
- Measurement errors are assumed to be in the form of Gaussian white noise.
- In order to generate a 5% Gaussian white noise, a normal distribution having a mean of 0 and a standard deviation of 0.015 is applied.
- The central controller used is the PD controller, not the PID (proportional integral derivative) controller.
- Relay-based auto-tuning approach is utilised to tune the PD controller.
- Train characteristics are constrained as defined in subchapters 4.1.4 and 5.1.1.
- For the sake of brevity, the word 'Fuzzy' alone sometimes is used to refer to Fuzzy logic.
- Fuzzy gain scheduling is implemented to improve PD control.
- Fuzzy membership functions that are used are of Gaussian type.
- Fuzzy inference approach used is the Mamdani method.
- The defuzzification approach used is the centre of gravity method.
- Kalman filter method is applied to noisy environments in regard to the speed profile.
- The value of the error (i.e. the difference between the speed reference and the actual speed) is considered as the input for the Kalman filter since the controller and the system are assumed to be a cohesive system.
- The equation for the modelling of the train dynamics using a Kalman filter is assumed to be able to represent the regular model, as described in subchapter 4.3.2.
- The covariance matrix of the process noise for the Kalman filter is considered to be small and is implemented only to balance the value of the estimate and the measurement.
- DLR B2007 rolling stock and its route from Stratford International to Woolwich Arsenal are considered as the real case study used to examine the methodology.

1.5 Methodology

In order to achieve the aim and objectives, this study employs a methodology which consists of the following:

- A literature review is undertaken to analyse any similar studies.
- The system is modelled and simulated using MATLAB.
- The train dynamics system is modelled mathematically.
- PD controller is designed and applied to the system.
- Fuzzy gain scheduling-based PD controller is designed and implemented into the system.
- Gaussian white noise of 5% measurement error is introduced.
- Filtering method, i.e. the Kalman filter, is designed and utilised.
- Artificial train trajectory is performed to assess the system.
- A real case study is carried out to examine the entire system when running in an actual environment.
- The entire system is validated and analysed based on the controller objectives.

1.6 Thesis Structure

The study is organised into 6 chapters. After this chapter, some related works are discussed and analysed in Chapter 2, which also specifies the research contributions of this study. In Chapter 3, all technical terminology involved in this thesis, namely the development of railway control systems and the controller methods, are explained for background knowledge. The stages of designing the train dynamics model, the types of controller, the introduction to the measurement errors and the approach to dealing with such errors are demonstrated in detail in Chapter 4. Analysis and discussion, employing a constant speed reference and an artificial trajectory, are described as well. After being evaluated in the previous chapter, the system is then examined in a real case study, i.e. the DLR, as described in Chapter 5. Finally, in Chapter 6, all findings and recommendations are identified.

2 Literature Review

This chapter presents some of the studies that are related to the aim of this thesis. The methods used in each item of research are explained concisely and then analysed, in particular those which employ a methodology similar to that used in this thesis. At the end of this chapter, the author determines the research contributions of this work that will fill in the gaps in knowledge left by previous studies.

2.1 Recent Studies on ATO

ATO developments consist of two major themes (Wang et al., 2016). The first relates to research aimed at optimising the ATO speed profile, the so-called high-level ATO, in order to meet specific criteria, such as passenger comfort, train capacity, energy consumption and punctuality. This type of study is subject to rolling stock performance, infrastructure data and so on. The algorithms employed are usually, for example, genetic algorithms, Fuzzy algorithms (Chang & Sim, 1997; Hwang, 1998; Ke & Chen, 2005; Ho et al., 1999), discrete dynamic programming (Franke, Terwiesch, & Meyer, 2000), MAX–MIN ant system (Ke, Chen, & Lin, 2009; Ke & Chen, 2007), brute force (Zhao, Roberts, & Hillmansen, 2012), hybrid algorithms (Carvajal-Carreño, Cucala, & Fernández-Cardador, 2014; Domínguez, Fernández-Cardador, Cucala, Gonsalves, & Fernández, 2014; Xu, Li, & Li, 2016) and so on. Some improvements have been made, such as considering the effect of the error in the positions of the train following the optimised trajectory to energy efficiency (Hamid, Nicholson, Douglas, Zhao, & Roberts, 2016), the effect of the behaviour of the ATO control system following the optimal speed profile for energy consumption (Carvajal-Carreño, Garcia, Fernández-Cardador, & Söder, 2015; Su, Tang, Chen, & Liu, 2014) and the effects of other factors (e.g. train mass, kinematic resistance, gradients, enhancing the maximum traction and braking forces, regenerative braking and optimising the timetable) to reduce traction energy consumption (Su, Tang, & Wang, 2016).

The second theme, called the low-level ATO, regards research to develop a reliable controller to track such optimised train trajectories. It is pivotal, as any optimised trajectory cannot function according to its purposes if the ATO control system is unable to follow it accurately. Some studies have developed the controller to track both the actual speed and the distance of the train, such as that conducted by Dong et al. (2017), while others have focused on only one of them, such as the work of Mao et al. (2017) focusing on position tracking and that of Fu et al. (2017a) focusing on speed tracking. On the other hand, there are also some studies

that consider both ATO research themes, such as those carried out by Ke et al. (2011), Wang et al. (2014) and Xiaojuan et al. (2015).¹

2.2 Related Works in ATO Control Systems

As described previously, this thesis can be categorised into the second type of ATO theme, focusing on tracking the actual train speed. Considering the control methods employed in this thesis, as described in 1.5, in terms of related works of the second type, the author classifies these works into four categories: PID-based, Fuzzy-based, Fuzzy-PID-based, other approaches and that considering measurement errors.

2.2.1 PID Based ATO Control Systems²

Some works developing PID for train control system are, for example, the studies performed by (1) Ke and Chen (2005) which are mainly focuses on optimising the speed code of the speed profile but also on using PID to track such a speed code; (2) Xiangxian, Yue, and Hai (2010) developing single-neuron PID; (3) H. Liu, Zhang, and Chang (2009) developing a nonlinear PID to tackle the Maglev train control system; and (4) Song and Sun (2017) considering more advanced PID, i.e. neuroadaptive PID-like fault-tolerant control. Furthermore, there are also some studies comparing PID and Fuzzy control (Huang & Her, 1997; Utomo, Sumardi, & Widiyanto, 2015; Yasunobu, Miyamoto, & Ihara, 1983).

2.2.2 Fuzzy Based ATO Control Systems

One of the old-fashioned implementations of Fuzzy system to the ATO is the study performed by Yasunobu et al. (1983). Since then, there have been many developments in Fuzzy logic implementation to the ATO. For example, there are the works combining Fuzzy with neural networks. Sekine and Nishimura (1995) proposed a Fuzzy neural network control with two-degrees-of-freedom, but their work was too short and general such that the control rules are tuned (Sekine, Imasaki, & Endo, 1995). A recent study in such a combination is the one undertaken by Yang, Fu, and Zhang (2012) in which neuro Fuzzy is employed to model the Electric Multiple Unit (EMU). Another work is the one using Fuzzy control based on the partition of complex process and hierarchical intelligent control (Chang, Jia, Xu, & Zhang, 1996).

There is also study which utilises multiple working conditions, i.e. actual speed, speed error, acceleration error and actual distance, for the Fuzzy logic controller (Dong, Li, & Ning, 2010),

¹ More explanations regarding both high level and low level are discussed in 3.2.

² It is noted that the PID controller was first applied on the first ATO system in the world, i.e. the Victoria Line of the London Underground, in 1968 (Dong, Ning, Cai, & Hou, 2010).

which was then improved (Dong, Li, Ning, & Hou, 2010) by adding another criterion: the predicted distance. In the meantime, Dong, Gao, Ning, and Li (2011b) used two Fuzzy methods to develop a self-regulating Fuzzy control algorithm to improve the accuracy of Fuzzy logic control, whereas (Dong et al. (2011a)) compared two types of Fuzzy, i.e. a direct Fuzzy controller and a Fuzzy controller incorporating the implication logic, which are applied to two different types of train model, i.e. a single-mass model and a unit-displacement multi-particle model, respectively. Moreover, a very recent research in Fuzzy implementation for ATO control is by Wang and Tang (2017) who employ Takagi–Sugeno (TS) Fuzzy models to model train dynamics and a Fuzzy predictive controller to track the speed profile subject to safety, passenger comfort, energy and speed tracking.

2.2.3 Fuzzy-PID Based ATO Control Systems

Besides employing PID or Fuzzy separately, there are some works combining both using various approaches. For instance, there is some work involving Fuzzy-PID integration in a way such that PID and Fuzzy are switched alternately, e.g. Gou (2014) who is developing a switching approach based on the Fuzzy decision and Bing, Hairong, and Yanxin (2009) who are designing two switching approaches, based on a threshold and Fuzzy rules. Furthermore, the other works generate the integration based on Fuzzy gain scheduling to tune the PID parameters, such as that of Wang, Wang, Sun, and Hao (2017) and Ke et al. (2011) who use the integration to track the train trajectories they optimise. However, Ke et al. also consider the track gradient as a Fuzzy gain scheduling input besides the speed error and delta error (i.e. the difference of speed errors). Implemented on a freight train, the research by Yang, Jia, Fu, and Lu (2017), despite also employing Fuzzy-gain-scheduling PID, considers a multi-modal Fuzzy-PID approach to cope with different conditions, i.e. starting, accelerating, cruising, coasting, regenerative braking and emergency braking, for train traction and braking. They also design backpropagation neural networks to replace the conditions of accelerating and cruising.

Besides the methods mentioned above, which have been implemented in various systems, such combinations are also developed in other approaches. Karasakal, Guzelkaya, Eksin, Yesil, and Kumbasar (2013) have designed an integrated Fuzzy-PID approach assisted by a Fuzzy weight regulator. Dounis, Kofinas, Alafodimos, and Tseles (2013) use Fuzzy gain scheduling to tune PID as well, but develop the Fuzzy system based on scaling factors to tune such Fuzzy scheduling. Dequan, Guili, Zhiwei, and Peng (2012) and Sinthipsomboon, Hunsacharoonroj, Khedari, Pongaen, and Pratumsuwan (2011) integrate the switching approach and Fuzzy gain scheduling in which their controllers can select either Fuzzy gain scheduling PID or expert

control, and Fuzzy gain scheduling PID or Fuzzy logic control, respectively. Ahn and Truong (2009) employ a robust extended Kalman filter to tune the membership functions and rules of Fuzzy gain scheduling PID.

2.2.4 Other Approaches and Developments in ATO Control Systems

Besides PID, Fuzzy and their hybrid methods, there are also other methods implemented to track the train speed profile. For example, Li, Yang, and Gao (2015) made a breakthrough in controlling multiple HST (high-speed train) to track each desired speed in specified headways. Yin, Chen, and Li (2016) include experienced drivers as sources of expert knowledge. There are some works considering actuator saturation on traction and braking, such as the studies carried out by Song, Song, Tang, and Ning (2011) and Gao, Dong, Chen, Ning, and Chen (2013). Some develop neural networks (Gao, Dong, Ning, Roberts, & Chen, 2016; Lin, Dong, Yao, & Bai, 2017) and iterative learning control approaches (Li, Hou, & Yin, 2015; Sun, Hou, & Tang, 2011), and Sun et al. consider the influence of weather conditions as well.

2.2.5 Accounting for Measurement Errors

As described in 1.2, measurement noise is considered in this thesis, therefore the author details the works considering it in ATO, or at least in railway control systems, in this subchapter. To the best of the author's knowledge, in fact, studies of speed tracking for a train control system, taking into consideration measurement errors, are exceptionally scarce in the literature. There are only three studies addressing this issue. Zhang, Chen, Sun, Hou, and Cai (2014) employed a sliding mode observer in a high-speed train, Li and Hou (Z. Li & Hou, 2015) implemented iterative learning control for an ATO control system and Fu, Yang, and Wang (2017b) applied generalised predictive control tuned using ANFIS (Adaptive Neuro-Fuzzy Inference System) on a high-speed train.³

On the other hand, many researchers have studied noise measurement in railway applications. However, such applications are not utilised for train control systems to track the given trajectories but rather for, for instance, velocity and/or position estimations (Allotta, Colla, & Malvezzi, 2002; Colla, Vannucci, Allottay, & Malvezzi, 2003; Monica Malvezzi, Allotta, & Rinchi, 2011; Pichlík & Zďěnek, 2017; Yuan, Zhao, Li, & Zhou, 2013; Zhuan & Xia, 2010). Besides, the Kalman filter and its developments are widely implemented for such estimations in order to attenuate noise measurement (Cui & Dong, 2018; Geistler & Bohringer, 2004; Jones, Franca, Zhou, & Forsberg, 2009; J. Liu, Cai, & Wang, 2016; M Malvezzi

³ Although Faiegghi, Jalali, and Mashhadi (2014) state that they will consider measurement noise for their future works, such research has not been realised yet.

et al., 2014; Siebler, Heirich, & Sand, 2018; Talvitie et al., 2018; Zhou, 2012). These studies simply resemble other works applied, for example, to cars (Daiss & Kiencke, 1995; Fangjun & Zhiqiang, 2000; Kobayashi, Cheok, & Watanabe, 1995; Liang, Yanru, Yongsheng, Hongwei, & Mingfa, 2010). Meanwhile, measurement errors are commonly included in other controller systems besides train control system, such as in Ahrens and Khalil (2004), who worked on track trajectories of pendulum systems, and Ball and Khalil (2008) and Ahrens and Khalil (2009) who worked on the track reference signal of a field controlled DC motor. Juang and Tsao (2008) performed adaptive noise cancellation in nonlinear modeling simulations, and Thornhill, Huang, and Shah (2003) researched a tank reactor.

2.3 Research Contribution

Examining previous subchapters, it can be inferred that in classical research, measurement noise has only been taken into consideration in specific types of railway studies, e.g. velocity and position estimations, and the previous works have shown minor interest in such noise, which exists in train control systems.

Hence, the main contribution of this thesis is in integrating Fuzzy gain scheduling PD and the Kalman filter for speed tracking in the ATO control system taking consideration of measurement errors, and verifying the designed controller using a case study on the DLR line.

3 Introduction to Railway Control Systems

This chapter supplies the necessary insights into the development of such complex systems, as denoted in Figure 1. However, it is only the control and signalling systems, especially the ATP, ATO and their development, which are described extensively since both systems directly form the background to the aims of this thesis. Moreover, the concept behind the controller, measurement errors and the filter applied in the methodology are explained.

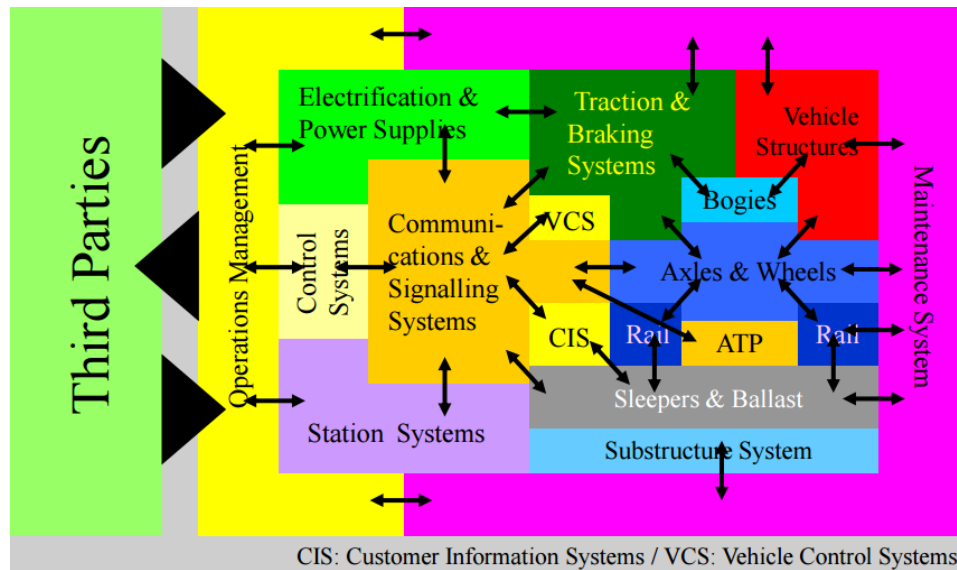


Figure 1 – Railway Systems (Schmid, 2015)

3.1 Protection Systems

With the development of railway transport, ensuring the safety of this transport has become essential. Human error can result in failure in railway operation and this triggers railway engineers to implement automatic controller systems in order to maintain a safe railway transport system. Train protection systems, which apply controller systems, must possess at least five fundamental functions that are the following (Chen, 2017):

- Maintaining a safe separation.⁴
- Protecting against obstructions.⁵

⁴ Each train must be segregated with a practically safe distance. This is carried out so that each has a guaranteed occupied track in accelerating or decelerating.

⁵ One also must protect these from any crash caused not only by a train collision, but also other causes, such as derailment and colliding with any object entering the train tracks.

- Ensuring a safe speed.⁶
- Ensuring safe boarding.⁷
- Ensuring a generally safe environment.⁸

With development, the train protection system evolves. There are several systems applying automation technology to ensure the safety of railway transport. To date, the ATP system is the most recent train protection system able to provide speed supervision in order to maintain a safe and permitted train speed.

3.1.1 Tripcocks and Trainstops⁹

This system consists of two components, i.e. a tripcock¹⁰ mounted underneath each driving cab, and a trainstop¹¹, a piece of trackside equipment integrated with the signal (Connor, 2015). Figure 2 illustrates a tripcock about to be hit by a trainstop.

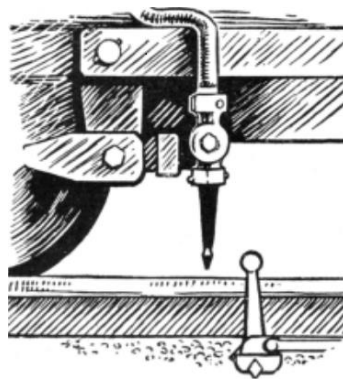


Figure 2 – An illustration of tripcock and trainstop (Connor, 2015)

However, this system suffers from several drawbacks. The tripcock could also, for example, meet other obstructions, e.g. a shovel and ballast stacked too high, that causes a false emergency brake. The driver then has to alight and crawl under the cab in order to close the lever manually. However, after 1914, this was no longer required as a cord-operated trip valve

⁶ The trains must be coerced to run within the tolerated speed limit for each specific route in order to maintain train safety.

⁷ In order to ensure passenger safety, a train, whenever passengers alight or board, must stop at the correct platform side and open the doors of the correct side.

⁸ The trains must provide safe circumstances along the journey and cope with any incident that happens.

⁹ The first train protection system which involved the signalling system in the London Underground was the tripcocks/trainstops system (Connor, 2015).

¹⁰ The tripcock is a lever with a valve connected to a brake pipe line. In the closed position, it faces downwards, but when an obstacle hits it, e.g. a trainstop, it is pushed back, causing it to open the valve resulting in the release of air inside the brake pipe and the application of the emergency brake.

¹¹ The trainstop, by implementing a spring-loaded arm, is connected to each stop signal. It works by utilising compressed air pressure at 60 psi to hold it down when the signal shows a proceed aspect and springs up during a danger aspect (Connor, 2015).

provided a more convenient way to reset it from inside the cab. Besides, since the trainstops need to be positioned close to the stop signals, tripping the traincock to apply the emergency brake when there is a signal passed at danger (SPAD) could only be executed when the train has passed, or is going to pass, the signal. This condition leads to a long overlap distance (usually 300 metres for a metro railway and more than 1500 metres for a mainline railway (Fenner, 2002)) which must be provided to avoid worst-case conditions. Headways can even be seriously affected by such overlap. In addition, the system is unable to reduce the train speed gradually when there is an incoming red signal instead of applying instant emergency brakes when there is a SPAD (Woodland, 2004).

3.1.2 Automatic Warning System¹²

First introduced in the 1950s, the AWS (Automatic Warning System) is one of the types of train protection system which is still in current use. (IRSE, 2008). It comprises two components, i.e. the train and track equipment¹³ (Rail Safety and Standards Board [RSSB], 2015a). Figure 3 denotes a schematic of the AWS arrangement.

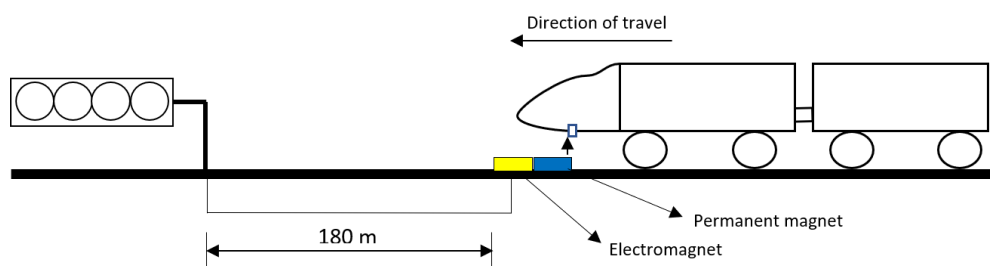


Figure 3 – AWS scheme (Author, 2017)

AWS works by using a receiver mounted beneath the cab that detects the magnetic fields from both magnets, i.e. the permanent magnet and the electromagnet. Subsequently, whether the receiver detects the presence of an electromagnetic field subject to the aspect shown by the signal is followed by two scenarios. The first occurs when a train runs towards the magnets and the signal displays a green or clear aspect; the electromagnet is energised. In this case, after the receiver detects the permanent magnet, the system starts a timer in order to capture the electromagnetic field within one second. As the electromagnet is active, the system rings a bell, and a black indication appears (see Figure 4, left side) in the cab, and the driver takes no action. If the receiver fails to detect the electromagnetic field due to a

¹² In other countries, it is called different names, e.g. ‘the Crocodile’ in the French and Belgian railway systems and “INDUSI” in the German and Austrian railways (IRSE, 2008).

¹³ In the train equipment, there is a receiver, audible indicator, a visual indicator (called the ‘sunflower’) and an acknowledgement button. In the track equipment which is normally placed 180 metres ahead of the signal, there are two types of magnet; a permanent magnet and an electromagnet connected to the signal (RSSB, 2015a).

caution aspect (single or double yellow aspect) or red aspect, the electromagnet is de-energised, and in this second scenario, the system sounds a horn, and the yellow and black indication occurs (see Figure 4, right side). In this event, within two to three seconds, the driver must press the acknowledgement button to deactivate the audible warning as otherwise the system applies the emergency brake.

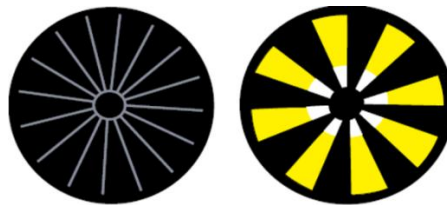


Figure 4 – AWS indicators of the black indication (left side) and the yellow and black indication (right side) inside the cab (RSSB, 2015a)

Regardless of its contributions to the prevention of many accidents, the AWS also has several limitations. Since the electromagnet is de-energised for a single or double yellow and red aspect, it is unable to differentiate among them so that the emergency brake can be applied even if the signal shows only a single yellow signal. Also, after being acknowledged, the system is unable to control the driver's next actions as the protection system has then been overridden. More importantly, the AWS is not equipped with speed supervision which would safeguard the train speed (IRSE, 1993).

3.1.3 Train Protection and Warning System¹⁴

Originally developed from the AWS of British Rail and Railtrack in 1994 due to the high expenditure associated with ATP implementation, TPWS (Train Protection and Warning System) started to operate in 1997. Moreover, it was later developed further and was encouraged by the Railway Safety Regulations 1999 (Rail Accident Investigation Branch [RAIB], 2008).

The system is mainly designed to reduce the possibility of any train passing a TPWS-fitted signal at danger or approaching such a signal or any permanent speed restriction or buffer stop area with a greater speed than allowed, by applying the brake (RSSB, 2004). It has two functions: to act as both a train stop system (TSS) and an overspeed sensor system (OSS)¹⁵, as

¹⁴ Exclusively applied in Britain, TPWS is a protection system technology between the AWS and ATP.

¹⁵ On the one hand, for TSS, when a TPWS-installed signal shows a red aspect, the TSS equipment is energised. At this moment, as long as the arming frequency of the TSS is still detected, if the train, regardless of its speed, also detects the trigger frequency of the TSS, the TSS demands the application of the brakes. On the other hand, for OSS application, it operates based on the time difference measured between the detections of the arming

denoted in Figure 5. Each transmitter of the TSS and OSS is connected to the TPWS trackside unit.

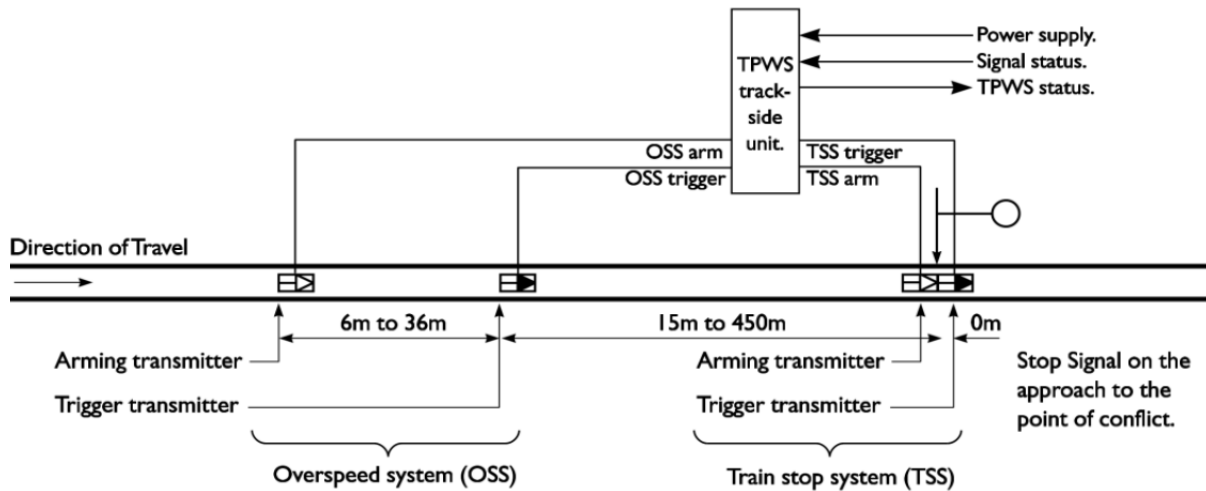


Figure 5 – Layout of TPWS equipment (RSSB, 2015b)

Regardless of TPWS performance, based on the report of Davies (2000),¹⁶ however, the TPWS indeed has limitations, that are the following:

- Not fail safe.
- Limited speed, i.e. only up to 75 mph (120.7 km/h).
- Assumes a higher emergency brake demand than the actual performance of most rolling stock.
- Not very effective on freight trains.
- No speed and braking supervision.

frequency of the OSS and the trigger frequency of the OSS. The system initiates the brake if the time is less than the predefined time which depends on the distance between two transmitters and their delays. This principle works when the signal shows a danger aspect so that both transmitters are energised (RSSB, 2004).

¹⁶ At that time, the need to improve the safety factor, especially the risk of SPADs, increased, resulting in, for instance, the introduction of the European ATP system, i.e. ETCS. Even the installation of TPWS could not meet the safety demand in the long-term future. Therefore, this suggested that all stakeholders should migrate to more sophisticated train protection systems. Due to the high cost, however, any improvement from TPWS to ATP was carried out only by developing the system's capabilities, resulting in the enhanced TPWS, i.e. TPWS+ and TPWS-E. TPWS+ means a TPWS with enhanced performance able to protect trains running up to 100 mph (160.9 km/h), whereas TPWS-E (Train Protection and Warning System Eurobalise) is an upgraded TPWS implementing similar train-to-trackside communications to ETCS so that in the Immediate future, such a TPWS can be improved to ETCS completely.

3.1.4 Automatic Train Protection¹⁷

The need to stop trains when they are in danger, particularly SPADs, led not only to the automatic application of the train brakes but also to the invention of train speed supervision, i.e. an automatic system functioning to continuously monitor the train speed and intervene in the case of unauthorised train speeding (IRSE, 1993). As illustrated in Figure 6, without the speed supervision intervention, the train could stop further (see dashed line). In order to consider a train protection system as an ATP system, therefore, it must have such a crucial function, i.e. guaranteeing that such unsafe movements do not occur (Woodland, 2004).

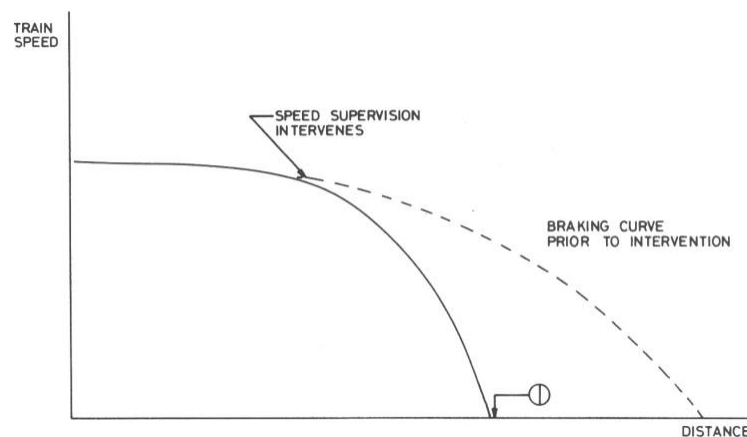


Figure 6 – ATP speed supervision (IRSE, 1993)

The ATP system has evolved in accordance with the improvements in information and communication technology. The introduction of transistor circuits, first produced in 1948, initiated the development of the first type of ATP in the 1960s. This system utilised coded track circuits to create so-called equi-block ATP in order to restrict the allowable speed line of each fixed block.

In the UK in 1989, the first two ATP systems, the so-called BR-ATP (British Rail Automatic Train Protection), were implemented on the HST between London Paddington and Bristol Parkway of Great Western produced by ACEC (now Alstom) and on multiple-unit trains on the Chiltern Line manufactured by SELCAB (Davies, 2000). In other countries in Europe, other ATP systems were implemented, namely ATB-NG in the Dutch Railway and TBL in the Belgian Railway systems.

¹⁷ Woodland (2004) found that the definitions of train control systems are widely interpreted by each author, company and country. He, at least, categorised those into four definitions and went on to use the one which regards the ATP, ATO and other automatic systems, e.g. ATS (Automatic Train Supervision), that mutually form the ATC (Automatic Train Control) as a cohesive system. In this thesis, the author intends to implement his definition.

3.2 Automatic Train Operation

Unlike train protection systems, the ATO system works on the operational section of the train control system. Since first introduced to the world in the Victoria Line of the London Underground in the early 1960s,¹⁸ it has provided crucial functions in driving a train, i.e. traction and braking. The Central, Jubilee and Northern Lines, thenceforth, also installed ATO systems. For example, the driver's console inside the cab of the Northern Line 1995 Rolling Stock driven by ATO is shown in Figure 7. Progressively, the ATO system has developed, resulting in the fully automatic control of trains (FACT) which is today known as a driverless train.¹⁹ The DLR is one of the ATO developments which no longer requires any driver, albeit that a member of staff is always on board (Connor, 2015).

In ATO systems, the train's position when it runs between station stops is tracked, and this creates an interlocking thanks to the two-way transmission between train-borne passive balises—sometimes called beacons or transponders—and active balises located at certain positions along the tracks. This communication can be developed to provide platform screen doors—in order to enhance safety—where the train is able to stop at specified platform gates (Hitachi Rail, 2013).



Figure 7 – Inside a cab of Northern Line 1995 Stock assisted by ATO system (Connor, 2015)

Moreover, in their applications on urban railways, ATO systems consist of two levels, i.e. high-level control and low-level control, as conceptually shown in Figure 8. By using any particular algorithm, such as a genetic algorithm, least-squares optimization, etc., and in order to

¹⁸ At that time, this system was supervised by so-called single manning or one-man operation (OMO) in which a driver controlled only the start of the train, the opening and closure of train doors and the observation of the platform when the train is about to depart. In the UK, the term arises since, by implementing ATO, the drivers' functions are obviously reduced, causing their duties to be similar to an operator (Connor, 2015).

¹⁹ This type of automatic train is described extensively in subchapter 3.3.

achieve specified targets, i.e. energy consumption, punctuality and passenger comfort, the high-level control generates and renews the optimised speed profile subject to speed restrictions of the ATP profile and the train and track conditions, such as maximum tractive effort and braking force, running resistances, track gradient, curvatures, tunnels and so on.²⁰ In the meantime, in the low-level control, by implementing a specific control method—such as PID control, robust control or adaptive control—to manage traction and braking forces and the data obtained from the sensors and the two-way communication in real time, the ATO system tracks the predefined optimal train trajectory as the reference (Wang et al., 2016).

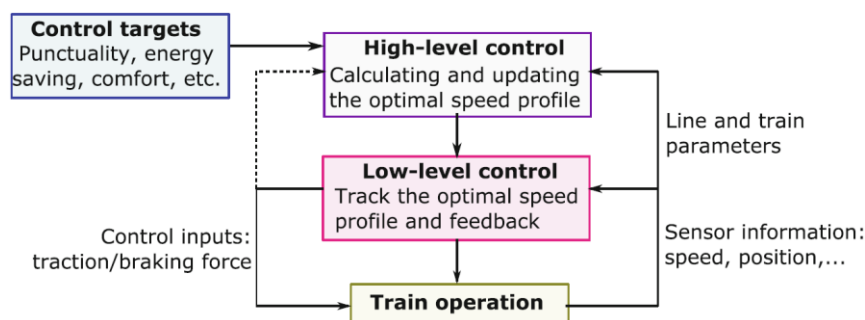


Figure 8 – Diagram of control actions of ATO (Wang et al., 2016)

The ATO system, moreover, offers essential advantages, i.e. shortening headway, increasing train capacity, improving train safety and reducing energy consumption (Siemens, 2016). Nonetheless, due to the fact that it is not a fail-safe system, in its implementation, the ATO system is integrated with the ATP system to guarantee that the train does not exceed the permitted speed (IRSE, 2008). As shown in Figure 9, where LMA stands for limit of movement authority, the ATP speed profile, generated on the upper speed, secures the ATO speed profile in any failure case by the ATO.

The ATP and ATO, supported by the ATS (Automatic Train Supervision), form an integrated system called ATC (Automatic Train Control), as denoted in Figure 10 (IRSE, 2009). The ATO system, which is connected to the train cab, drives both traction and brake, but the service brake only, whereas the ATP merely controls the brakes, i.e. both the service brake and the emergency brake.

²⁰ Such high-level control, on the other hand, is also applied on freight railways, for example, not as an ATO system but rather as a driver advisory system (DAS) which can provide the optimal train trajectory to be followed manually by the driver (Wang et al., 2016).

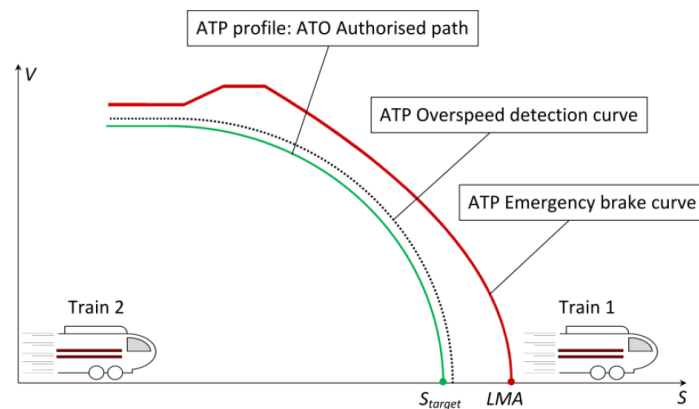


Figure 9 – The speed profiles of ATO and ATP system (Carvajal-Carreño, 2017)

The ATO and ATP communicate with trackside equipment; the ATO has two-way communication, while the ATP only works as a receiver. The sensors provide the tracking data of both the actual train speed and the position to the ATP and ATO. Then, the ATS system monitors the entire system so that, in order to optimise the train operation, the ATS can adjust the actual circumstances to the predefined schedule and traffic. In other words, it serves as an interface between the ATC and the operators at the control centre (Li et al., 2017).

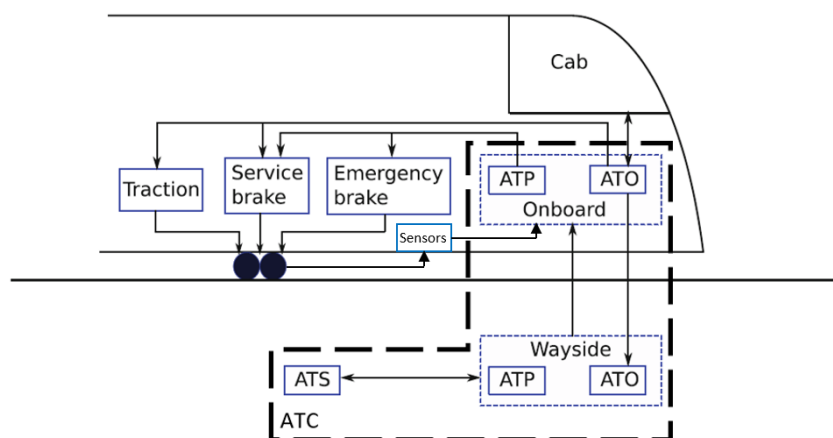


Figure 10 – The structure of ATC system (Dong, Ning, et al., 2010)

3.3 Grades of Automation²¹

According to the International Electrotechnical Commission (IEC) 62267 standard (as cited in the International Association of Public Transport [UITP], 2014, 2015), metro railway transport is categorised into four levels, the so-called GoA (Grades of Automation). Such grades refer

²¹ The summary of all GoAs' functions can be seen in Table 6 in Appendix A – Table of Difference among GoAs. It shows increasing GoA and their increasing number of functions.

to how the train operation is controlled, either manually by the driver or in a fully automated manner. As shown by the UITP (2015), normally the GoA are classified into GoA1, GoA2, GoA3 and GoA4 although the term GoA0²² is sometimes also used (Keevill, 2016). The figure denotes that at GoA3 and GoA4, the driver is no longer required, whereas the other 2 levels need a driver.

- GoA1

As the first degree of the GoA, GoA1 applies to an ATP whose functions are as described in 3.1.4. Since this refers only to ATP installation, i.e. it is a safety system and not a train operation system, GoA1 still requires a driver to operate the train from starting, traction, cruising, coasting, braking, parking, door opening and closure and even tackling any emergency circumstances.

- GoA2

In GoA2, along with the ATP, an ATO is also installed to operate the acceleration, cruising, coasting and stopping of the train. However, the driver, sometimes in this case called the operator, is needed only for starting the train, opening and closing the doors and handling any emergency circumstances. This system is also referred to as semi-automatic operation (STO).

- GoA3





Still implementing the ATP and ATO, GoA3 no longer requires a driver since the system is able to open the doors automatically after arriving at the station and to detect any obstacle, including a person on the track in order to prevent collisions. Nonetheless, an on-board staff member is still necessary to perform crucial duties, e.g. closing the doors and ensuring the safety of the passengers, driving the train manually if the system fails and dealing with any emergency. GoA3 is called Driverless Train Operation (DTO).

- GoA4

As the most recent metro signalling system, GoA4, sometimes called UTO (Unattended Train Operation), is a fully automatic system capable of operating without any personnel on board. Besides the ATP and ATO, this system also integrates an ATS and then creates an ATC system. UTO provides the integrated subsystems capable of not only operating safety and operational functions, e.g. safe speed, train operation and doors opening and closing, but also optimises the timetable and handles disruptions and emergency situations. In order to establish such

²² Practically, GoA0 is not included in the GoA term. It implies that it is an on-sight operation, that is controlled manually and fully by the driver, i.e. without any assistance from an ATP or even an ATO system (Keevill, 2016).

an integrated system reliably, the operation control centre (OCC) continuously monitors the system and provide high-reliability bi-directional communications.

| Grade of Automation | Type of train operation | Setting train in motion | Stopping train | Door closure | Operation in event of Disruption |
|-----------------------------------------------------------------------------------------|-------------------------|-------------------------|----------------|-----------------|----------------------------------|
| GoA 1  | ATP with driver | Driver | Driver | Driver | Driver |
| GoA 2  | ATP and ATO with driver | Automatic | Automatic | Driver | Driver |
| GoA 3  | Driverless | Automatic | Automatic | Train attendant | Train attendant |
| GoA 4  | UTO | Automatic | Automatic | Automatic | Automatic |

ATP - Automatic Train Protection ATO - Automatic Train Operation

Figure 11 – Grades of Automation (UITP, 2014)

Keevill (2016) has formulated two aspects in relation to enhancing GoA, i.e. the advantages and challenges. In general, there are four benefits in upgrading GoA, namely:

- Safety.
- Operational Service.
- Line Capacity.
- Cost.

And there are six challenges in upgrading GoA, namely:

- Rolling Stock Upgrades.
- Communication Enhancements.
- Detection of Track Intrusion.
- Risks.
- Culture.
- Cost-Benefit Assessment.

3.4 Automatic Controller

Many controller applications are implemented in the railway transport system as previously described. Several methods to accomplish such automatic applications were also mentioned

in Chapter 2. This subchapter defines the basic knowledge regarding the controller methods considered in this thesis.

3.4.1 PID Controller²³

This comprises of three terms: proportional (P element), integral (I element) and derivative (D element). Equation 1 shows the mathematical definition of the PID controller.

Equation 1 – PID Control Law

$$u(t) = K_p e(t) + K_i \int_0^t e(t) dt + K_d \frac{de(t)}{dt}$$

$u(\cdot)$ is the control signal produced by the PID; this will become the input to the regulated system. K_p is called the proportional gain. $e(\cdot)$ is the error, which is the difference between the set point value and the value of the output of the system. K_i is called the integral gain. K_d refers to derivative gain.

As shown in Figure 12, which illustrates a block diagram of PID control when applied to a system, the PID utilises feedback to calculate the deviation between the desired value and the system output value. y_r is the set point value; whereas y is the process value.

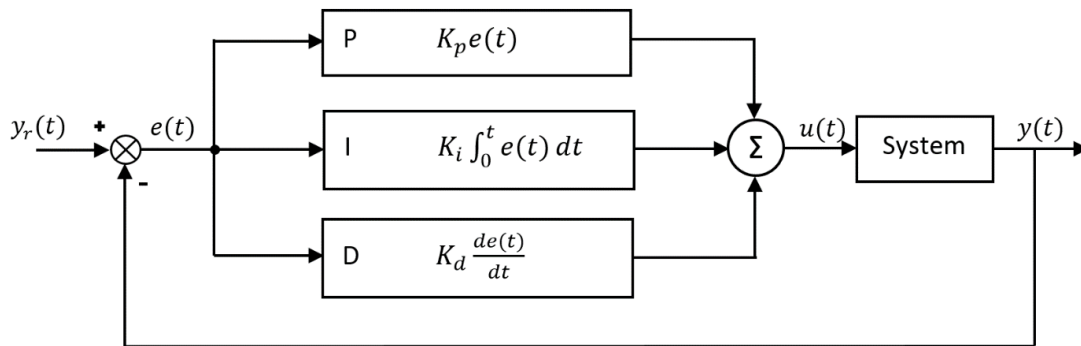


Figure 12 – Block diagram of PID controller (Author, 2017)

In addition, there is another equivalent PID control form which is shown in Equation 2 (Åström & Hägglund, 1995).

²³ PID control is one of the favourite controllers used to regulate various systems. It has evolved over 250 years and is still in use today (Åström & Hägglund, 2006). In its development, specifically in order to meet its control objectives, e.g. transient response and noise attenuation, PID control evolves. Many attempts have been made to improve PID control including designing new structures, or incorporating it with other controllers, and developing proper tuning methods in order to establish more desirable performance of the PID. Such efforts can be classified into five types of development, namely employing the methods of analytics, heuristics (artificial intelligence), frequency response, optimization and adaptive tuning (Heong, Chong, & Yun, 2005).

Equation 2 – Equivalent PID Control Law

$$u(t) = K_p[e(t) + \frac{1}{T_i} \int_0^t e(t) dt + T_d \frac{de(t)}{dt}]$$

This type of PID control has slight differences, i.e. it uses T_i (reset time) and T_d (derivative time). However, these values are defined as $T_i = \frac{K_p}{K_i}$ and $T_d = \frac{K_d}{K_p}$, respectively.

- Integrator Windup

In PID control, there is a common issue which can adversely impact its performances. This problem is integrator windup (Åström & Häggglund, 1995). The culprit is an integral part of the PID and this is the risk of implementing the integral part in PID. This case takes place when the actuator reaches its limit. For example, when a valve reaches its maximum opening, the controller may still command it to open since the error value will continue to be integrated with respect to time, resulting in a very large output value exceeding the actuator's capacity. This means that the controller needs a longer time to return the system to normal. Figure 13 illustrates the output signal from the system and the control signal that occurs when integrator windup occurs.

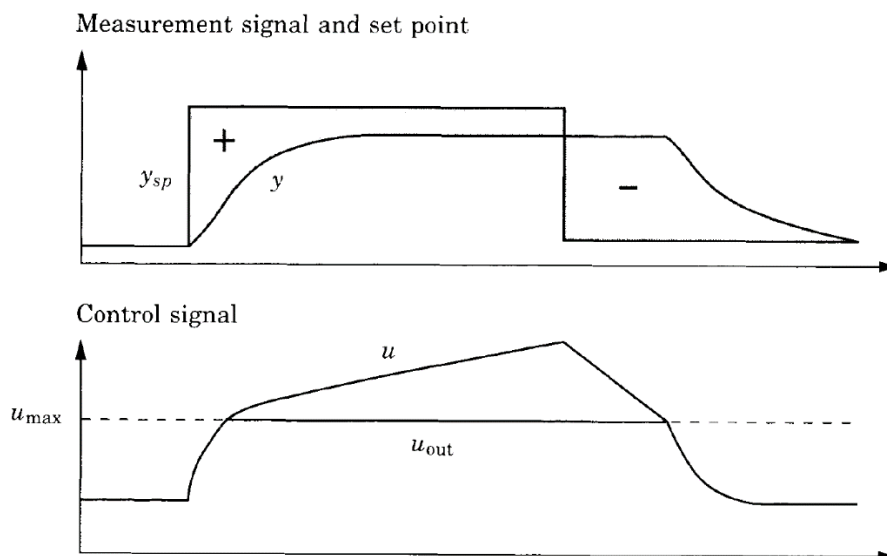


Figure 13 – Example of integrator windup (Åström & Häggglund, 2006)

- Ziegler-Nichols PID Tuning Method

Prior to implementing PID on a system, it is necessary to determine the appropriate parameters for the PID. This is called tuning of the PID Controller. There are many methods to tune PID control, for example (Åström & Häggglund, 2006), manual tuning, Ziegler-Nichols methods, pole placement methods, algebraic tuning methods, optimisation methods and

loop shaping methods. However, as Ziegler-Nichols methods can be regarded as among the most popular PID tuning methods, they have been employed in many developments. Therefore, it is practicable to implement one of the Ziegler-Nichols PID tuning methods on ATO control systems.

One of the Ziegler-Nichols methods, known as optimum pre-act time adjustment (1942), works on the idea of setting PID tuning rules by finding the ultimate gain K_u and ultimate period T_u . The procedure for this consists of the following:

- a. Setting the controller either to use proportional controller only or to adjust T_i to infinity and T_d to zero.
- b. Setting a value for step response.
- c. Finding the value of K_u by gradually increasing K_p until the controller reaches continuous oscillations, as illustrated in Figure 14.
- d. The value of K_p in which the controller continuously oscillates is the value of K_u , whereas the value of T_u is the period of such a response.
- e. After both values are observed, find the real values of K_p , T_i and T_d using Equation 3.

Equation 3 – Rules for K_p , T_i and T_d

$$K_p = 0.6K_u$$

$$T_i = 0.5T_u$$

$$T_d = 0.125T_u$$

- Relay-Feedback PID Auto-tuning Method

One of the main drawbacks of the Ziegler-Nichols tuning method is that it is time consuming and it is not possible to tune the PID automatically. This has led to the development of another method; one which uses a relay feedback approach. Initially introduced by Åström and Hägglund (1984; 1984a, 1984b),²⁴ this technique proposes a reliable method to tune the PID parameters automatically based on the implementation of a relay control feedback, as shown in Figure 15 (top).

²⁴ They suggest that when a system runs by using an input d from a relay, it will generate oscillations in a harmonic way as with the Ziegler-Nichols method (see Figure 15 (bottom)). Such oscillations occur since a system will oscillate with specific period if it has a phase lag greater than 180° .

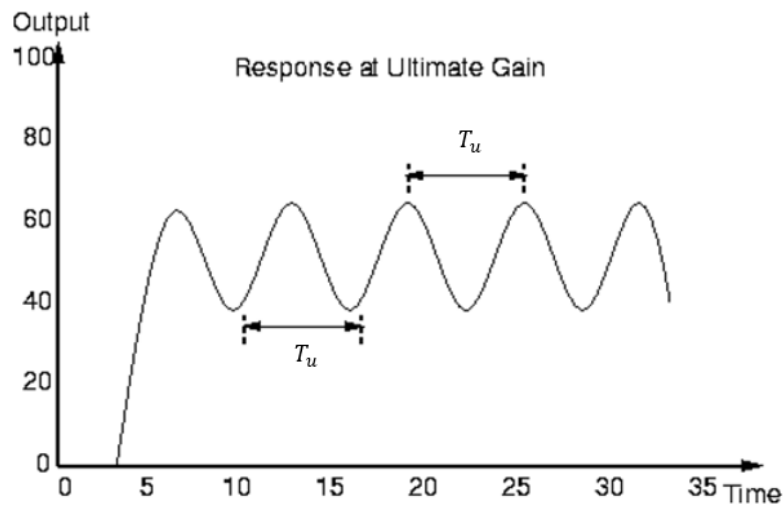


Figure 14 – Response from the controlled system (Ponton, 2007)

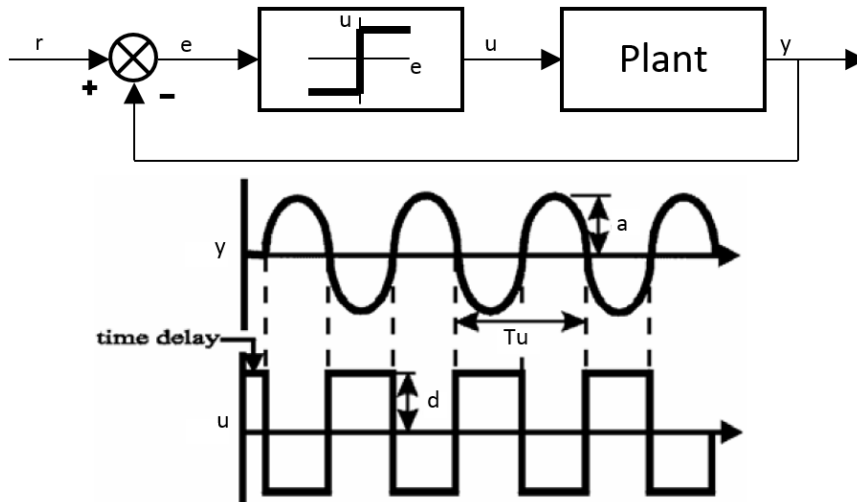


Figure 15 – Block diagram (top) and output and control signal responses (bottom) of relay feedback control (Yu, 2006)

Equation 4 – The output of relay

$$d = \begin{cases} d; & e > 0 \\ -d; & e < 0 \end{cases}$$

If d is the relay output amplitude when error e is greater than zero and $-d$ when e is less than zero, as defined in Equation 4, and a is the amplitude of the system output which can be determined by measuring the distance between the upper peak and the lower peak, then on dividing the amplitude by 2, then ultimate gain K_u can be approximately described as:

Equation 5 – Interaction between relay and ultimate gain

$$K_u = \frac{4d}{\pi a}$$

Furthermore, since the frequency f depends on the ratio between the number of oscillations N in a wave and the total time required T_{total} for a wave to travel, so that $f = N \frac{1}{T_{total}}$, one could operate the system to produce a wave in a certain time T_{total} using relay control in order to obtain the value of N by counting the number of peaks produced and then subtracting 1. Then, the critical period T_u can be found based on its relationship with the frequency, as shown in Equation 6. After K_u and T_u have been found, one could utilise the Ziegler-Nichols rules, as explained in Equation 3.

Equation 6 – Interaction between critical period and frequency

$$T_u = \frac{1}{f}$$

Subsequently, after the PID parameters have been tuned using the relay feedback approach, PID control itself can be set to operate automatically, as shown in Figure 16. Therefore, the method is called PID auto-tuning.

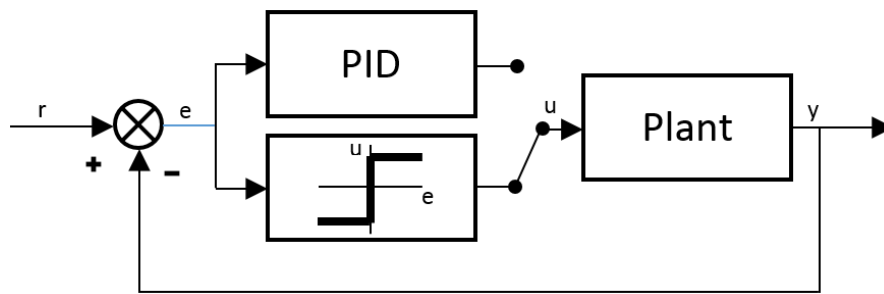


Figure 16 – Block diagram of relay-feedback PID auto-tuning method

3.4.2 Fuzzy Logic

First introduced by Zadeh (1965), Fuzzy set theory is a concept in which a set in a space of points is defined to have membership function (MF), namely a real number between 0 and 1, that is obviously different from the classical set theory where each individual is determined as either a member or not in straightforward and unambiguous manner. In other words, an point in Fuzzy set can be said to be both a member and not a member, that is, it is partially a member and partially not a member (Chen & Pham, 2000).

If an element x is included in a universe of discourse X , then the Fuzzy notation for mapping x as a member of Fuzzy set A in X is given by Equation 7, where $\mu_A(x) \in [0,1]$ is the MF of Fuzzy set A .

Equation 7 – Fuzzy notations

$$A = \{(x, \mu_A(x)) | x \in X\}$$

To explain the concept of the Fuzzy set more clearly, Mendel, Hagra, Tan, Melek, and Ying (2014) consider the temperature of a room using linguistic measuring, i.e. cold and hot. By employing the classical set, one has to divide explicitly between what is a hot temperature and what is a cold temperature, for example, “cold” is defined as between 0 and 18 degrees Celsius and “hot” is greater than 18 degrees Celsius, as shown in Figure 17 (a). Since the crisp sets recognise the concept that an element is either a member or not a member, the degree of membership of “cold” is fully 1 and that for “hot” fully 0.

However, an issue arises when the measured temperature is 17.99999°C or 18.00001°C , where is unreasonable to classify it as either fully cold or hot. Thus, by implementing Fuzzy sets, as denoted in Figure 17 (b), such an issue can be solved by considering that the temperature belongs to both sets with different degrees of membership. In Fuzzy sets, the temperature of 26°C can have membership values of $\mu_{\text{cold}}(26^{\circ}\text{C}) = 0.2$, i.e. 0.2 for “cold”, and $\mu_{\text{hot}}(26^{\circ}\text{C}) = 0.8$, i.e. 0.8 for “hot”.

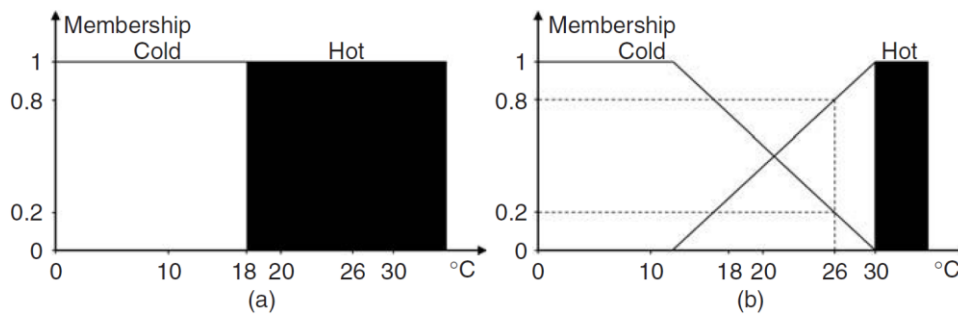


Figure 17 – Example of membership functions of (a) crisp sets and (b) Fuzzy sets (Mendel et al., 2014)

Like the classical sets, Fuzzy sets have the same fundamental operations, namely union, intersection and complement (Jang, Sun, & Mizutani, 1997). Consider A , B and C are Fuzzy sets in a universe X , then the definition of three operations is the following:

- Union

The union is written as $C = A \cup B$ or $C = A \text{ OR } B$ where, for given x element of X , the operation of union is defined by Equation 8.

Equation 8 – Operation of union

$$\mu_C(x) = \mu_{A \cup B}(x) = \mu_A(x) \vee \mu_B(x) = \max(\mu_A(x), \mu_B(x))$$

- Intersection

The intersection is written as $C = A \cap B$ or $C = A \text{ AND } B$ where, for given x element of X , the operation of intersection is defined by Equation 9.

Equation 9 – Operation of intersection

$$\mu_{A \cap B}(x) = \mu_A(x) \wedge \mu_B(x) = \min(\mu_A(x), \mu_B(x))$$

- Complement

The complement is written as \bar{A} , i.e. *NOT A* or $\neg A$ where, for given x element of X , the operation of complement is defined by Equation 10.

Equation 10 – Operation of complement

$\mu_{\bar{A}}(x) = 1 - \mu_A(x)$ In addition to the Fuzzy operations, MFs of Fuzzy sets also have to be defined in order to map an element x into the Fuzzy sets. There are many types of MF to parameterise such an element. However, in this thesis, the author only presents three possibilities, namely the triangular MF, trapezoidal MF and Gaussian MF.

- Triangular MF

Suppose there are three parameters (a, b, c) where $a < b < c$. Then the triangular MF is given by Equation 11. Figure 18 (left) denotes the triangular MF.

Equation 11 – Triangular MF

$$\text{triangle}(x; a, b, c) = \begin{cases} 0; & x \leq a \\ \frac{x-a}{b-a}; & a \leq x \leq b \\ \frac{c-x}{c-b}; & b \leq x \leq c \\ 0; & c \leq x \end{cases}$$

- Trapezoidal MF

Suppose there are four parameters (a, b, c, d) where $a < b \leq c < d$. Then the trapezoidal MF is given by Equation 12. Figure 18 (middle) denotes the trapezoidal MF.

Equation 12 – Trapezoidal MF

$$\text{trapezoid}(x; a, b, c, d) = \begin{cases} 0; & x \leq a \\ \frac{x-a}{b-a}; & a \leq x \leq b \\ 1; & b \leq x \leq c \\ \frac{d-x}{d-c}; & c \leq x \leq d \\ 0; & d \leq x \end{cases}$$

- Gaussian MF

Suppose there are two parameters (c, σ) where c is the centre of MF and σ is the deviation from the centre. Then the Gaussian MF is given by Equation 13. Figure 18 (right) denotes the Gaussian MF.

Equation 13 – Gaussian MF

$$gaussian(x; \sigma, c) = e^{-\frac{1}{2}\left(\frac{x-c}{\sigma}\right)^2}$$

As mentioned by Chen and Pham (2000), the selection process for proper membership functions is more or less subjective. Hence, there is no precise and strict rule to specify them; they are usually chosen based on scientific background, expert experience and the specific requirements of the application considered.

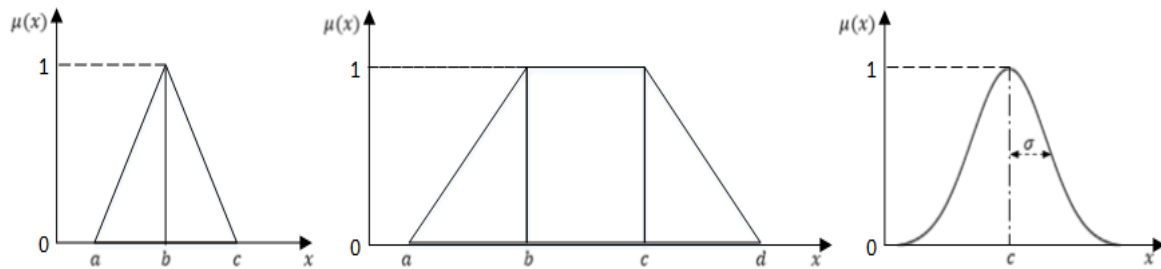


Figure 18 – Membership functions of (left) triangle, (middle) trapezoid and (right) Gaussian (Author, 2018)

In addition, the developments in the field of Fuzzy logic have led to many new applications, such as in biomedicine, data mining, image processing, pattern recognition and control applications (Sivanandam, Sumathi, & Deepa, 2007). Particularly for the latter example, based on the concepts of Fuzzy logic, the Fuzzy logic controller (FLC) was first developed by Mamdani and Assilian (1975). Its principle is to imitate human reasoning based on imprecise linguistic information, in manually controlling a system into numerical control rules that can be applied to the controller systems.

The architecture of FLC is shown in Figure 19. For a nonlinear controller $u = f(x)$, where f is a nonlinear function ruled by Fuzzy sets mathematics and Fuzzy logic operations, FLC has crisp values of inputs x and outputs u . Then, its four components, i.e. fuzzification, rule base, inference engine and defuzzification are the following (Mendel et al., 2014):

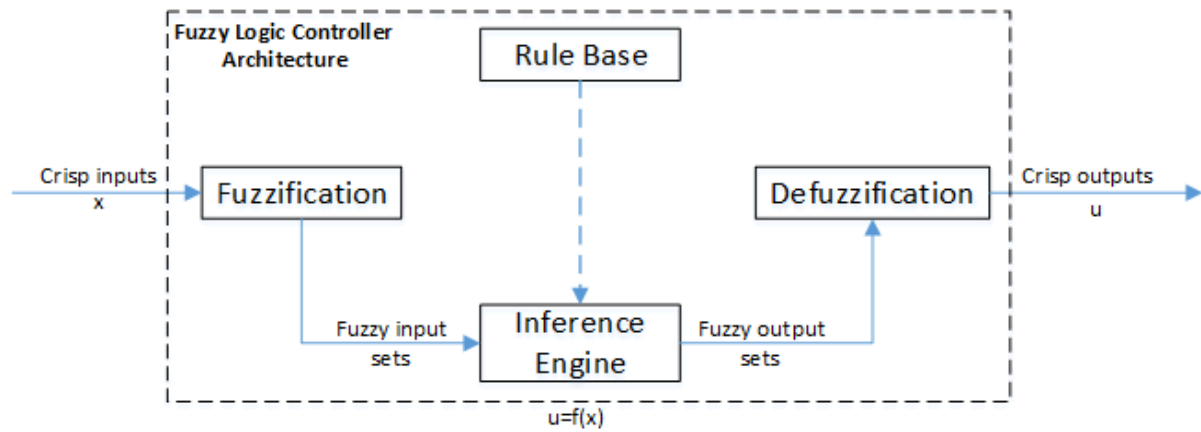


Figure 19 – Architecture of Fuzzy logic controller (Mendel et al., 2014)

- Fuzzification

By using Fuzzy set theory, this component converts the inputs in the form of classical sets into Fuzzy sets. Therefore, such inputs can be processed further by the inference engine. For instance, as mentioned earlier regarding the measured temperatures of cold and hot, such a crisp value is then mapped into Fuzzy sets, as shown in Figure 17 (b).

- Rule Base

This component consists of the rules, which are initially determined by the designer, governing FLC behaviours. A rule comprises of antecedent and consequent. For example, in the rule saying “*IF temperature is cold AND pressure is high THEN heater is high*”, the antecedent is the *IF* part, whereas the consequent is the *THEN* part. Equation 14 shows an example of Fuzzy rules.

Equation 14 – Example of Fuzzy rules

Rule 1: *IF input x_1 is A_1 AND/OR input y_1 is B_1 THEN output z_1 is C_1*

⋮

Rule n : *IF input x_n is A_n AND/OR input y_n is B_n THEN output z_n is C_n*

- Inference Engine

After defining the rule base, the rules are executed and managed by the inference engine to perform the mathematics of Fuzzy sets, i.e. determining the degree of membership of each crisp input by employing membership functions and the operations of Fuzzy logic, as explained earlier. Consequently, the aggregated Fuzzy output can be produced for the next step: defuzzification. For example, suppose two *AND* rules whose two inputs and output are x , y and z , respectively. The process of defining the degree of membership of each input and

combining them based on the rules to produce the aggregated Fuzzy output can be seen in Figure 20. The upper part of the figure shows the inference process, which applies implication method *min* (intersection) for the output of each rule. Meanwhile, the lower right corner side shows the aggregated Fuzzy output using the *max* operation (union) and the lower left corner shows the input distributions.

- Defuzzification

This component is the last stage of FLC in which the aggregated Fuzzy output is reconverted into crisp values so that the system can utilise them directly since most systems use such crisp values. Some defuzzification methods include the centre of gravity (centroid) and mean of maximum methods. As shown in Equation 15, z_{cog} is the centroid method where $\mu_C(z_i)$ is the membership degree at which z_i crisp value is applied and N is the number of crisp values calculated; z_{mom} is the mean-of-maximum method where z_j is the crisp value when it reaches the maximum value of membership degree, e.g. $\mu_C(z_j) = 1$, and l is the number of times of such the crisp value on the maximum value of membership degree.

Equation 15 – Defuzzification methods of centroid and mean of maximum

$$z_{cog} = \frac{\sum(\text{value of member} \times \text{membership value})}{\sum(\text{membership value})} = \frac{\sum_{i=1}^N z_i \cdot \mu_C(z_i)}{\sum_{i=1}^N \mu_C(z_i)}$$

$$z_{mom} = \sum_{j=1}^l \frac{z_j}{l}$$

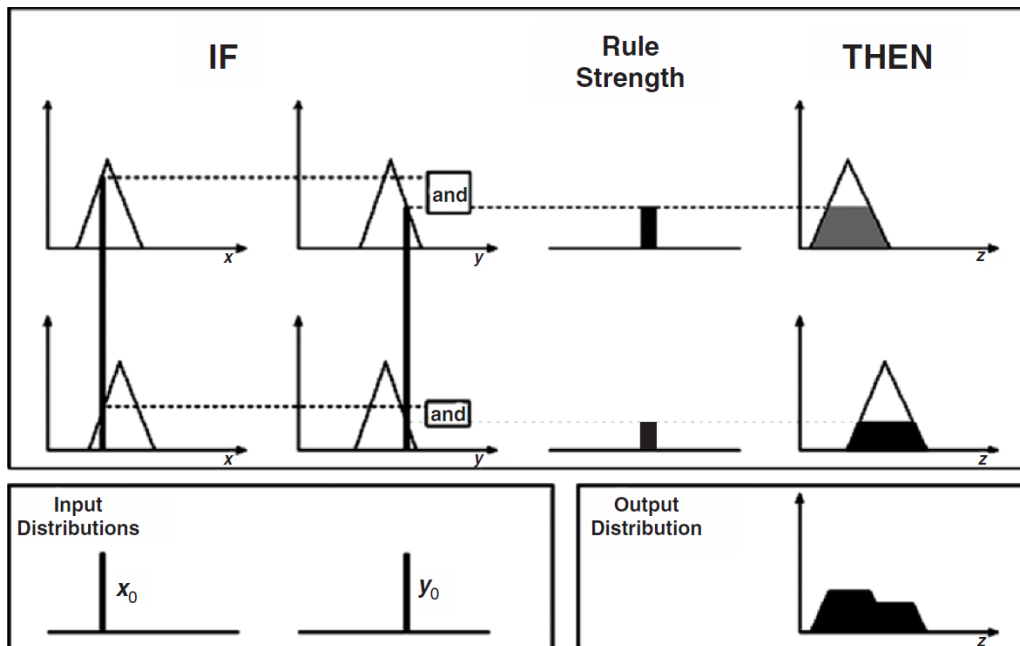


Figure 20 – Example of Fuzzy inference (Sivanandam et al., 2007)

Furthermore, the developments of FLC has triggered many types of Fuzzy implementations in control systems, particularly the PID controller. Some of these are, for example, the Fuzzy-PD controller, Fuzzy-PI controller, Fuzzy-PID controller and even a designed FLC for updating the PID parameters online as an adaptive controller (Chen & Pham, 2000). The latter type is called Fuzzy gain scheduling of the PID controller (Zhao, Tomizuka, & Isaka, 1992, 1993) or, sometimes, Fuzzy self-tuning of the PID controller (He, Tan, Xu, & Wang, 1993).

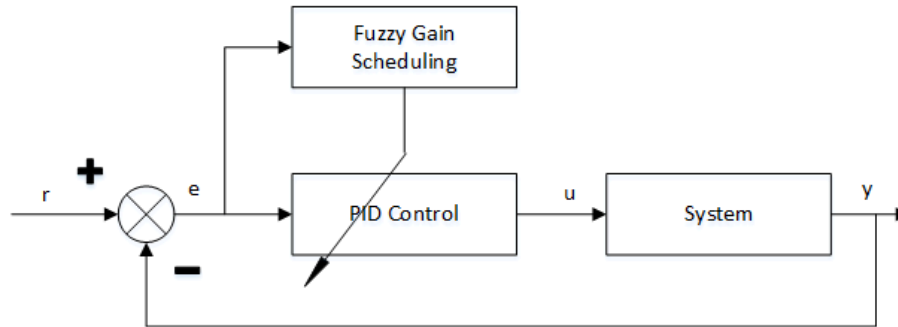


Figure 21 – Simplified block diagram of Fuzzy gain scheduling based PID (Zhao et al., 1993)

3.4.3 Measurement Errors in Sensor

In train applications, speed measurement plays a significant role since it provides critical information for train control systems to work safely and properly. However, measurement error, sometimes also called measurement noise, exists in every instrument and disrupts the original data. This is the condition where the measured speed and position are distorted by an undesirable signal (Yuan et al., 2013). Such errors occur in almost every field of study, such as image processing, signal processing, sampling error and instrument error (Buonaccorsi, 2010). In the latter example, the noise is often modelled to represent the deviated information of the system output obtained from the devices. Moreover, it is common to model the noise in the form of a normal distribution, additive zero mean white Gaussian noise: $X \sim N(0, \sigma^2)$, and to improve the performance of the controller, e.g. by implementing a filter or an estimator, in dealing with such noise (Bavdekar, Deshpande, & Patwardhan, 2011).

Suppose that there is a variable x with mean μ , variance σ^2 and standard deviation σ . Then the probability density function (PDF) of the normal distribution of x is shown in Equation 16 (Bryc, 1995). One could employ Equation 17 and Equation 18 to calculate the mean, variance, standard deviation and covariance, respectively, where N is the number of data points. Further, Figure 22 shows an example of the PDF of a normal distribution. In addition to x , if there is a variable y , one could calculate the covariance of both variables, as shown in Equation 19.

Equation 16 – Probability density function of normal distribution

$$f(x) = \frac{1}{\sqrt{2\pi}\sigma} e^{-\frac{(x-\mu)^2}{2\sigma^2}}$$

Equation 17 – Equation of mean

$$\mu = \frac{1}{N} \sum_{i=1}^N x_i$$

Equation 18 – Equations of variance and standard deviation

$$\text{var}(x) = \sigma_x^2 = \frac{1}{N} \sum_{i=1}^N |x_i - \mu_x|^2$$

$$\sigma_x = \sqrt{\frac{1}{N} \sum_{i=1}^N |x_i - \mu_x|^2}$$

Equation 19 – Equation of covariance

$$\text{cov}(x, y) = \sigma_{xy} = \frac{1}{N} \sum_{i=1}^N (|x_i - \mu_x| |y_i - \mu_y|)$$

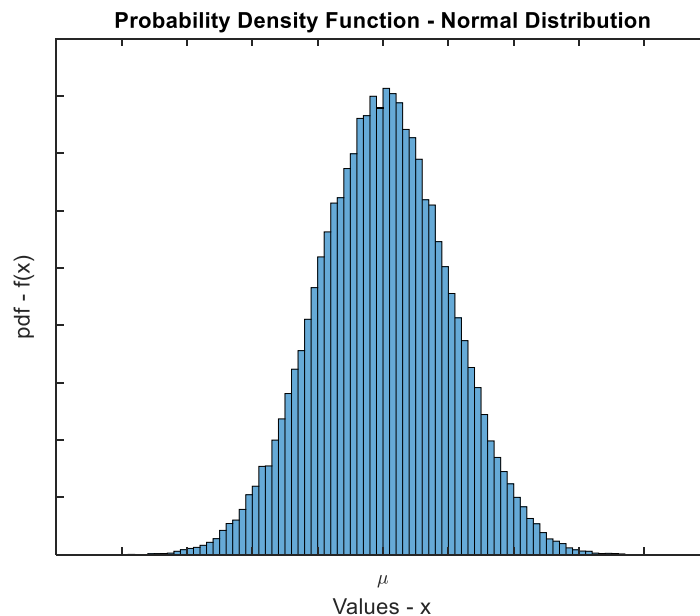


Figure 22 – Probability density function of normal distribution (Author, 2018)

3.4.4 Kalman Filter

First developed by Kalman (1960; 1961), the Kalman filter is a statistical estimation algorithm. Its function is to estimate the states of linear dynamical systems corrupted by Gaussian white noise. In more detail, modelled in a state space, the system state containing Gaussian process noise is estimated based on the initial parameters and measured data with Gaussian noise. The estimation is iterated and updated continuously over time (Narayan, Mahesh, & Andreas, 2013).

The basic concept of the Kalman filter is to estimate optimal solutions $\hat{x}_{t|t}$ between predicted state $\hat{x}_{t|t-1}$ (obtained from initial state $\hat{x}_{t-1|t-1}$) and measurement z_t . All states have a Gaussian PDF (Faragher, 2012). Figure 23 shows the illustration of how the Kalman filter works to estimate a car's position x in the x -axis, while the y -axis is the PDF.

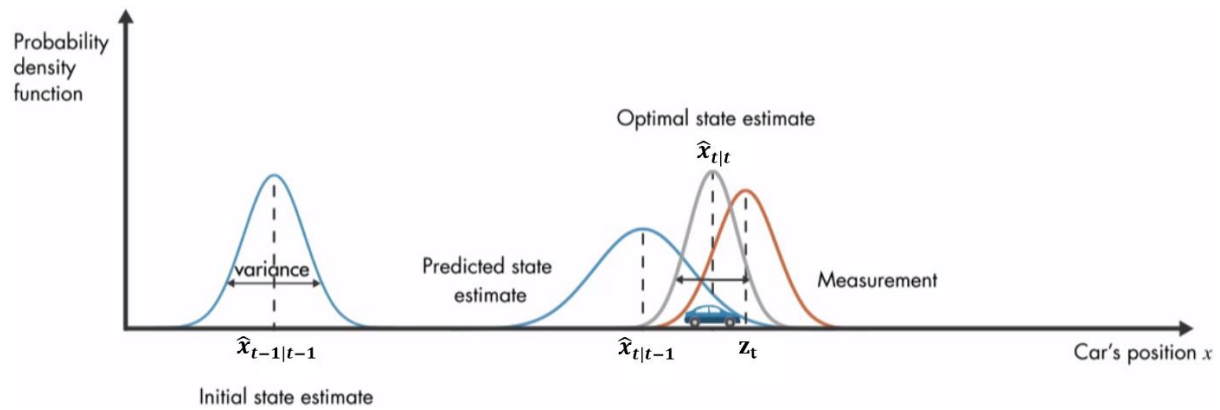


Figure 23 – Illustration of the concept of Kalman filter (Ulusoy, 2017)

In more detail, assume a state space model given by Equation 20.

Equation 20 – State space model

$$x_t = F_t x_{t-1} + G_t u_t + v_t$$

where x_t is the n state vector of the linear dynamical system at time t ; u_t is the m state vector of the inputs of the system; where $m \leq n$; F_t is the $n \times n$ state transition matrix corresponding to x_{t-1} ; G_t is the $n \times m$ state transition matrix corresponding to u_t ; v_t is the n state vector of Gaussian random process noise with zero mean and covariance matrix Q_t : $v_t \sim N(0, Q_t)$. Moreover, also consider measurements of the system as defined by Equation 21.

Equation 21 – Measurement model

$$z_t = H_t x_t + w_t$$

where z_t is the p state vector of the measurements (or outputs) of the system; H_t is the $p \times n$ state transition measurement matrix; where $p \leq n$; w_t is the n state vector of Gaussian measurement noise with zero mean and covariance matrix R_t : $w_t \sim N(0, R_t)$.

To estimate the system state, there are several stages that must be undertaken, i.e. prediction and estimate update. In the prediction stage, two equations are employed, as defined in Equation 22.

Equation 22 – Prediction equations

$$\begin{aligned}\hat{x}_{t|t-1} &= F_t \hat{x}_{t-1|t-1} + G_t u_t \\ P_{t|t-1} &= F_t P_{t-1|t-1} F_t^T + Q_t\end{aligned}$$

where $\hat{x}_{t|t-1}$ is the state estimate at time t based on collected data until time $t - 1$; $\hat{x}_{t-1|t-1}$ is the state estimate at time $t - 1$ based on collected data until time $t - 1$; $P_{t|t-1}$ is the error covariance matrix at time t based on collected data until time $t - 1$; $P_{t-1|t-1}$ is the error covariance matrix at time $t - 1$ based on collected data until time $t - 1$; F_t^T is the transpose of the matrix F_t ; Q_t is the covariance matrix of v_t at time t .

Subsequently, after both $\hat{x}_{t|t-1}$ and $P_{t|t-1}$ have been obtained, in the estimate update, the following equations are solved:

Equation 23 – Estimate update equations

$$\begin{aligned}S_t &= H_t P_{t|t-1} H_t^T + R_t \\ K_t &= P_{t|t-1} H_t^T S_t^{-1} \\ \hat{x}_{t|t} &= \hat{x}_{t|t-1} + K_t (Z_t - H_t \hat{x}_{t|t-1}) \\ P_{t|t} &= (I - K_t H_t) P_{t|t-1} = P_{t|t-1} - K_t H_t P_{t|t-1}\end{aligned}$$

where R_t is the covariance matrix of the vector w_t at time t ; K_t is the Kalman gain at time t ; $\hat{x}_{t|t}$ is the state estimate at time t based on collected data until time t ; $P_{t|t}$ is the error covariance matrix at time t based on collected data until time t ; I is an identity matrix.

In executing the above equations, keep in mind that the epoch from prediction to estimate update is conducted at every time t ($t = 1, 2, \dots, T$) where at the first time, the initial conditions for $\hat{x}_{t-1|t-1}$ and $P_{t-1|t-1}$ are adjusted to $t = 0$. After one performs one epoch, the time is updated to $t = t + 1$, moreover the previous $\hat{x}_{t|t}$ and $P_{t|t}$ are used for the next $\hat{x}_{t-1|t-1}$ and $P_{t-1|t-1}$. See Figure 24 for an illustration of this process.

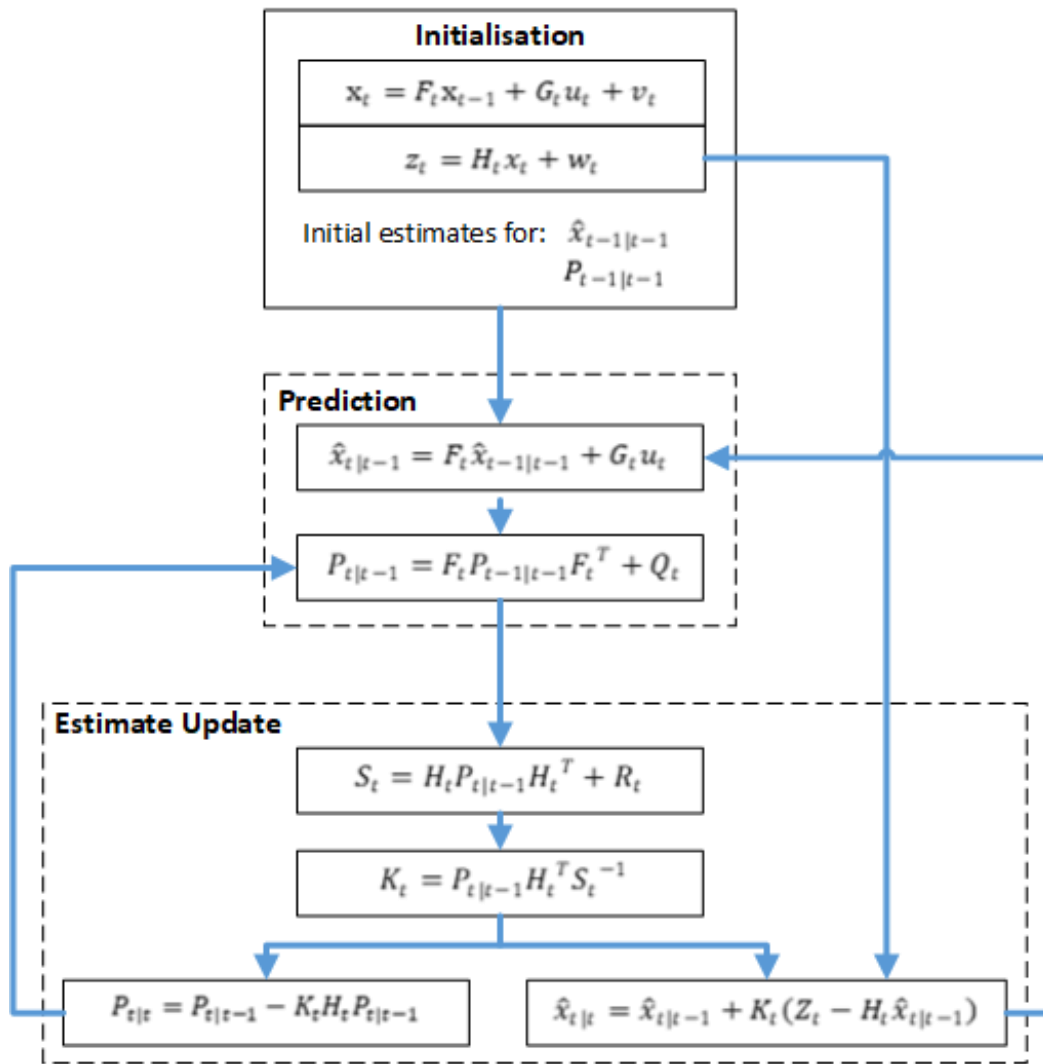


Figure 24 – Recursive procedures of Kalman filter (Author, 2018)

4 Proposed Controller Design of Metro ATO

In order to realise an ATO system, a control design is required. In this chapter, the train dynamics model is defined as a system to be used by the controller. Afterwards, the functions of the controller, mainly consisting of PD control and Fuzzy gain scheduling, are illustrated in detail so as to design an ATO system subject to the factors assigned in Chapter 1. Furthermore, measurement errors and their suppression are described as well. Finally, analysis and discussion of the methodology are presented.

4.1 Train Modelling

Train modelling in this thesis is derived from Newton's second law $F = ma$, where F , m and a respectively are the applied net force in Newtons, the object's mass in kilograms and the object's acceleration in metres per second squared. In a train, the total force applied, F , is the sum of many entities, namely traction force, braking force, gradient resistance, running resistance, curvature resistance and tunnel resistance.²⁵ The forces can be seen in Equation 24 in time-independent form.

Equation 24 – Time-independent train modelling

$$ma(t) = k_t F(v(t)) - k_b B(v(t)) - R_G(s) - R_R(v) - R_C(s) - R_T(s, v)$$

Due to the fact that normally any resistance data are saved digitally and depending on the position value (e.g. for every 1 metre), it is more convenient to apply train modelling in distance-independent form. Therefore, as denoted by Howlett and Pudney (1995), $a = v \frac{dv}{ds}$ as shown in Equation 25, and such modelling can be written as shown in Equation 26.

Equation 25 – Transformations of derivative of speed

$$\frac{dv}{ds} = \frac{dv}{ds} \cdot \frac{dt}{dt} = \frac{dv}{dt} \cdot \frac{dt}{ds} = a \cdot \frac{1}{v}$$

Therefore, in this thesis, Equation 26 is used to model the train.

Equation 26 – Distance-independent train modelling

$$m \cdot v(s) \cdot \frac{dv}{ds} = k_t F(v(t)) - k_b B(v(t)) - R_G(s) - R_R(v) - R_C(s) - R_T(s, v)$$

where m is the total train mass (kg); $a(\cdot)$ is acceleration (m/s^2); $v(\cdot)$ is speed (m/s); k_t is control signal of the relative tractive effort; $F(\cdot)$ is maximum available tractive effort (N); k_b

²⁵ As curvature resistance provides minor values (Rochard & Schmid, 2000) and most DLR tracks are open, one can neglect the curve and tunnel resistance parameters and employ the other parameters only.

is control signal of relative braking force; $B(\cdot)$ is maximum available braking force (N); $R_G(\cdot)$ is gradient resistance (N); $R_R(\cdot)$ is running resistance (N); $R_C(\cdot)$ is curvature resistance (N); $R_T(\cdot)$ is tunnel resistance (N).

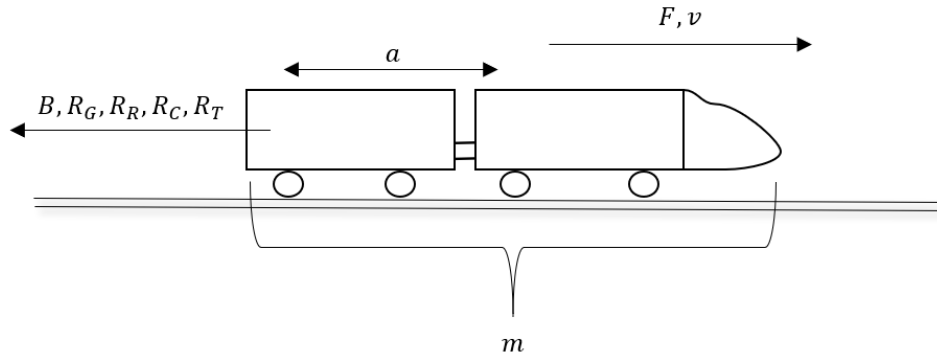


Figure 25 – Train modelling (Author, 2017)

Figure 25 illustrates the modelling of a train with mass m where the train travels from left hand side to right hand side of the figure. Tractive effort F and speed v have the same direction as that in which it runs; therefore, they give a forward movement to it. On the other hand, braking force B and all resistances, i.e. R_G , R_R , R_C and R_T , have the opposite direction so that they give a backward movement to it. Besides, the value of acceleration a has both directions or, in other words, could be positive, i.e. having a forward direction, or negative, i.e. having a backward direction. When it has a negative value, this refers to deceleration which leads the train to reduce its speed. From the standstill position, to make the train have forward motion, the value of the traction force F must exceed all backward forces.

4.1.1 Calculating Speed and Time Values

Subsequently, considering that the train model depends on the distance, i.e. the distance value is known, but the time value is unknown, and to calculate the actual speed at each metre without the time value, one could use Equation 27.

Equation 27 – Speed equation without predefined time value

$$2a(s) \cdot \Delta s = v(s+1)^2 - v(s)^2 \text{ or } v(s+1) = \sqrt{v(s)^2 + 2a(s) \cdot \Delta s}$$

Then, to find time values, by employing the derivative of speed $\frac{dv}{dt} = a$, one could find $dt = \frac{dv}{a}$ which can be written in discrete functions as shown in:

Equation 28 – Difference of time

$$\Delta t = \frac{\Delta v}{a(s)} = \frac{v(s+1) - v(s)}{a(s)}$$

The values of the time difference are calculated using Equation 28 and the total running time is also computed in discrete functions using Equation 29.

Equation 29 – Total running time

$$T(s) = \sum_{i=0}^s \Delta t(i)$$

$\Delta t(\cdot)$ is the time difference in seconds at every one metre displacement; Δs is the distance difference constant with a value of 1 metre; $v(\cdot)$ is the train actual speed at a certain distance s ; $a(\cdot)$ is the acceleration at a specified distance s ; $T(\cdot)$ is total running time from the beginning of the train starting to move, $i = 0$, until specified distance s .

4.1.2 Traction and Braking

There are two main forces applied to train modelling, i.e. the traction force and braking force. Traction force or tractive effort causes the train to move forward. Therefore, this force has a positive value. On the other hand, braking force generates backward movement on the train so that it has a negative value, as shown in Equation 24. Moreover, it is assumed that the train does not apply traction and braking force at the same time, therefore Equation 30 states:

Equation 30 – Relation between traction and braking forces and its values

$$k_t \cdot k_b = 0$$

$$k_t \in [0,1]$$

$$k_b \in [0,1]$$

4.1.3 Resistances

This study ignores curvature and tunnel resistances as these values are insignificant. Accordingly, the resistances consist of gradient and running resistances only.

- The First Resistance R_G

Gradient resistance arises when the train tracks have any height difference, whether it is climbing or a descending, over a certain distance. Otherwise, this resistance is zero. Therefore, a steep slope produces more resistance than a gradual slope. Equation 31 shows the expression for gradient resistance.

Equation 31 – Definition of gradient resistance

$$R_G(s) = mg \sin \theta(s)$$

g is the gravitational acceleration constant, i.e. 9.81 m/s^2 ; θ is the slope angle, as shown in Figure 26.

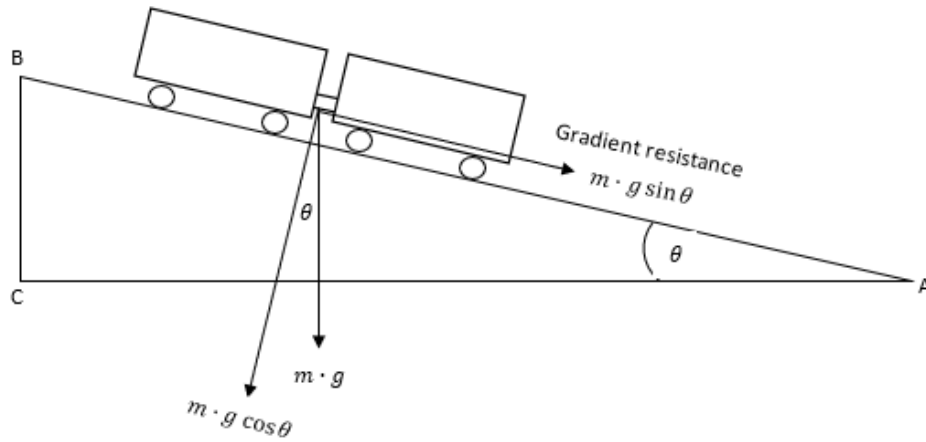


Figure 26 – Gradient resistance (Author, 2017)

Since gradient resistance utilises the sine function, instead of defining the value of θ and then calculating $\sin \theta$, it can also be defined as a height change over a certain distance. For example, according to Figure 26, there is a height change of CB along distance AB . Thus, $\sin \theta$ can be described as $\frac{CB}{AB}$ (Rochard & Schmid, 2000).

- The Second Resistance R_R

Running resistance comprises three components, i.e. the coefficient for mass-dependent resistance A in Newtons, the coefficient for rolling stock resistance B in Ns/m and the coefficient for aerodynamic resistance C in Ns^2/m^2 . Equation 32 expresses the resulting relationship. This type of resistance is determined only by experimental observation.

Equation 32 – Definition of running resistance

$$R_R(v) = A + Bv(s) + Cv(s)^2$$

Since R_R mainly depends on speed v , whether it is first order or second order, running resistance will increase with respect to speed. Figure 27 shows that when the train speed is relatively low, i.e. approximately less than 4 m/s , the running resistance in total (solid line) produces nearly the same value as only applying the A coefficient (dotted line), whereas it gives a much higher resistive force when the speed increases. Bv (dash-dot line) and Cv^2 (dashed line) in fact provide a significant incline.

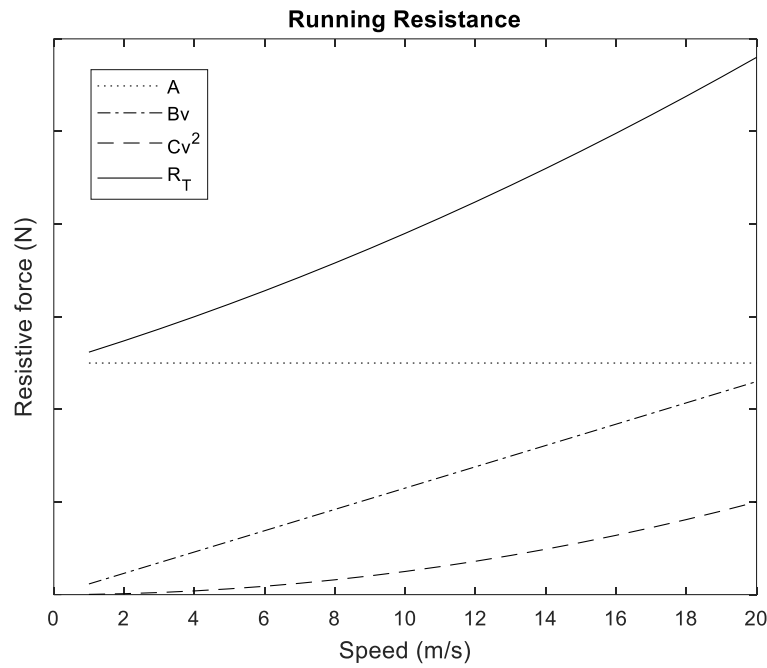


Figure 27 – Running resistance behaviour (Author, 2017)

4.1.4 Train Parameter Descriptions

Tractive effort and braking force are defined in Equation 33 and Equation 34 (Su et al., 2016).

Equation 33 – The definition of tractive effort

$$F(v) = \begin{cases} 310,000 \text{ N}; & v \leq 10 \text{ m/s} \\ 310,000 - 10,000(v - 10) \text{ N}; & 10 < v \leq 22.2 \text{ m/s} \end{cases}$$

Equation 34 – The definition of braking force

$$B(v) = \begin{cases} 260,000 \text{ N}; & v \leq 15 \text{ m/s} \\ 260,000 - 18,000(v - 15) \text{ N}; & v > 15 \text{ m/s} \end{cases}$$

4.2 Control Design

The ATO controller used in this thesis is designed in this subchapter. The main controller is PD control with an initial tuning method executed by relay-based auto-tuning, as defined in 3.4.1. Therefore, before employing PD control, a relay-based controller is performed to find appropriate values for K_u and P_u . Subsequently, immediately after both parameters and the three parameters for PID, i.e. K_p , T_i and T_d , have been acquired, the controller will shift automatically to PD control. Furthermore, Fuzzy gain scheduling also assists in renewing those three parameters to adapt to the system behaviours.

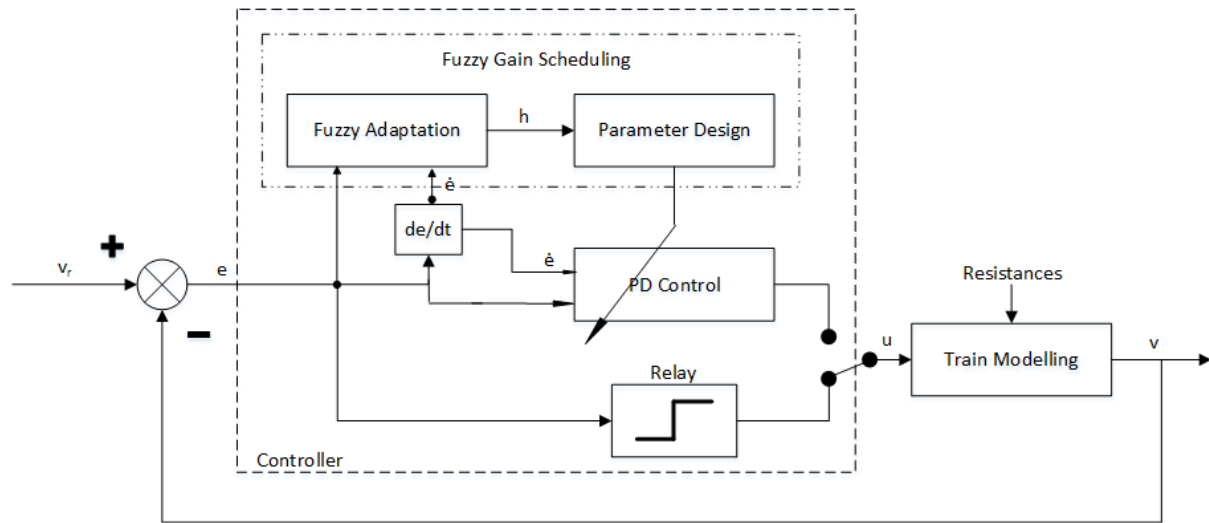


Figure 28 – Block diagram of train modelling and the controllers (Author, 2017)

Figure 28 illustrates a block diagram of the entire controller with the train system. v_r is speed reference which is assumed as the optimised train trajectory. v is actual speed obtained directly from the output of the system. e is the error value which is the difference between the speed reference v_r and the actual speed v ; a positive value of error means v is lower than v_r , and vice versa; whereas a zero value occurs when both have the same value. h is a Fuzzy control signal generated by the Fuzzy scheme used to modify the PD parameters. u is the main control signal used by the system to supply traction or braking forces.

4.2.1 PID Control

In applying PID control to train dynamics modelling, the author implements a discrete time PID control function, as shown in Equation 35, which is equivalent to the continuous form in Equation 2.

Equation 35 – Discrete-time PID control

$$u(t) = K_p \{e(t) + \frac{1}{T_i} \sum_{i=0}^t (e(i) \cdot \Delta t) + T_d \frac{(e(t) - e(t-1))}{\Delta t}\}$$

However, since both k_t and k_b are constrained, and the braking force k_b has a negative value, implicitly, one could define that the control signal only has values between 1 (full traction) and -1 (full braking). This means that there is actuator saturation. Moreover, as explained in 3.4.1, the “I” element in PID control is the culprit for the controller windup because, as the nature of an integral accumulates all values, making it larger, it gives a value of the control signal greater than the actuator capability, i.e. saturation occurs. Thus, in this study, instead

of using a PID controller, the author employs PD control only, to avoid any controller windup. Then, Equation 35 is replaced by Equation 36.

Equation 36 – Discrete-time PD control

$$u(t) = K_p\{e(t) + T_d \frac{(e(t) - e(t-1))}{\Delta t}\}$$

Then, according to subchapter 4.1.1, that states that it is distance difference which is set to constant, Equation 36 is replaced by Equation 37.

Equation 37 – Distance constant based discrete-time PD control

$$u(s) = K_p\{e(s) + T_d \frac{(e(s+1) - e(s))}{\Delta t(s+1)}\}$$

Subsequently, as discussed earlier, relay feedback is employed to auto-tune the PD parameters at the beginning. Here, one could determine the parameters for such an auto-tuning method as introduced in 3.4.1. First of all, based on Equation 4 and using the values from Equation 30, relay output amplitude d is determined by Equation 38.

Equation 38 – The output value of relay

$$d = \begin{cases} 1; & e > 0 \\ -1; & e < 0 \end{cases}$$

By using the values of d and directly measuring a , i.e. the amplitude of the system output, then, based on Equation 5, the ultimate gain K_u can be calculated. Moreover, one could easily find the ultimate period T_u also. Finally, by exploiting both K_u and T_u , the Ziegler-Nichols PID tuning rules in Equation 3 can be implemented automatically.

4.2.2 Fuzzy Gain Scheduling

After the PD controller has been designed along with the relay-based auto-tuning, Fuzzy gain scheduling is formulated in this section. As described in 3.4.2, it is employed to create a PID-based adaptive controller able to manipulate on-line the controller parameters at every time instance subject to the system output's conditions. Here, to adjust K_p , T_i and T_d of the PID controller, as denoted in Figure 29, the Fuzzy approach comprises of two components: Fuzzy adaptation and parameter design (He et al., 1993). The former acts as the Fuzzy logic controller inputting error e and delta error \dot{e} and outputting the h parameter, where the three are in crisp value form, to be used by the next stage. Outputting K_p , T_i and T_d , the latter component includes the α equation, which utilises the h parameter, and converts α to the three PID parameters. By employing a single parameter only from the Fuzzy core, i.e. h

converted to α , it is more meaningful and convenient to combine human experience, i.e. Fuzzy logic, and controller mathematics, i.e. PD controller and relay-based auto-tuning, since α is formulated based on the Ziegler-Nichols rules so the higher the value of α is, the higher and the lower the proportional and derivative element of PD are, respectively, and vice versa. Thus, specifically, Fuzzy gain scheduling can promote PD control to both accelerate the system output v to meet the desired value v_r and decelerate any overshoot and undershoot.

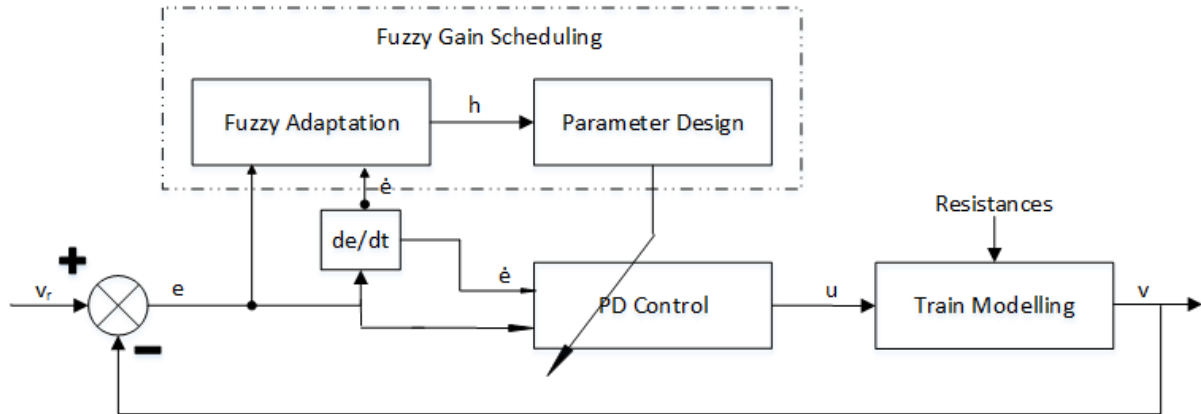


Figure 29 – Block diagram of proposed Fuzzy gain scheduling (Author, 2018)

- Fuzzy Adaptation

As the core of Fuzzy gain scheduling, Fuzzy adaptation performs the function of Fuzzy logic. Its two inputs e and \dot{e} are mapped into Fuzzy sets E and R , respectively, while the aggregated Fuzzy output is H which is then defuzzified into crisp values of h . Figure 30 shows that Fuzzy adaptation implements the Mamdani method with two Fuzzy inputs (E and R) having seven MFs, one output H having five MFs, and 49 rules.

In the fuzzification process, the crisp values of inputs e and \dot{e} are mapped using seven MF-based Fuzzy sets, as characterised by Equation 39. N and P in the first letter of each Fuzzy set indicating “negative” and “positive”, respectively, whereas L , M and S in the second letter mean “large”, “medium” and “small”, respectively. ZE denotes “zero”. Nonetheless, to provide simpler notations, each Fuzzy set of E and R is defined based on integers where $NL = -3$, $NM = -2$, and so forth, as denoted in Equation 39.

Equation 39 – Fuzzy sets of E and R

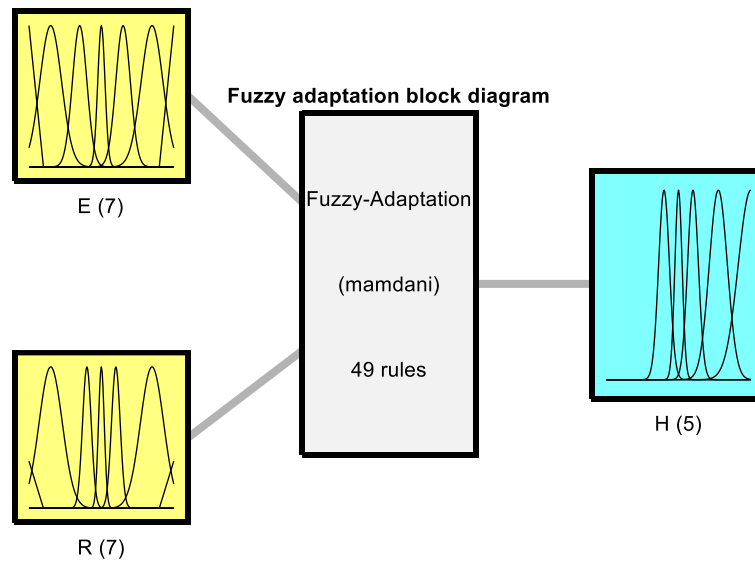
$$E = \{NL, NM, NS, ZE, PS, PM, PL\} = \{-3, -2, -1, 0, 1, 2, 3\}$$

$$R = \{NL, NM, NS, ZE, PS, PM, PL\} = \{-3, -2, -1, 0, 1, 2, 3\}$$

Subsequently, for Fuzzy output H , the author determines five MF-based Fuzzy sets, as formulated in Equation 40. The naming of each Fuzzy set and the usage of integers for notation are carried out in the same way as for the Fuzzy inputs.

Equation 40 – Fuzzy sets of H

$$H = \{NS, ZE, PS, PM, PL\} = \{-1, 0, 1, 2, 3\}$$



System Fuzzy-Adaptation: 2 inputs, 1 outputs, 49 rules

Figure 30 – Block diagram of Fuzzy adaptation (Author, 2017)

MFs of Fuzzy input E are shown in Figure 31. Fuzzy sets -3 and 3 utilise trapezoidal MFs, while the rest use Gaussian MFs. Based on Equation 12 and Equation 13, one could fuzzify the crisp input e into Fuzzy input E using the parameters in Equation 41 of each Fuzzy set:

Equation 41 – Parameters of Fuzzy input E MFs

$$(-3|a, b, c, d) = -25, -25, -1, -0.8$$

$$(-2|\sigma, c) = 0.15, -0.7$$

$$(-1|\sigma, c) = 0.1, -0.3$$

$$(0|\sigma, c) = 0.05, 0$$

$$(1|\sigma, c) = 0.1, 0.3$$

$$(2|\sigma, c) = 0.15, 0.7$$

$$(3|a, b, c, d) = 0.8, 1, 25, 25$$

MFs of Fuzzy input R are shown in Figure 32. All apply the same MF type as the Fuzzy input E . Based on Equation 12 and Equation 13, one could fuzzify the crisp input \dot{e} into Fuzzy input R using the parameters in Equation 42 of each Fuzzy set:

Equation 42 – Parameters of Fuzzy input R MFs

$$(-3|a, b, c, d) = -10, -10, -0.7, -0.4$$

$$(-2|\sigma, c) = 0.08, -0.35$$

$$(-1|\sigma, c) = 0.03, -0.1$$

$$(0|\sigma, c) = 0.02, 0$$

$$(1|\sigma, c) = 0.03, 0.1$$

$$(2|\sigma, c) = 0.08, 0.35$$

$$(3|a, b, c, d) = 0.4, 0.7, 10, 10$$

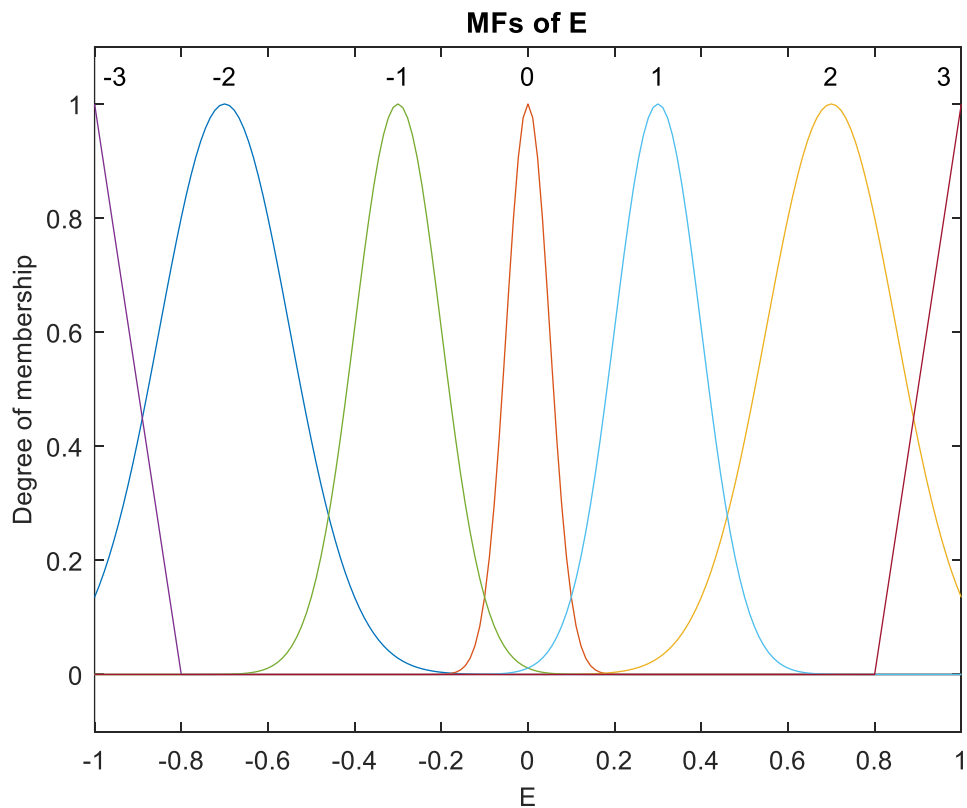


Figure 31 – Membership function of error (Author, 2017)

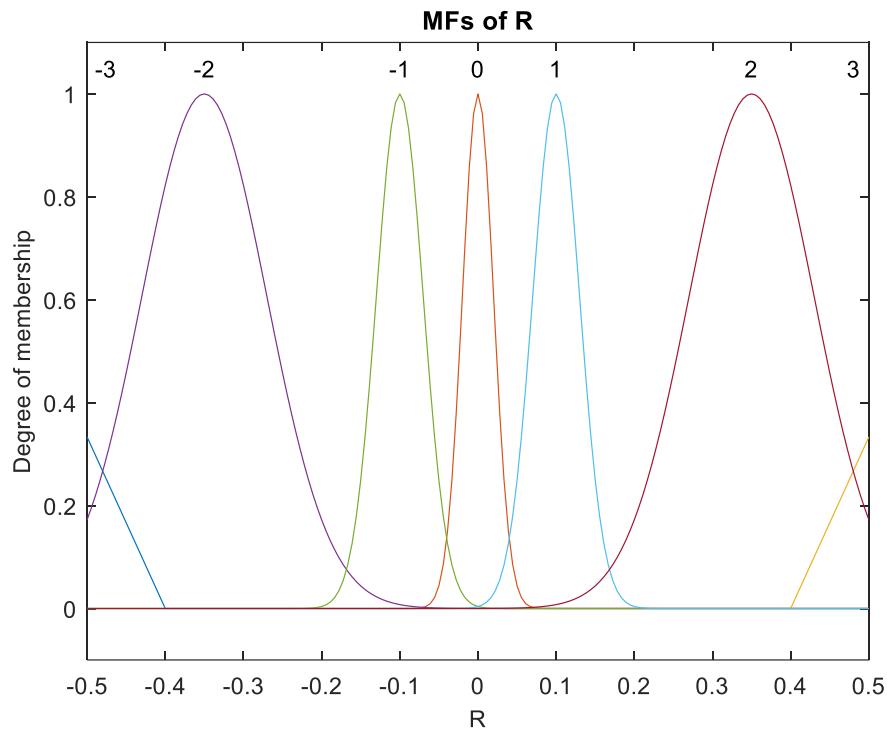


Figure 32 – Membership function of delta error (Author, 2017)

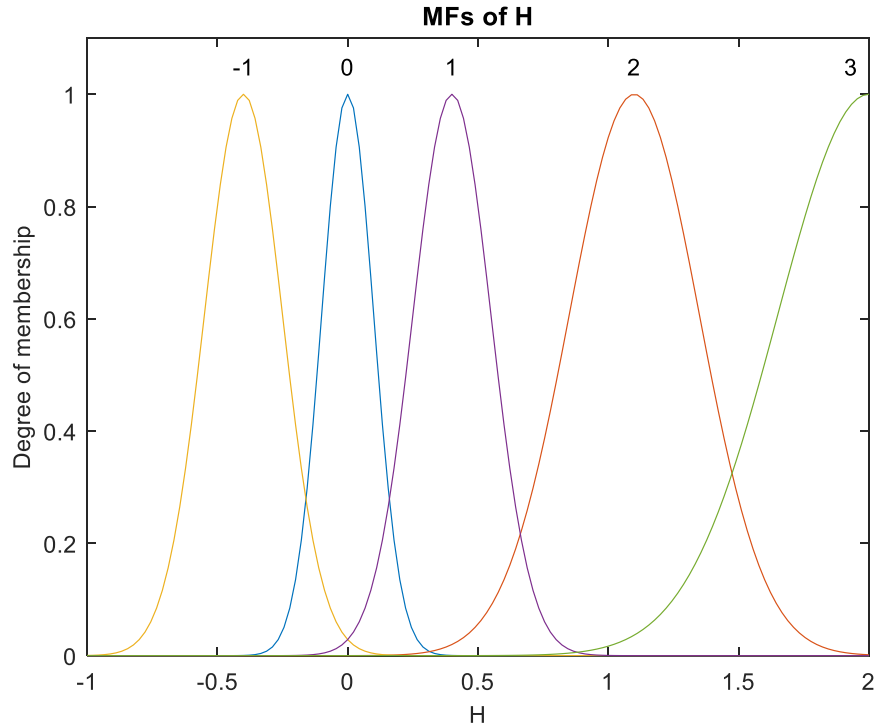


Figure 33 – Membership function of h (Author, 2017)

MFs of Fuzzy output H is shown in Figure 33. All employ Gaussian MFs. Then, based on Equation 13, Fuzzy output H is defined using the parameters in Equation 43 of each Fuzzy set:

Equation 43 – Parameters of Fuzzy output H MFs

$$(-1|\sigma, c) = 0.15, -0.4$$

$$(0|\sigma, c) = 0.1, 0$$

$$(1|\sigma, c) = 0.15, 0.4$$

$$(2|\sigma, c) = 0.25, 1.1$$

$$(3|\sigma, c) = 0.35, 2$$

Before executing the inference, one could use the Fuzzy rules connecting two Fuzzy inputs and Fuzzy output as stated in Table 1. The way to read such rules is, for example *IF E is – 3 AND R is 3 THEN H is 0*, and so on and so forth.

Table 1 – Rule Base of Fuzzy adaptation

| | | H (output) | | | | | | |
|---------------------------|----|---------------------------|----|----|---|---|---|---|
| | | R (2 nd input) | | | | | | |
| | | -3 | -2 | -1 | 0 | 1 | 2 | 3 |
| E (1 st input) | -3 | 3 | 3 | 3 | 3 | 2 | 1 | 1 |
| | -2 | 3 | 2 | 2 | 1 | 1 | 1 | 1 |
| | -1 | 2 | 1 | 1 | 0 | 1 | 1 | 2 |
| | 0 | 2 | 0 | 0 | 0 | 0 | 1 | 2 |
| | 1 | 1 | 1 | -1 | 0 | 1 | 1 | 1 |
| | 2 | 1 | 2 | 1 | 1 | 1 | 2 | 3 |
| | 3 | 1 | 2 | 1 | 2 | 2 | 3 | 3 |

In the inference engine, which is the standard Mamdani inference method, the methods of implication and aggregation implemented are *min* (intersection) and *max* (union) operations, as defined in Equation 9 and Equation 8, respectively. After executing the inference engine and obtaining the aggregated Fuzzy output, to produce the crisp value h , the author applies the centroid method for defuzzification, as formulated in Equation 15 (upper equation).

- Parameterisation Design

The second component of the proposed Fuzzy gain scheduling is parameter design. Here, the crisp value h from Fuzzy adaptation is employed to produce the α parameter for directly controlling the PD parameters. Equation 44 describes the $\alpha(s + 1)$ parameter which has two definitions, i.e. at $\alpha(s) > 0.5$ and $\alpha(s) \leq 0.5$, where $\alpha(s)$ denotes the α parameter at specified distance s , $h(s)$ is the crisp value h from the Fuzzy stage at specified distance s and

γ is a positive constant within the interval [0.2, 0.6] implemented to adjust the convergence rate of the α formula. At distance $s = 0$, $\alpha(0)$ is set to 0.5. By employing Equation 44, it is assured that the α parameter is constrained between 0 and 1 and generates smooth adjustment for the PD control.

Equation 44 – Definition of alpha

$$\alpha(s + 1) = \begin{cases} \alpha(s) + \gamma h(s) \cdot (1 - \alpha(s)); & \alpha(s) > 0.5 \\ \alpha(s) + \gamma h(s) \alpha(s); & \alpha(s) \leq 0.5 \end{cases}$$

For each $\alpha(s)$, one could regulate K_p , T_i and T_d as shown in Equation 45. Although the main controller used is PD control, T_i is still needed since, to obtain T_d , one has to find T_i in advance. Such equations are initially derived from the Ziegler-Nichols rules, as shown in Equation 3, when $\alpha(0)$ set to 0.5.

Equation 45 – Relation among PID parameters, alpha and ultimate gain and period

$$\begin{aligned} K_p &= 1.2\alpha K_u \\ T_i &= 0.75P_u \cdot \frac{1}{1 + \alpha} \\ T_d &= 0.25T_i \end{aligned}$$

4.3 Noise Insertion and Improving the Controller

In this subchapter, Gaussian white noise, approximating the actual device measurement errors, is introduced into the system. Furthermore, due to its nature, which is to reduce the accuracy of the results, the controller has to be enhanced to counter the resulting defective speed profile, as explained in 3.4.3. Kalman filter design is presented for assisting the controller, as based on 3.4.4.

4.3.1 Introduction to Measurement Errors

In order to generate a 5% Gaussian white noise, based on Equation 16, Equation 17 and Equation 18, a normal distribution having a mean of 0 and a standard deviation of 0.015 is applied, and the random variable of such the distribution is multiplied by the actual speed to produce a noisy speed. As denoted in Figure 34, the centre of the PDF (when the noise is zero) is assumed as 100%; a negative value of noise represents the percentage of less than 100%, and vice versa. For example, the noise of -0.02 denotes $(100 - 0.02)\%$, and that of 0.03 indicates $(100 + 0.03)\%$. This means that the closer to the mean the noise is, the higher the PDF is and the smaller the noise is, and vice versa.

As shown in Figure 35, measurement errors are attached to the actual speed v_{actual} resulting in a noisy speed v_{noise} which is fed into v_r and generates errors. Unlike the system without measurement errors, as shown in Figure 28 which has v_{actual} as the output of the block diagram, Figure 35 shows that the output is obtained from v_{noise} . This certainly creates undoubtedly noisy and unstable error values able to produce catastrophic errors in the entire system. Since it is not feasible to gain the actual speed from v_{noise} directly, an improvement for the controller is required.

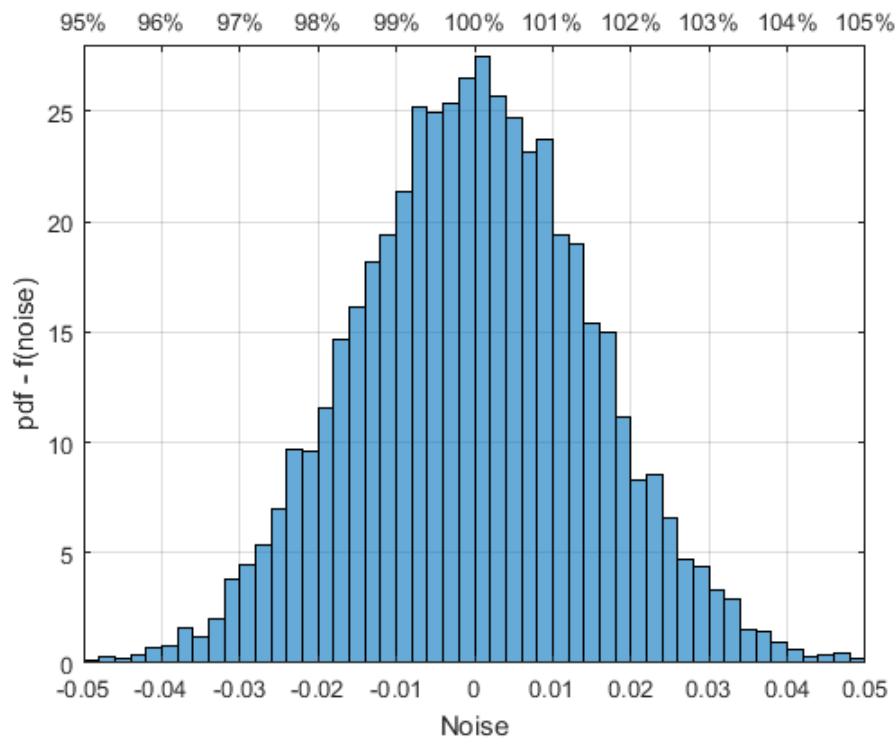


Figure 34 - Probability density function of measurement noise with mean 0 and standard deviation 0.015 (Author, 2018)

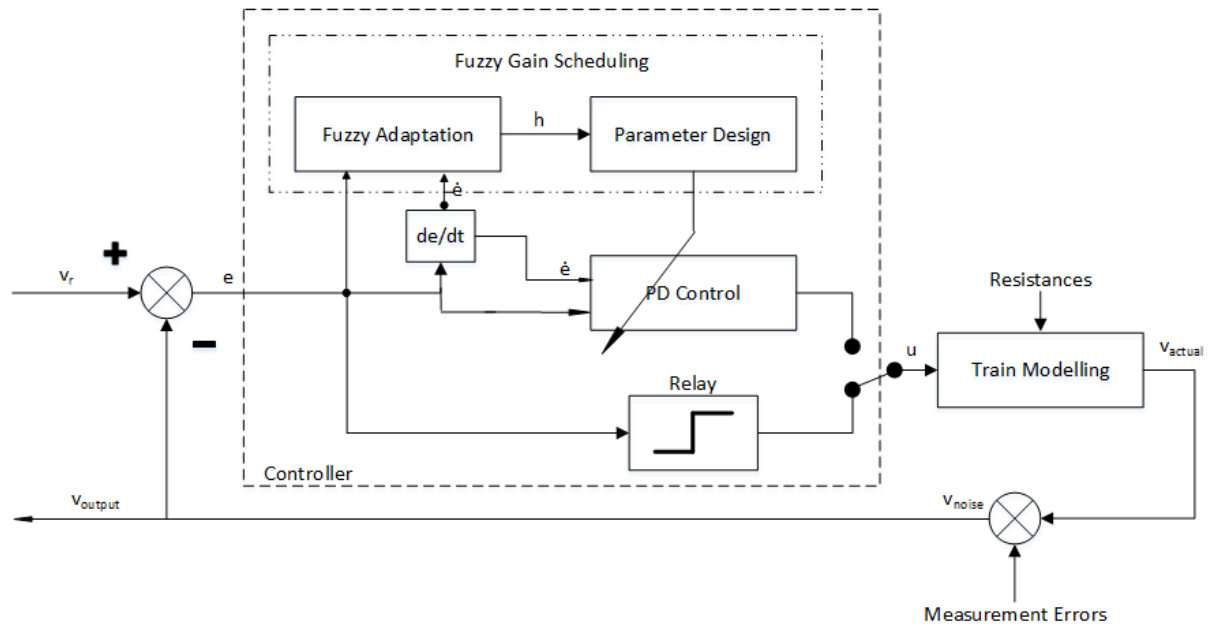


Figure 35 – Block diagram of train modelling, controller and measurement errors (Author, 2017)

4.3.2 Implementing the Kalman Filter

To attenuate the applied measurement noise, the author implements a Kalman filter. Its theory is described in 3.4.4. In the proposed ATO control and train system, for the inputs, the Kalman filter is connected to the error e between v_r and v_{output} and to the output of the addition of the measurement errors, i.e. v_{noise} , whereas its output, after being multiplied by -1 , is fed into the sum, as denoted in Figure 36. Both inputs form the input for $G_t u_t$, considering the controllers and the train model as an entire system, and that for measurements z_t , respectively, as defined in Equation 20 and Equation 21.

Another type of train model, equivalent to Equation 26, is defined in Equation 46 below by considering the model in the distance-independent form, as characterised in 4.1.

Equation 46 – Train speed modelling

$$\dot{x}_s = \dot{x}_{s-1} + \ddot{x}_s \cdot \Delta t_s + v_{s,1}$$

$$\ddot{x}_s = \ddot{x}_{s-1} + v_{s,2}$$

where \dot{x}_s and \dot{x}_{s-1} are the actual speed at specified distances s and $s - 1$, respectively; \ddot{x}_s and \ddot{x}_{s-1} are acceleration at specified distances s and $s - 1$; Δt_s is time at specified distance s ; $v_{s,1}$ and $v_{s,2}$ are Gaussian process noise with zero mean and covariance matrix Q_s .

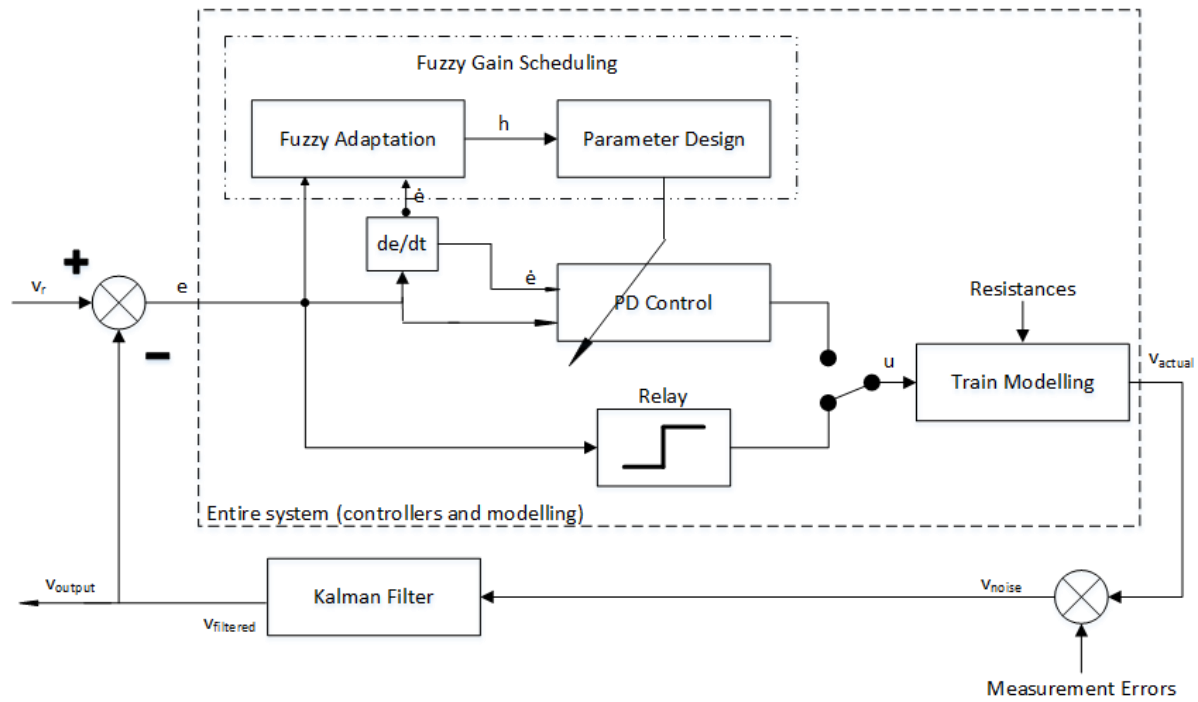


Figure 36 – Block diagram of the entire system with measurement errors and Kalman filter
(Author, 2017)

Afterwards, by considering that e is $G_t u_t$, Equation 46 can be defined in the form of matrix notation as follows:

Equation 47 – Train speed modelling in matrix notation

$$\begin{bmatrix} \dot{x}_s \\ \ddot{x}_s \end{bmatrix} = \begin{bmatrix} 1 & \Delta t_s \\ 0 & 0 \end{bmatrix} \cdot \begin{bmatrix} \dot{x}_{s-1} \\ \ddot{x}_{s-1} \end{bmatrix} + \begin{bmatrix} 1 \\ 0 \end{bmatrix} \cdot [e] + \begin{bmatrix} v_{s,1} \\ v_{s,2} \end{bmatrix}$$

where $x_t = \begin{bmatrix} \dot{x}_s \\ \ddot{x}_s \end{bmatrix}$, i.e. $n = 2$; $F_t = \begin{bmatrix} 1 & \Delta t_s \\ 0 & 0 \end{bmatrix}$ although F_t should be $\begin{bmatrix} 1 & \Delta t_s \\ 0 & 1 \end{bmatrix}$, but considering that it is only speed (excluding acceleration) that is measured and controlled, \ddot{x}_s is employed merely for assisting the Kalman filter calculations since one has to accomplish an $n \times n$ F -matrix, so that one can neglect the acceleration estimate; and $G_t = \begin{bmatrix} 1 \\ 0 \end{bmatrix}$ since it is only one input, i.e. vector $u_t = e$ ($m = 1$), so that it is more convenient to define G_s as a 2-by-1 matrix ($n \times m$).

Subsequently, for the measurement model, based on Equation 21, one could define:

Equation 48 – Measurement model of train speed

$$y_s = \dot{x}_s + w_{s,1}$$

where y_s is the measured speed disrupted by Gaussian measurement errors w_s with zero mean and covariance matrix R_s .

Then, for Equation 48, in the form of matrix notation, one could write:

Equation 49 – Measurement model in matrix notation

$$[y_s] = [1 \quad 0] \cdot \begin{bmatrix} \dot{x}_s \\ \ddot{x}_s \end{bmatrix} + [w_s]$$

where vector $z_t = [y_s]$ $p = 1$; $H_s = [1 \quad 0]$ ($p \times n$), considering that, as explained earlier, it is only speed (excluding acceleration) that is measured and controlled. Therefore, in operating the Kalman filter, especially in Equation 21, one could use v_{noise} directly as z_t .

Before executing Equation 22 and Equation 23 and running the epoch, initial conditions, i.e. $\hat{x}_{t-1|t-1}$ and $P_{t-1|t-1}$ at $t = 0$, and both covariance matrices, i.e. Q_s and R_s , are determined as follows:

Equation 50 – Initial conditions

$$\hat{x}_{0|0} = \begin{bmatrix} \dot{x}_0 \\ \ddot{x}_0 \end{bmatrix} = \begin{bmatrix} 0 \\ 0 \end{bmatrix}$$

$$P_{0|0} = I = \begin{bmatrix} 1 & 0 \\ 0 & 1 \end{bmatrix}$$

Equation 51 – Covariance matrices of process and measurement noise

$$Q = \begin{pmatrix} 10^{-6} & 0 \\ 0 & 10^{-6} \end{pmatrix}$$

$$R = var(noise)$$

4.4 Analysis and Discussion

The methodology of this study has been previously elucidated comprehensively. In this subchapter, the methods are assessed and analysed by utilising a constant speed reference and artificial train trajectory run on the model system. The total distance applied here is 5000 metres (5 km). Subsequently, the results are discussed and compared.

4.4.1 Performance Indices

To analyse and compare the proposed controllers based on control objectives, as interpreted in subchapter 1.2, the author determines the performance indices used to evaluate the controllers. Those are the following:

- $Error < 3\%$

The controllers must be able to track the given trajectories to satisfy a speed tracking error of less than 3%. In the test of constant speed reference in 4.4.2, instead of using 3% tracking

error, it uses a settling time of 3% steady state error. Lower values of settling time indicate better performance.

- $-30\text{ s} \leq \text{total time deviation} \leq +30\text{ s}$

The time difference between the running time of the given trajectory and that of the actual speed profile produced by the controllers must comply a punctuality of no more than 30 seconds early and no greater than 30 seconds late.

- IAE and ISE

The controllers must outperform the conventional controller, i.e. the PID-only controller, in both IAE and ISE performance. Moreover, IAE and ISE are calculated using Equation 52 below where S is the maximum distance. Lower values of both IAE and ISE indicate better performance.

Equation 52 – Equations of IAE and ISE

$$IAE = \int_0^{\infty} |e(t)| dt \sim \sum_{s=0}^S (|e_s| \cdot \Delta t_s)$$

$$ISE = \int_0^{\infty} (e(t))^2 dt \sim \sum_{s=0}^S (e_s^2 \cdot \Delta t_s)$$

4.4.2 Constant Speed Reference

The first type of test performed is by utilising a constant speed reference. This approach functions to assess the system performance with several controllers when running on a step input. As this type of test employs no train trajectory to be followed by the system, the author only considers a 3% steady state error, in which the settling time is used, and IAE and ISE as the controller criteria to be analysed. Such criteria are substantive as they specify the system as consistently following and rapidly reacting to the given train trajectory in strict shapes and constraints, which is the case discussed further in subchapter 4.4.3. Then, to run the system on a step input without any information regarding the track, the resistance applied to train model is merely the running resistance, as illustrated in Figure 37.

1. Testing the System with a Simple Controller

Before implementing more complex controllers in the system, a closed-loop system is designed, as shown in Figure 37, in order to analyse the system behaviour. It is adjusted to be as stable as possible, e.g. eliminating all resistance forces, except running resistance, and any noise, so that one is able to approximate its behaviour as precisely as possible.

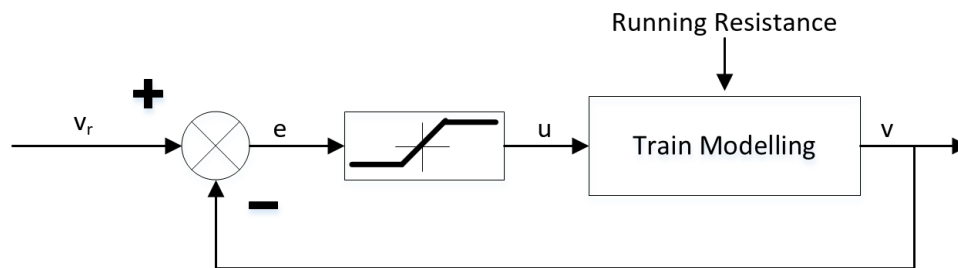


Figure 37 – The system with simple controller (Author, 2017)

Here, the value of the error employed immediately, after being saturated, as the input for the system. Furthermore, as stated in subchapter 4.1.2, the constraint on traction and braking is between 1 and -1 when the value of the error is higher than 1 or lower than -1 . In addition, since the system has two components, i.e. traction and braking, this test is divided into two sections.

a. Traction Force Test

By using a step input of 10, the system runs and approaches the reference. Figure 38 shows the output of the system (solid blue line) which increases towards the reference (black dashed line). One can see that it looks as though it is behaving normally.

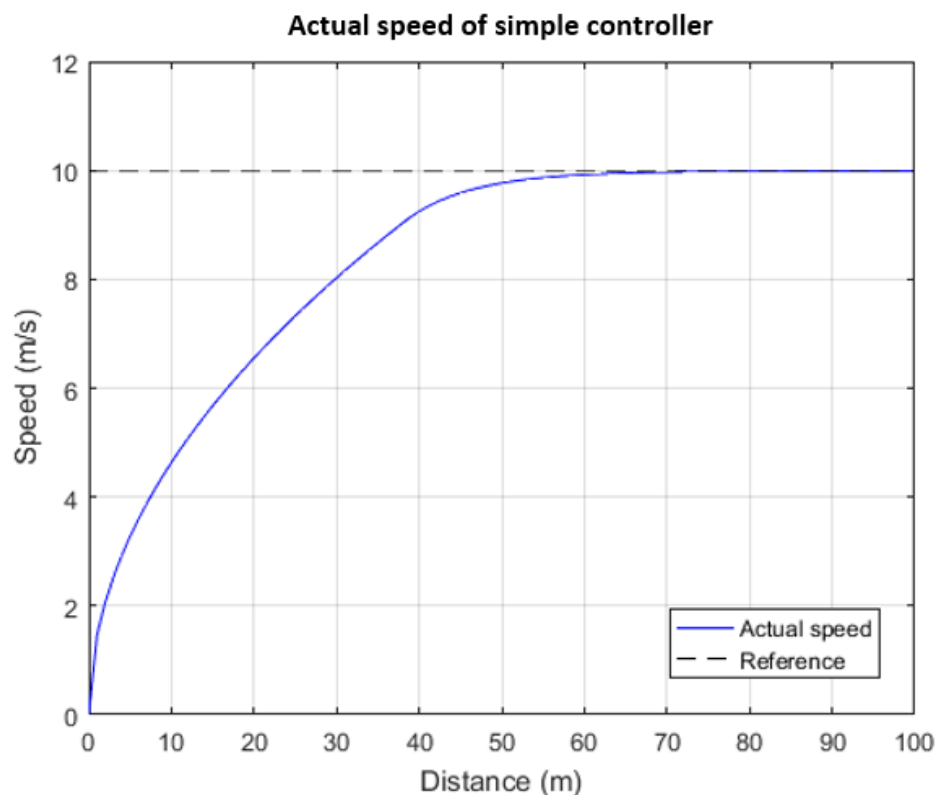


Figure 38 – Actual speed of the system with simple controller (traction part) (Author, 2017)

On the other hand, Figure 39 shows the system output with respect to time so that the settling time value can be measured easily, in this case it is 9.4736 seconds, which represents a 3% steady state error, i.e. 9.7 m/s. Moreover, the IAE and ISE values are 49.7694 and 282.1087, respectively.

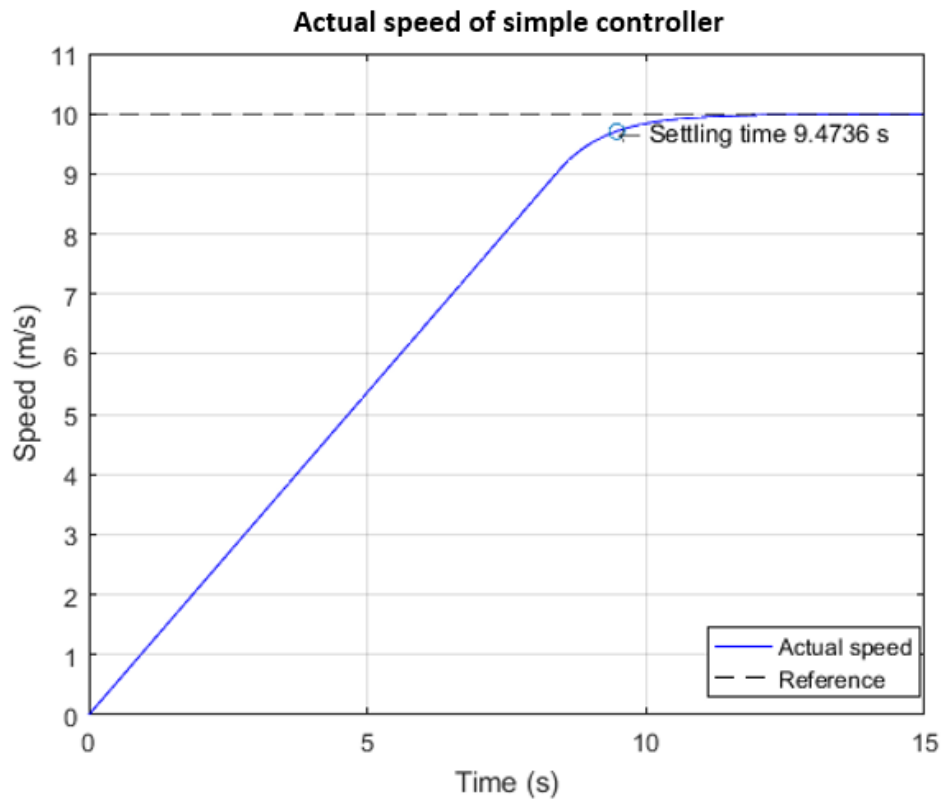


Figure 39 – Actual speed of the system with simple controller with settling time (traction part) (Author, 2018)

b. Braking Force Test

In order to assess the braking performance of the system, first, one could run it in the traction mode, then when it reaches a certain speed, a braking force can be applied to reduce the speed to specific value. Moreover, the approach of applying the braking force to make the train come to a standstill cannot be used to analyse the performance since when the system stops, the settling time cannot be measured anymore. In this braking force test, initially the traction force to achieve a speed of 20 m/s, then braking is carried out at a distance of 350 metres from the origin to decrease the speed to 5 m/s.

This speed reference (black dashed line) can be seen in Figure 40 along with the actual speed (solid blue line). As shown in Figure 41, the first point where there is a 3% steady state error, i.e. 5.15 m/s, for the system with the braking force, takes place at a settling time 46.5549 seconds. Moreover, the IAE and ISE values are 316.8766 and 3649.0045, respectively.

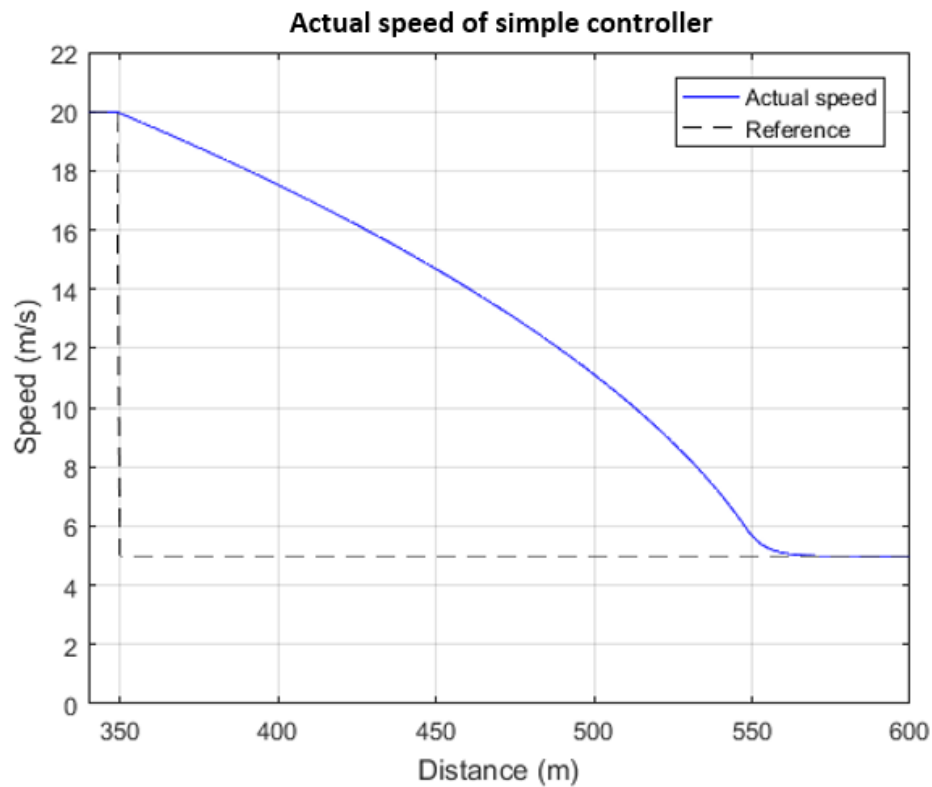


Figure 40 – Actual speed of the system with simple controller (braking part) (Author, 2017)

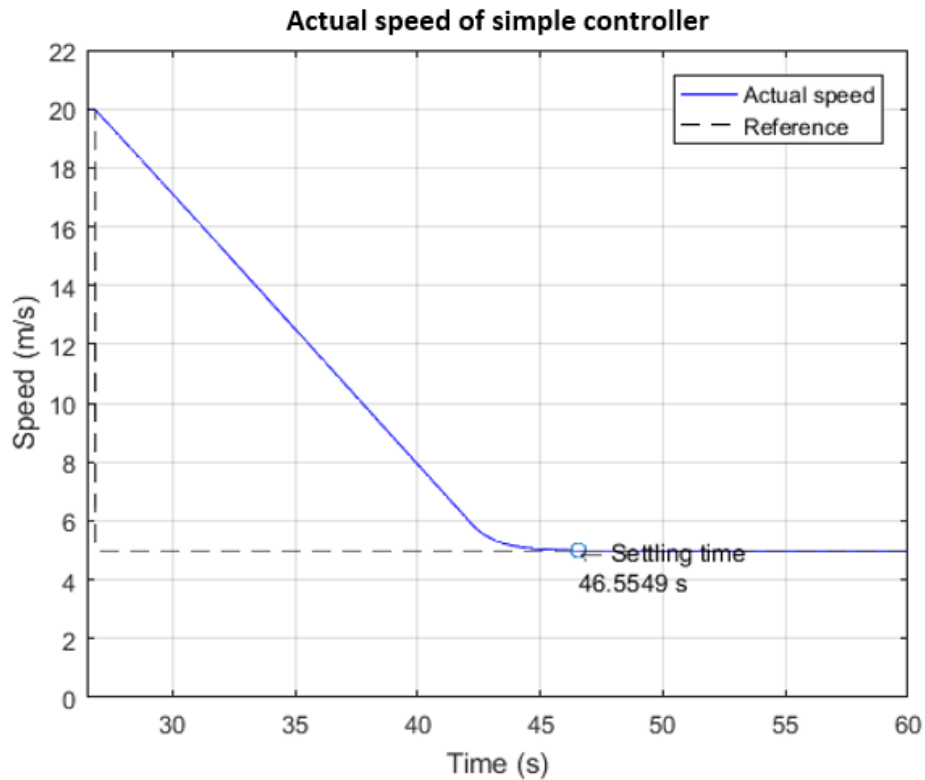


Figure 41 – Actual speed of the system with simple controller with settling times (braking part) (Author, 2017)

2. Assessing Auto-tuning Parameters for PID Controller

The step inputs used in this test are the same as those used for testing the system with a simple controller. As explained in 3.4.1 and 4.2.1, before implementing the PID or PD controller, the author next employs relay-based auto-tuning. Therefore, to analyse the system using the PID, relay feedback control is operated, and Figure 42 shows the result in terms of the control and output signals.

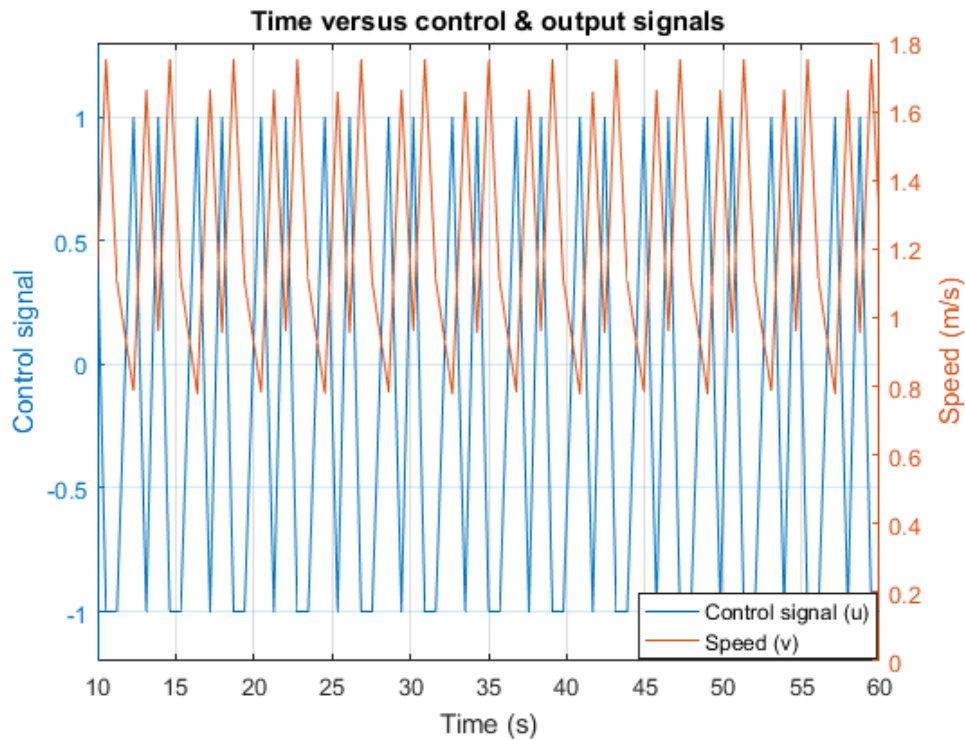


Figure 42 – Plot chart of control and output signals with respect to time (Author, 2018)

Based on Equation 5, Equation 6 and Equation 3, the important parameters can be obtained from above figure, i.e. $K_u = 2.126$, $T_u = 2.039$, $K_p = 1.28$, $T_i = 1.02$ and $T_d = 0.25$, and may then be implemented in the PID controller.

a. Traction Force Test

Figure 43 shows the output of the system (solid blue line) obtained by implementing the PID. It appears to be difficult for the PID to follow the reference (black dashed line). Even when the process output is seen with respect to time (see Figure 44), the system can maintain oscillations after 179.8768 seconds, which is its settling time. Moreover, its IAE and ISE values are extremely poor, i.e. 407.9013 and 1509.3524, respectively.

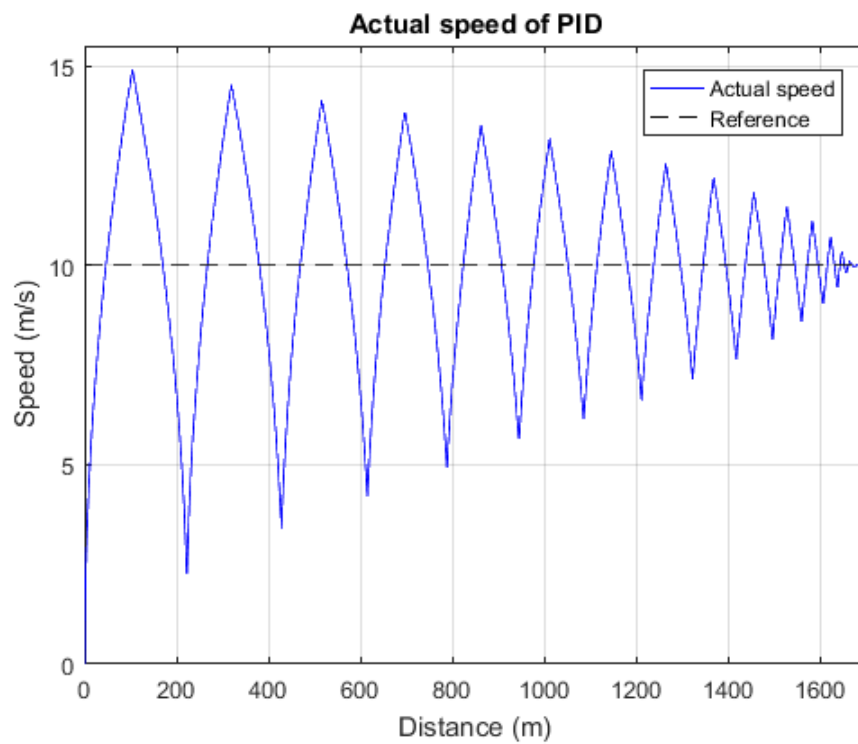


Figure 43 – Actual speed of PID (traction part) (Author, 2018)

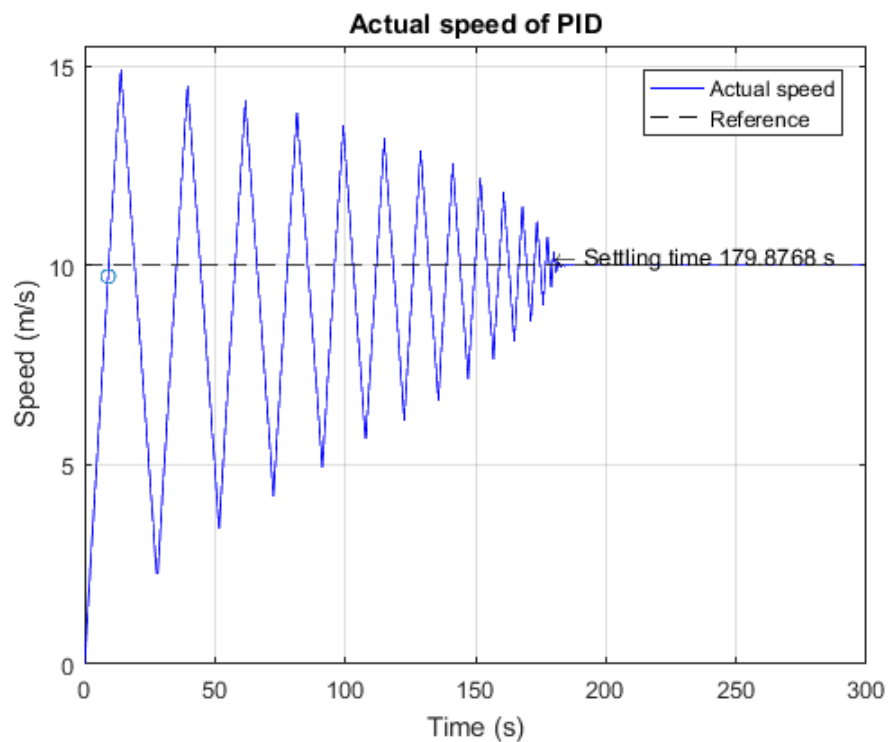


Figure 44 – Actual speed of PID with settling time (traction part) (Author, 2018)

b. Braking Force Test

As with the test of the traction force, the PID test for the braking force also shows poor results, as denoted in Figure 45. It's settling time also indicates deficient performance at 791.0235 seconds, as shown in Figure 46. Lastly, its IAE and ISE values are 3376.9993 and 17236.4372, respectively.

3. Assessing Auto-tuning Parameters for PD Controller

Due to the windup integrator, as explained in 3.4.1, the PID gives poor results. Therefore, the author considers removing the "I" element in PID so that it becomes PD control to eliminate the PID drawbacks, as discussed previously. In this test, the PD control utilises the same parameters as the PID control except for T_i .

a. Traction Force Test

Figure 47 shows the actual speed of the system using PD control. One can see that it yields comparable results to the system with a simple controller. However, when the PD is viewed with respect to time, as shown in Figure 48, it indeed produces superior results than for the simple control system, i.e. a 9.366 second settling time, 48.6 IAE value and 282.0277 ISE value.

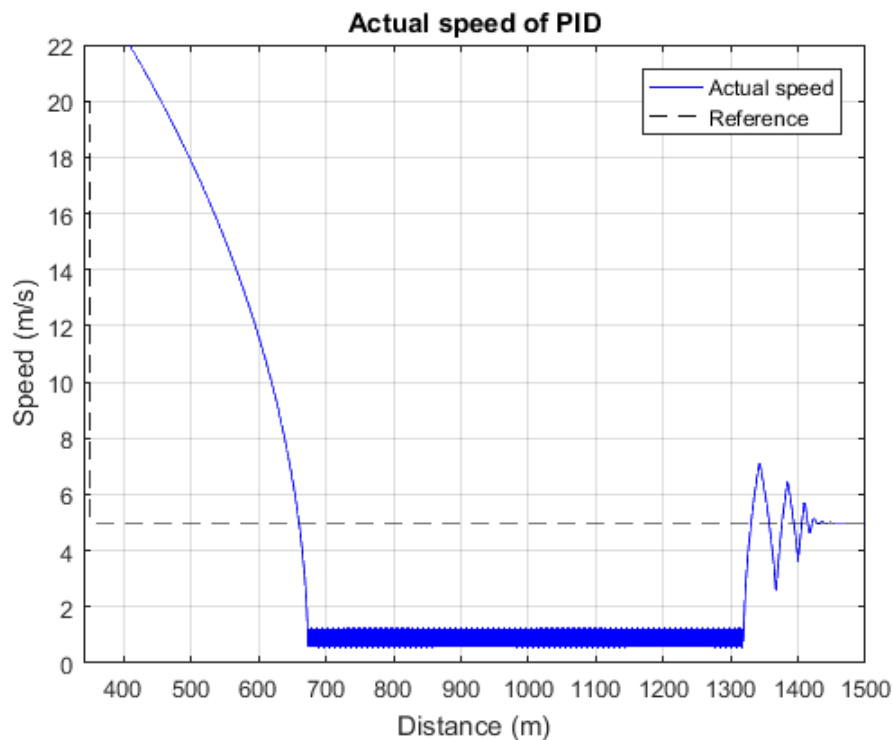


Figure 45 – Actual speed of PID (braking part) (Author, 2018)

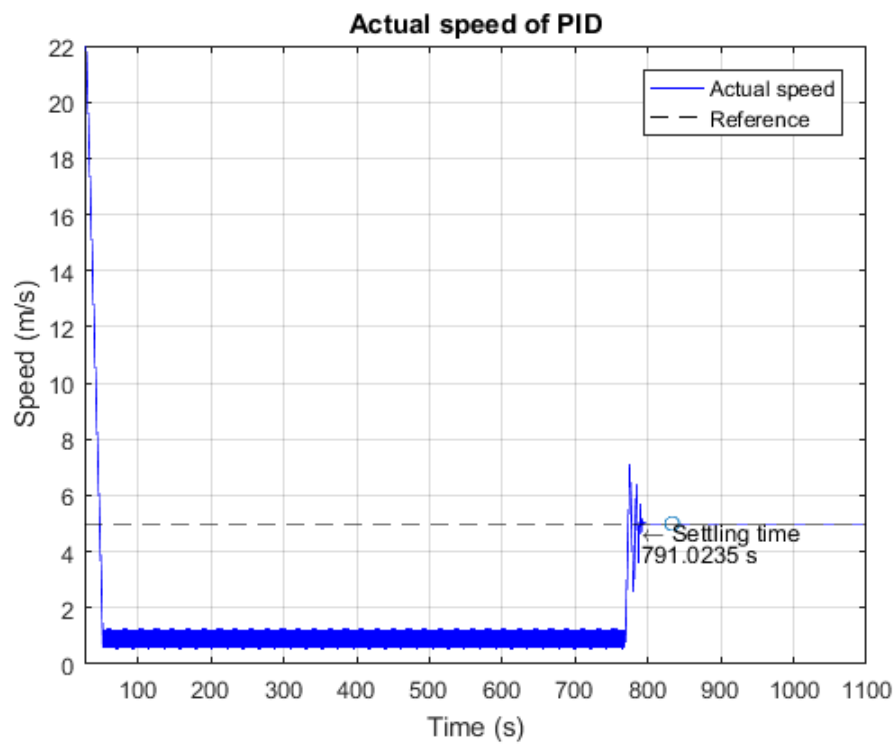


Figure 46 – Actual speed of PID with settling time (braking part) (Author, 2018)

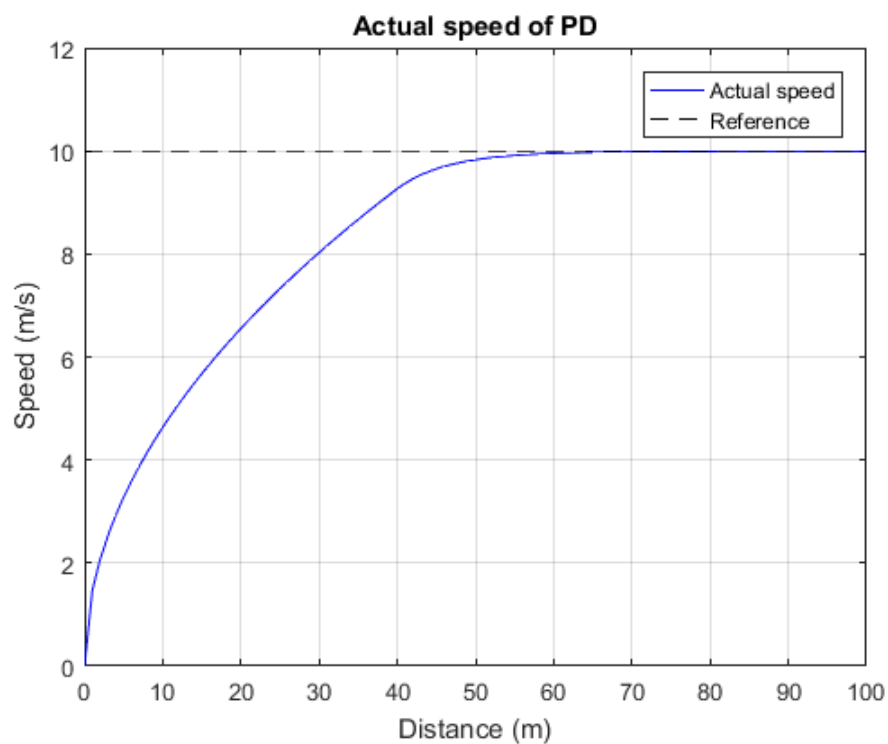


Figure 47 – Actual speed of PD (traction part) (Author, 2018)

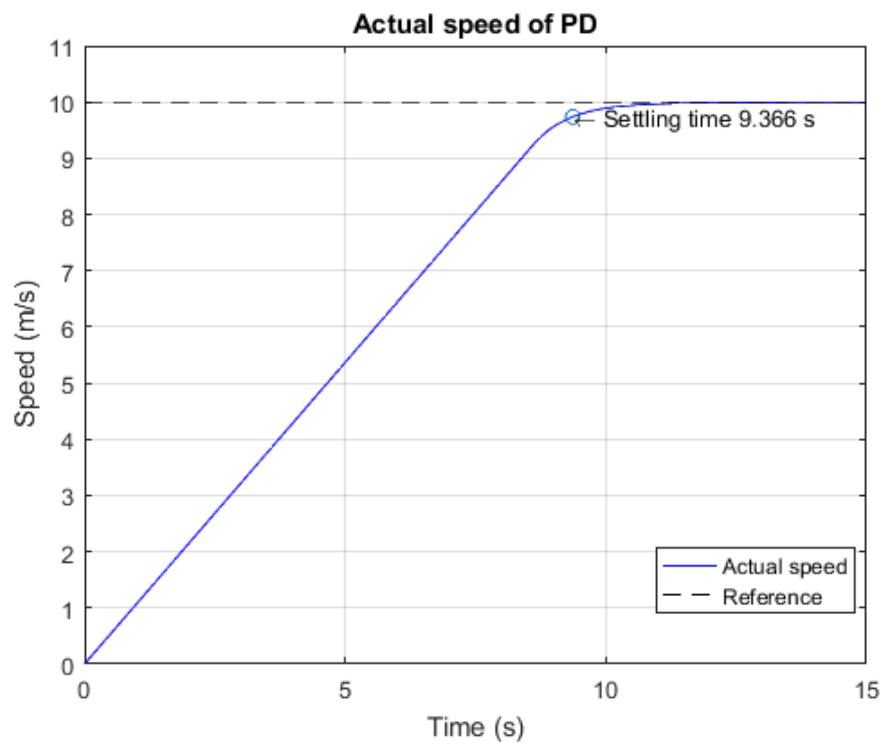


Figure 48 – Actual speed of PD with settling time (traction part) (Author, 2018)

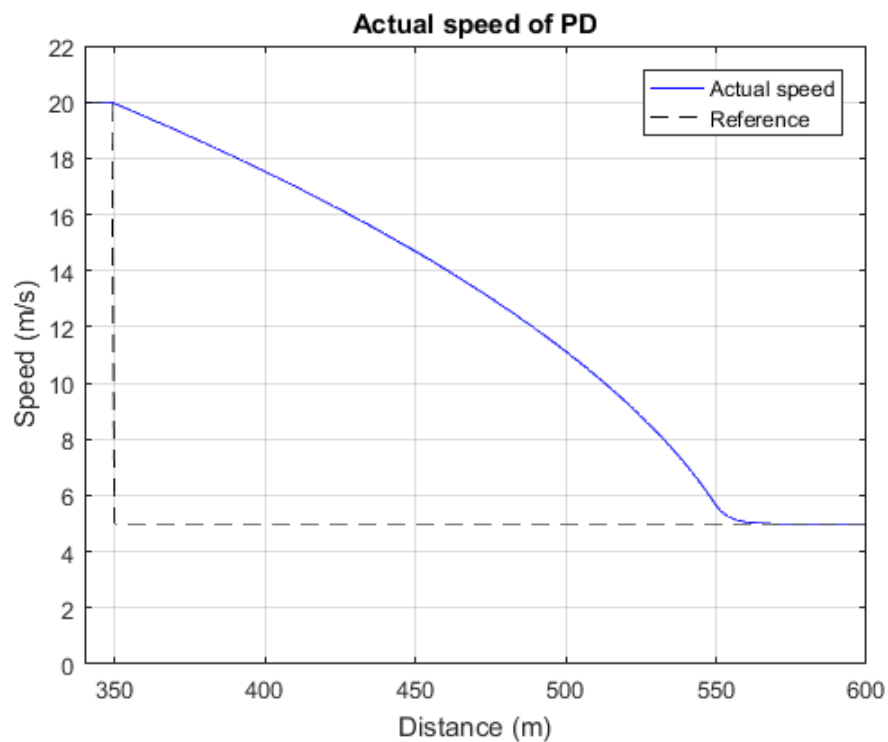


Figure 49 – Actual speed of PD (braking part) (Author, 2018)

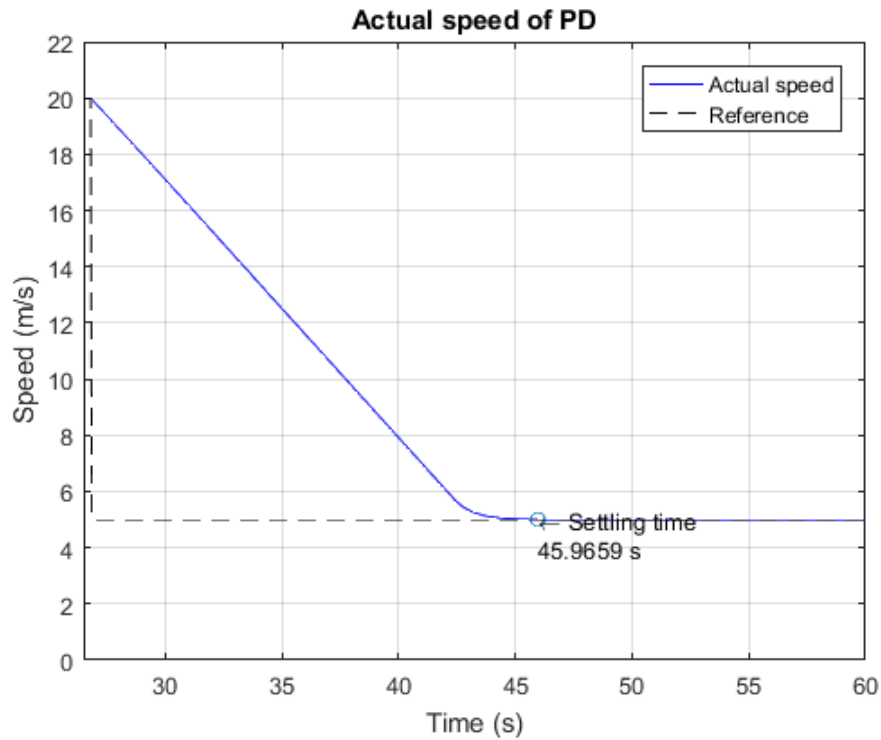


Figure 50 – Actual speed of PD with settling time (braking part) (Author, 2018)

b. Braking Force Test

For the braking force test, the PD control also yields excellent results, as shown in Figure 49. Its settling time (45.9659 seconds) outperforms the simple control system and even the PID control, as denoted in Figure 50. Finally, its IAE and ISE values are 314.7612 and 3649.3826, respectively.

4. Examining Fuzzy Gain Scheduling Based PD Controller

As described in 4.2.2, at distance $s = 0$, Fuzzy gain scheduling uses the same parameters as the PD at the beginning of the tests, i.e. K_u , T_u , K_p and T_d . Moreover, since the hybrid controller uses T_i to find T_d , after running, T_i is also employed. Then, for γ the author defines a value of 0.6.

a. Traction Force Test

The results are shown in Figure 51. One can see that this type of controller gives satisfactory results. Even its settling time indicates superior results, i.e. 9.0538 seconds, as shown in Figure 52. Further, its IAE and ISE values are 46.5358 and 281.9444, respectively.

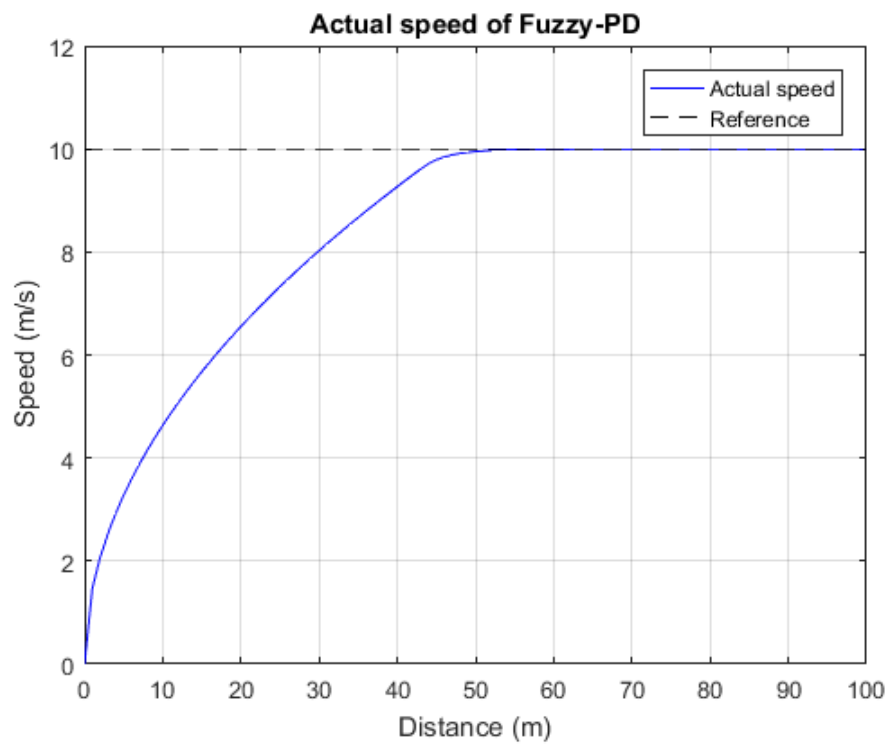


Figure 51 – Actual speed of Fuzzy-PD (traction part) (Author, 2018)

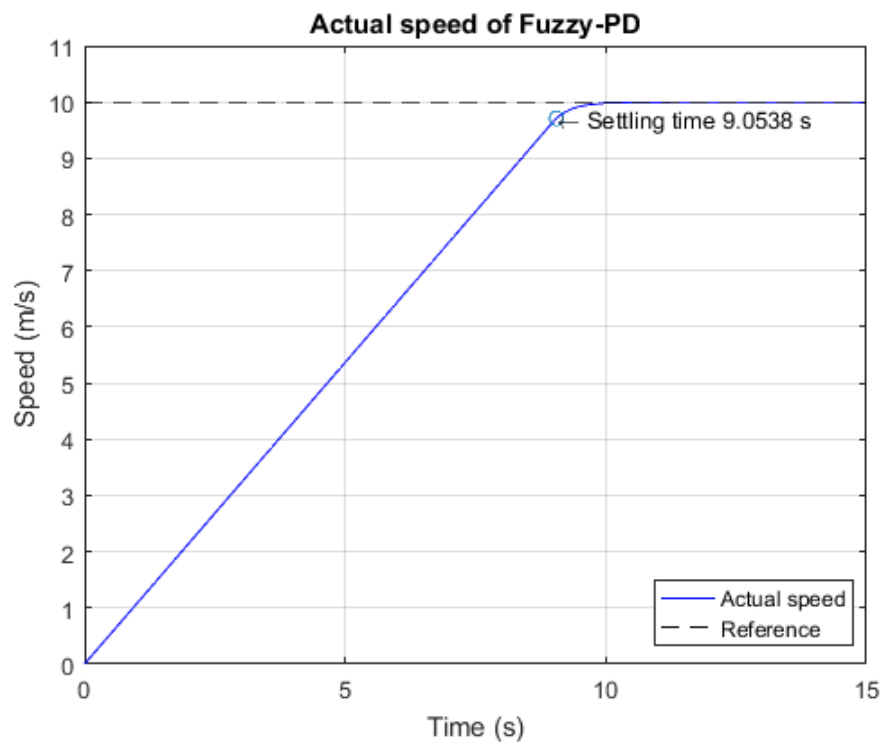


Figure 52 – Actual speed of Fuzzy-PD with settling time (traction part) (Author, 2018)

b. Braking Force Test

For the braking force test, Fuzzy gain scheduling of the PD control also indicates satisfactory performance, especially in regard to its settling time: 44.3842 seconds. Figure 53 and Figure 54 show its performance with respect to distance and time, respectively. Its IAE and ISE values are 311.0428 and 3650.1829, respectively.

5. Comparisons

In this section, all four controllers that have been discussed previously are compared with each other by means of three performance indices: T_s (settling time), IAE and ISE. In the first comparison, as denoted in Figure 55, the traction force tests of the four controllers are displayed in one chart. PID (blue dashed line) demonstrates the worst process output compared to the other three, whose results are relatively similar.

Likewise, in the second comparison, shown in Figure 56, for the braking force tests, the PID gives the worst performance. Eventually, in the third comparison, as shown in Table 2, one can see the performance of the controllers more clearly. For the settling time and IAE, Fuzzy-PD, i.e. Fuzzy gain scheduling of PD control, demonstrates the best results both in terms of traction and braking tests. Meantime, although Fuzzy-PD outperforms PD for the traction test, on the other hand, for the ISE index in the braking test, Fuzzy-PD is slightly inferior to PD and the simple control system. Ultimately, based on the results shown in the table, only the best two controllers, i.e. PD control and Fuzzy-PD control, are employed in the analysis and discussion in the next section.

Table 2 – Comparison indices of constant speed reference test

| Indices | Traction Test | | | |
|---------|---------------|------------|-----------|-----------|
| | Simple | PID | PD | Fuzzy-PD |
| T_s | 9.4736 | 179.8768 | 9.366 | 9.0538 |
| IAE | 49.7694 | 407.9013 | 48.6 | 46.5358 |
| ISE | 282.1087 | 1509.3524 | 282.0277 | 281.9444 |
| Indices | Braking Test | | | |
| | Simple | PID | PD | Fuzzy-PD |
| T_s | 46.5549 | 791.0235 | 45.9659 | 44.3842 |
| IAE | 316.8766 | 3376.9993 | 314.7612 | 311.0428 |
| ISE | 3649.0045 | 17236.4372 | 3649.3826 | 3650.1829 |

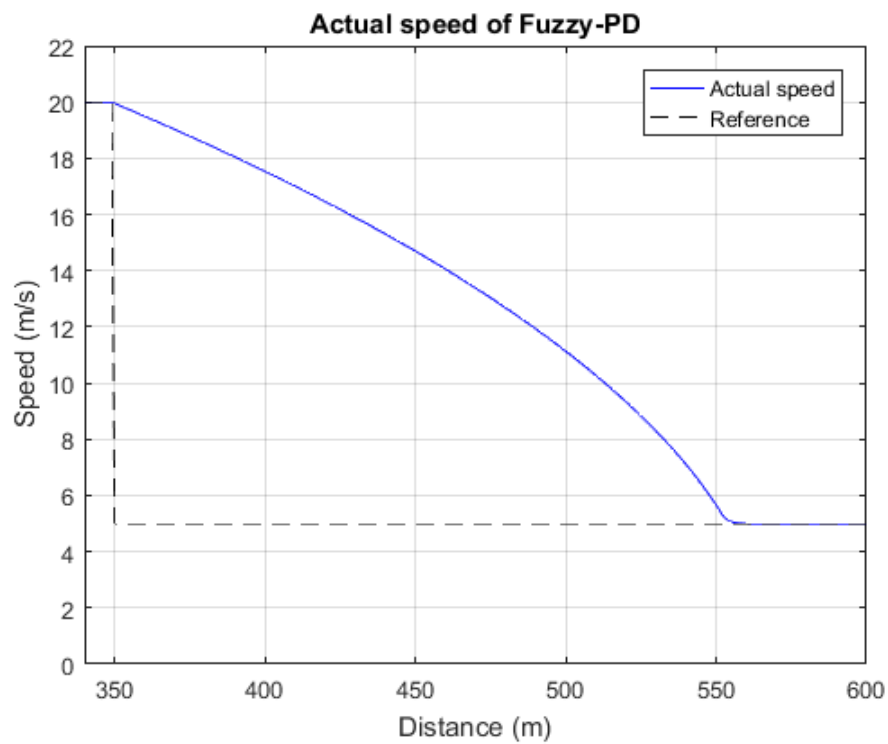


Figure 53 – Actual speed of Fuzzy-PD (braking part) (Author, 2018)

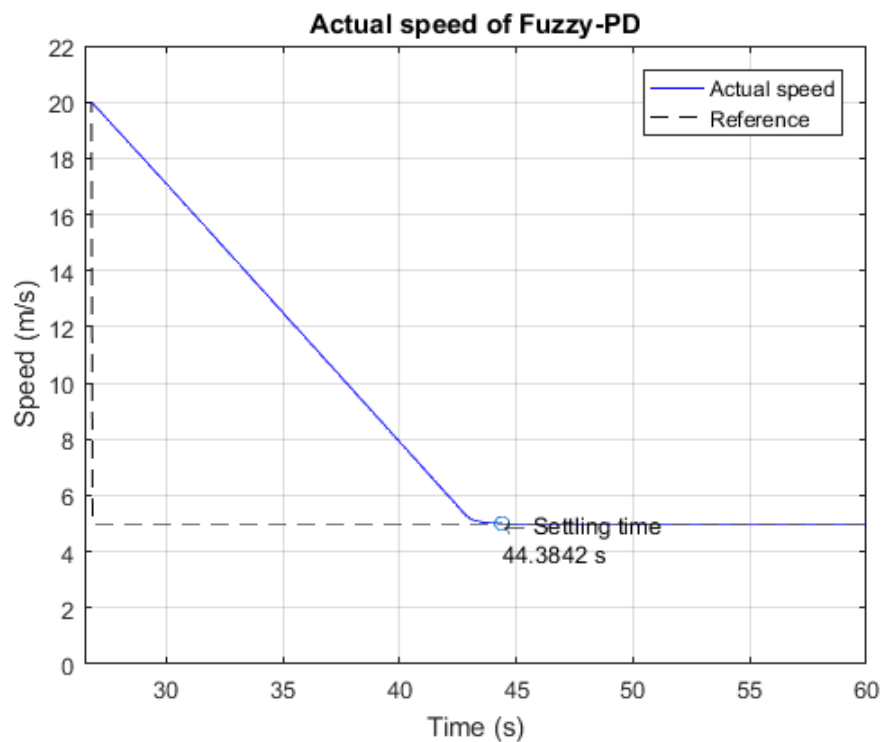


Figure 54 – Actual speed of Fuzzy-PD with settling time (braking part) (Author, 2018)

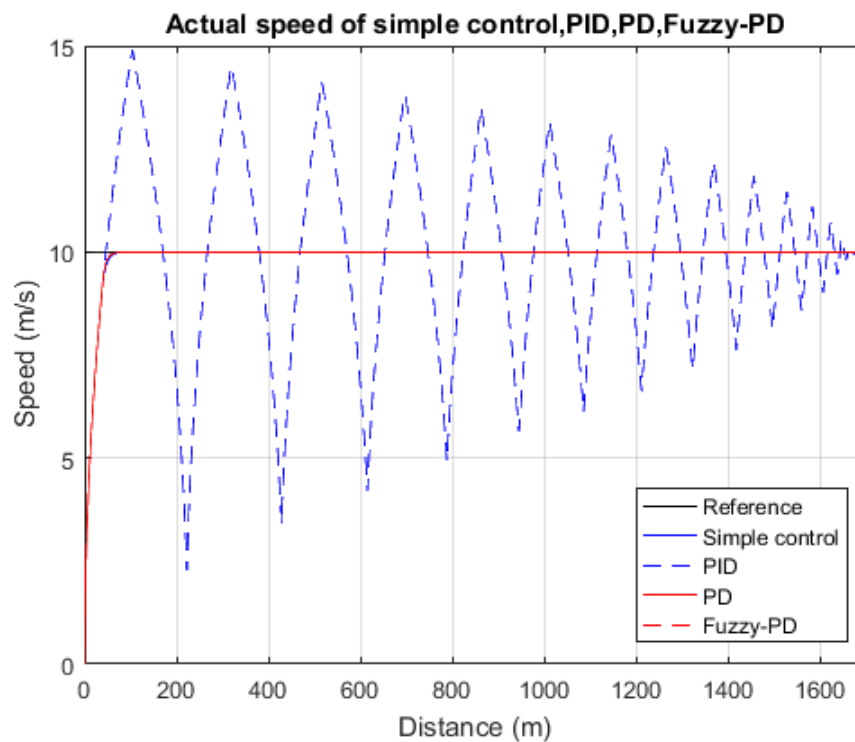


Figure 55 – Comparison of simple control, PID, PD and Fuzzy-PD (traction part) (Author, 2018)

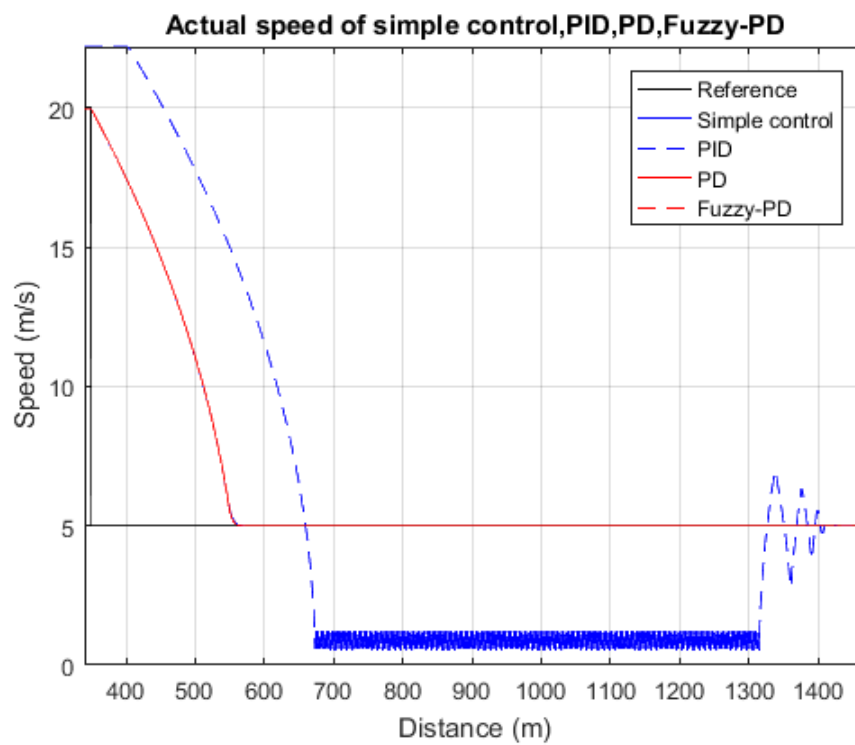


Figure 56 – Comparison of simple control, PID, PD and Fuzzy-PD (braking part) (Author, 2018)

4.4.3 Running on Artificial Train Trajectory

After running the system on a constant reference, here, an artificial train trajectory is used to assess the system performance. One could utilise this approach to test the system and even the controller in following variable speed references. Due to its linkage to a more realistic track than a constant speed reference test, the resistances, particularly, gradient resistance, affect this type of test.

1. Characteristics of the Trajectory

In this trajectory, the author applies the traction mode three times and the braking mode twice. The speed limit used along the running pattern can be seen in Figure 57. At a distance of between 0 and 200 metres, the speed limit is 12 m/s; at between 201 and 1000 metres, it is 17 m/s; between 1001 and 4500 metres, it is 22.2 m/s; at between 4501 and 4999 metres, it is 12 m/s; and finally, at a distance of 5000 metres, it is 0 m/s. Hence, the track length is 5 km.

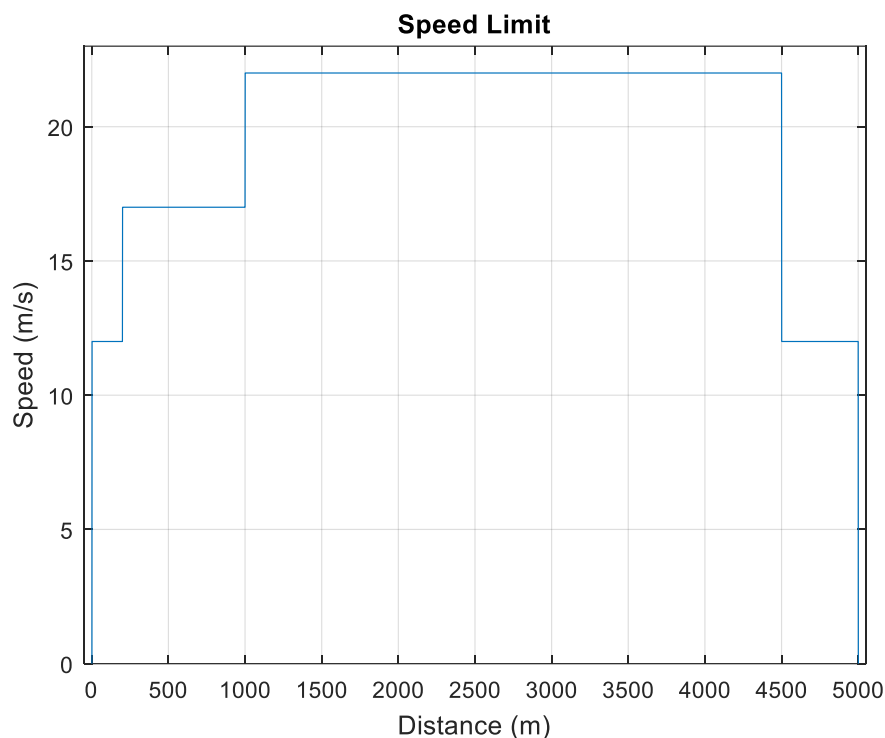


Figure 57 – Speed limit for artificial train trajectory (Author, 2017)

Subsequently, to create the gradient resistance, the author considers the altitude, as shown in Figure 58. Mostly uphill slopes influence the resistance, even though there is a steep downhill starting from 2500 metres. Based on this figure, one could calculate the height change over every, for example, 100 metres, and then compute the gradient resistance.

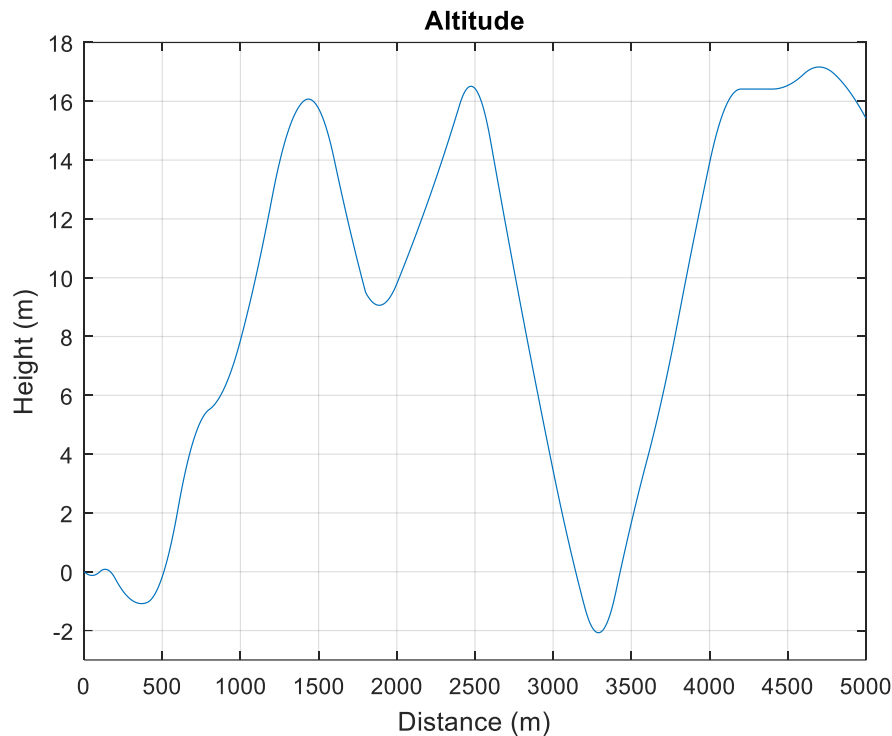


Figure 58 – Altitude for artificial train trajectory (Author, 2017)

In order to generate the train trajectory to be used by the controller, one could implement, for example, a coasting strategy, an approach which has been applied widely (Dong, Ning, et al., 2010) in order to produce a lower carbon footprint and more comfortable train journeys. Moreover, since energy consumption and passenger comfort are not considered as the controller objectives of this study, the approach of maximum performance to generate the train trajectory is also employed to evaluate the system and the controller.

a. Full Power Trajectory

The full performance of the train trajectory generates a running pattern based on a given speed limit at maximum capacity, i.e. traction and braking, of the system. Therefore, it exhibits a trajectory which consistently attempts to approach the speed limit. For the full performance, the following stages are carried out (Hwang, 1998):

1. By using the given characteristics of the train model as stated in subchapter 4.1, divide the train trajectory into two phases, i.e. forward and backward trajectories.
2. First, by performing maximum tractive effort, the forward trajectory is generated along the speed limit from A to E, as shown in Figure 59.
3. By applying the maximum braking force as the motion force, instead of the tractive effort, on the other hand, the backward trajectory is carried out during the braking parts of the path, i.e. between E and D and between C and B. This technique is

- calculated by utilising negative deceleration, as the interim acceleration, and the backward distances from E to D and from C to B.
4. When the calculation of the forward trajectory and backward trajectory intersect each other at points B and D, a combination of them produces complete train trajectory.
 5. In order to clarify both ways, synchronise the calculations of distance, speed and acceleration or deceleration between them.

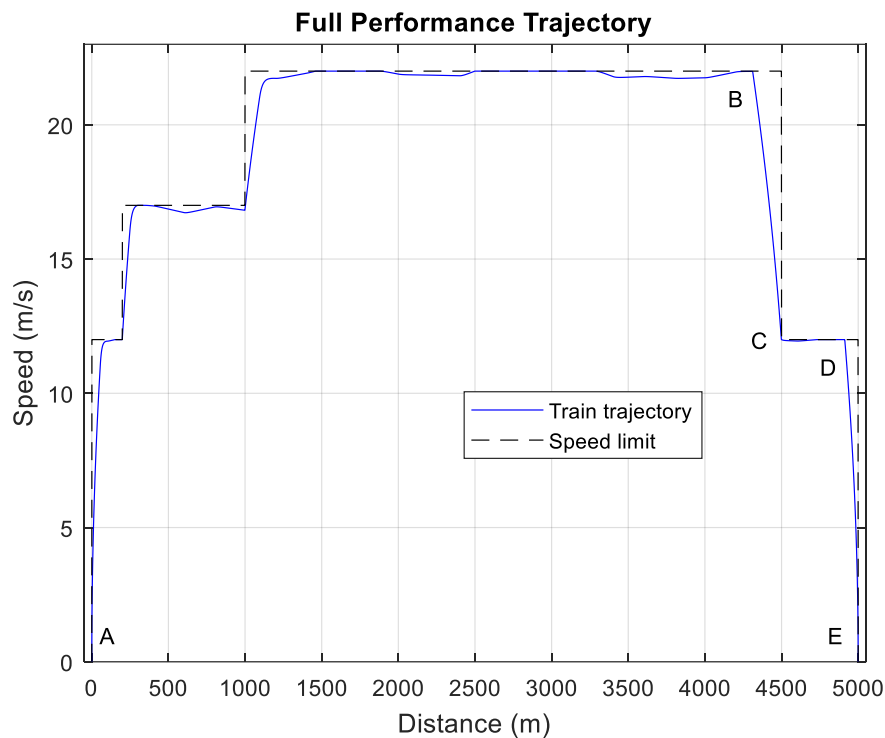


Figure 59 – Full-performance train trajectory (Author, 2017)

As shown in Figure 60, in producing the train trajectory of Figure 59, there are three types of acceleration, i.e. true acceleration from the tractive effort (blue dashed line), negative deceleration (red dashed line) and their composite (acceleration and deceleration) as exhibited by the solid black line. The negative deceleration, as described in step 3 above, is necessary to produce the backward trajectory. Afterwards, as explained in step 5, such a negative deceleration has to be inverted to create the true deceleration which is negative in value.

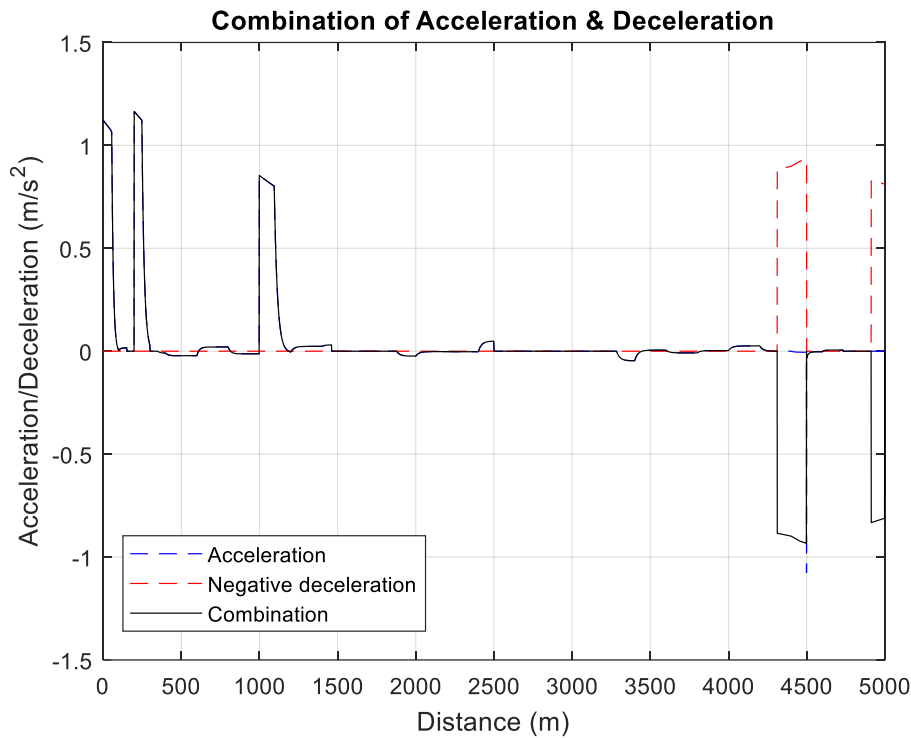


Figure 60 – Acceleration/Deceleration of full-performance train trajectory (Author, 2017)

b. Implementing Coasting Strategy

In this study, there are no complex algorithms implemented to generate the train trajectory with coasting strategy, it is assumed that the following simple technique to create a running pattern with coasting components is an optimised train trajectory. The procedure to produce such a trajectory is fundamentally based on the technique used to create the maximum performance train trajectory. Nevertheless, for braking modes, one should employ the coasting mode when the speed of the trajectory v_{ref} reaches coasting speed v_{coast} . The steps to perform this are as follows:

1. Follow step 1 and 2 of Full Power Trajectory, as shown in Figure 59.
2. Define the coasting speed v_{coast} value at which the speed of the train trajectory v_{ref} starts to coast. In this analysis, the author defines its value as 60 km/h or 16.7 m/s.
3. For the braking parts, as explained in step 3 of Full Power Trajectory, impose the condition as defined in Equation 53 where $-dec$ is the negative instantaneous deceleration of the system and $B(v)$ is the braking force. Albeit $-dec$ is zero when v_{ref} is greater than or equal to v_{coast} , despite being much less than the value of $-dec$, the deceleration still exists thanks to the resistance forces.
4. Execute steps 4 and 5 of Full Power Trajectory.

Equation 53 – Coasting strategy

$$-dec = \begin{cases} 0; & v_{ref} \geq v_{coast} \\ B(v); & v_{ref} < v_{coast} \end{cases}$$

After these steps have been executed, one could produce the train trajectory with a coasting strategy, as illustrated in Figure 61. At the point of braking between B and C, coasting is involved. This case occurs since the points B and C apply the braking mode with a coasting strategy and their v_{ref} is greater than v_{coast} .

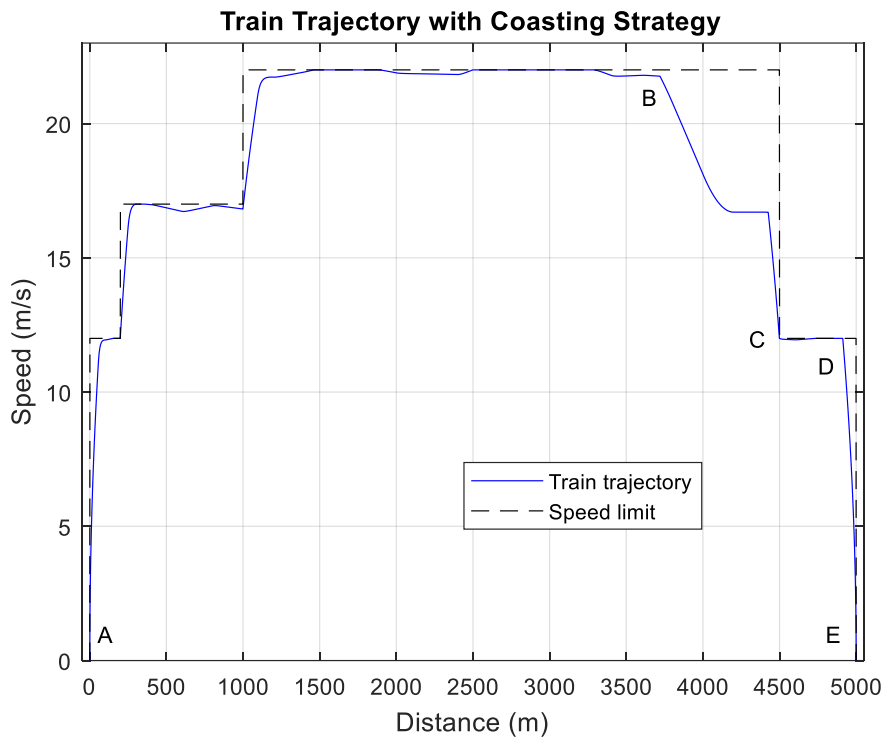


Figure 61 – Train trajectory with coasting strategy (Author, 2017)

As in Figure 60, in Figure 62 one can see the combination of acceleration and deceleration. The blue dashed line displays the true acceleration from the traction force; the red dashed line shows the negative deceleration; both acceleration and negative deceleration are integrated (solid black line) in terms such that the negative deceleration is transformed inversely.

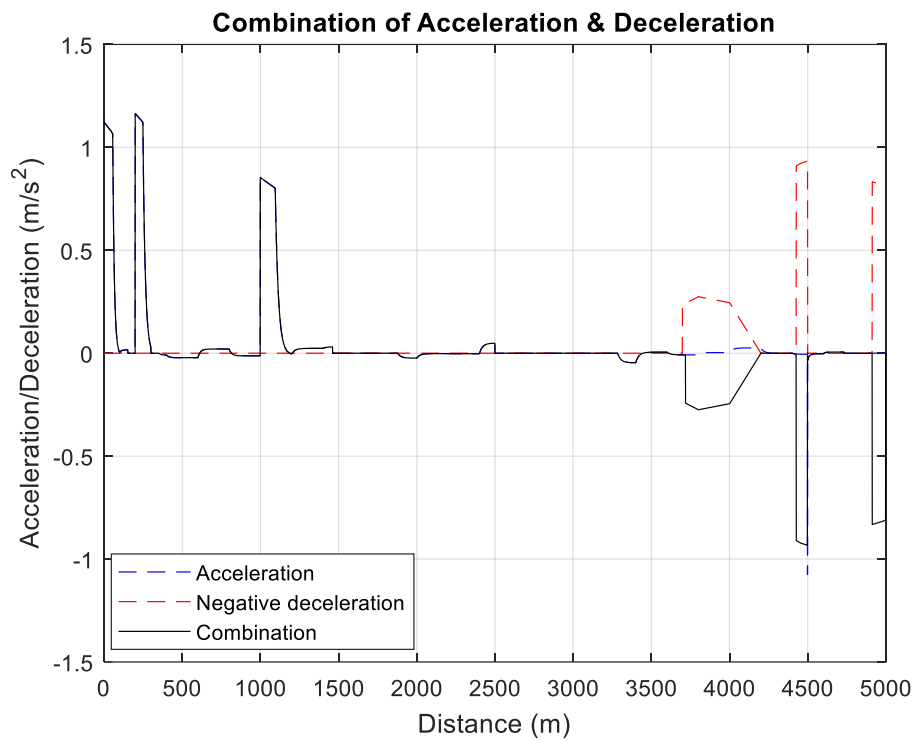


Figure 62 – Acceleration/Deceleration of train trajectory with coasting strategy (Author, 2017)

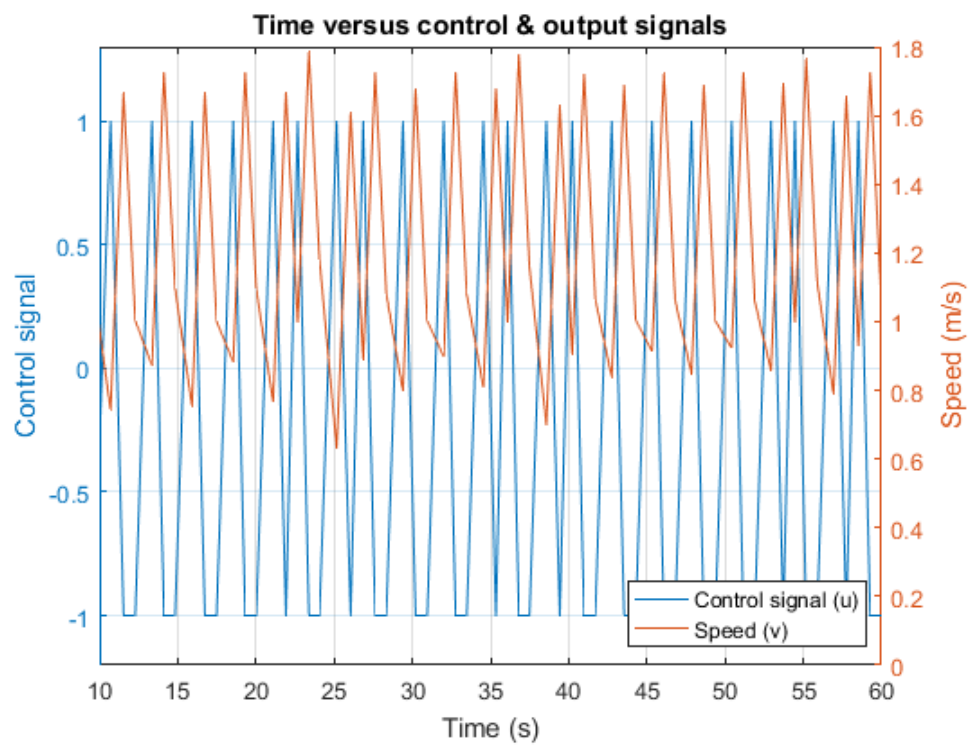


Figure 63 – Plot chart of control and output signals with respect to time (with gradient resistance) (Author, 2018)

2. Testing PD Controller

In this test, the PD controller is used to follow two types of trajectory. Overall, the steps undertaken for PD are the same as in 4.4.2. Nevertheless, due to the presence of a gradient resistance affecting the system behaviour, one has to perform relay-based auto-tuning again, as shown in Figure 63, and in calculating the parameters K_u and T_u , one could use the mean operation (see Equation 17) to create the average of the slightly disturbed process output. Subsequently, based on Equation 5, Equation 6 and Equation 3, the values of the parameters are as follows: $K_u = 1.344$, $T_u = 2.266$, $K_p = 0.81$, $T_d = 0.28$ and $T_i = 1.13$; T_i used later for the Fuzzy-PD.

Unlike the application in the constant reference test, when running on a full-power trajectory, as shown in Figure 64, the PD control is unable to cope with the given trajectory such that it creates a somewhat large error, exceeding the $\pm 3\%$ error limit. A similar case also occurs for the PD when running on a trajectory with a coasting strategy, as denoted in Figure 65. Again, the PD yields unsatisfactory results.

Furthermore, in terms of running time in the full-power trajectory, as shown in Figure 66, the PD control spends a maximum time of 280.565 seconds, or 4.6761 minutes, whereas the maximum time of the speed reference is 282.2025 seconds, or 4.7034 minutes. Therefore, the time difference between them is that the actual speed of the PD control is 1.6375 seconds earlier than the reference speed, meaning that the time constraint is satisfied.

Meanwhile, for running time in the trajectory with a coasting strategy, as shown in Figure 67, the PD control produces the maximum time of actual speed at 286.0793 seconds, or 4.768 minutes, or 0.95353 seconds earlier than the reference speed. Therefore, the time constraint is satisfied.

Then, the IAE and ISE performances of the PD control for the full-power trajectory are 80.2453 and 80.6098, respectively, whereas those in the trajectory with coasting are 49.7983 and 40.8824, respectively.

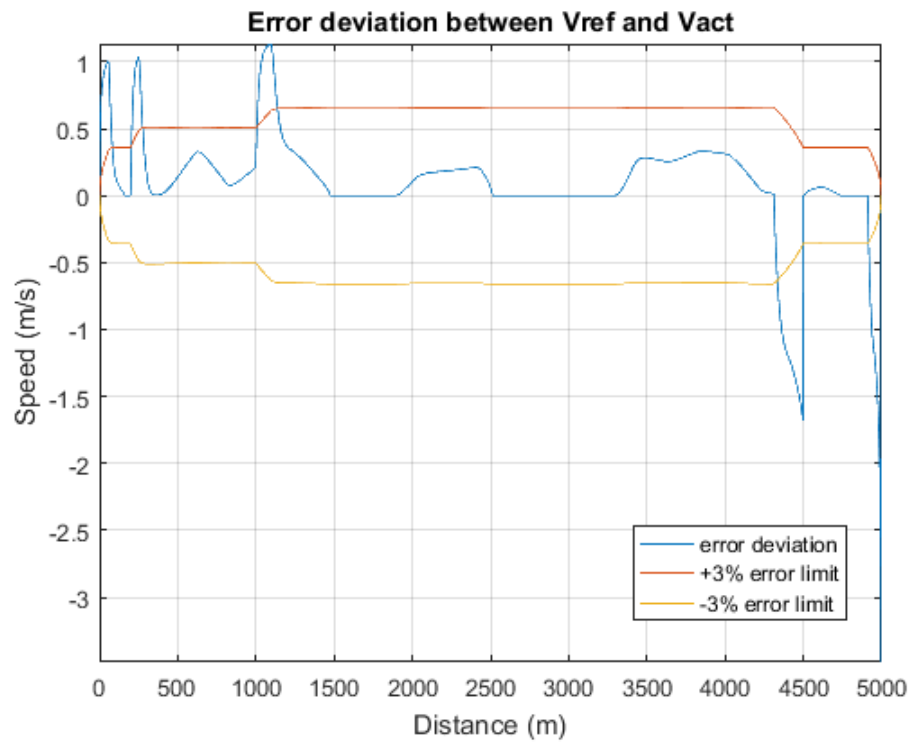


Figure 64 – Error deviation of PD control in full-power trajectory (Author, 2018)

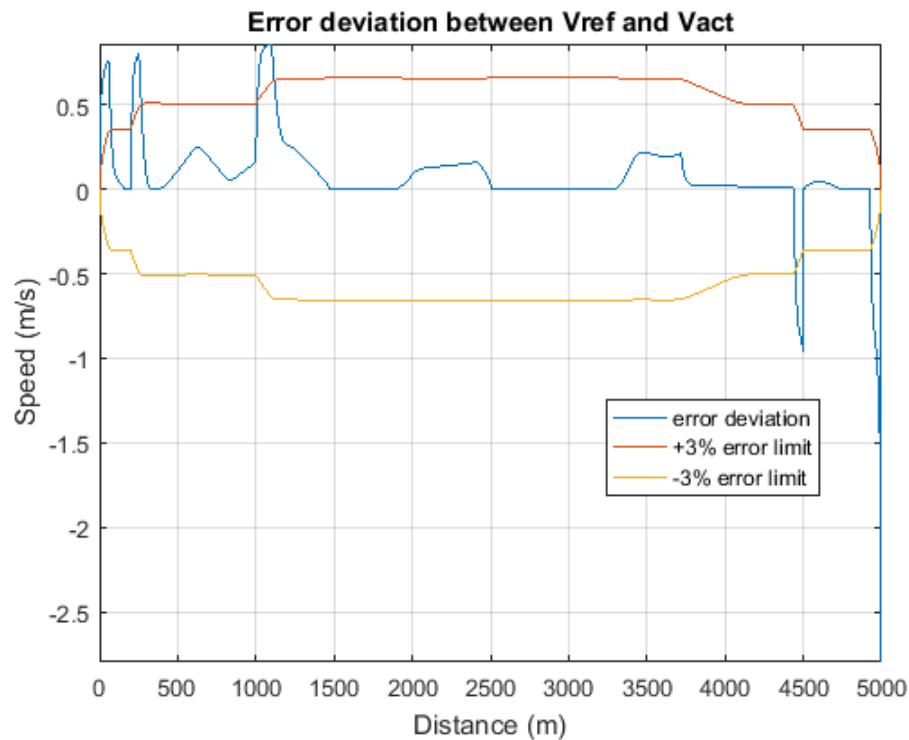


Figure 65 – Error deviation of PD control in trajectory with coasting (Author, 2018)

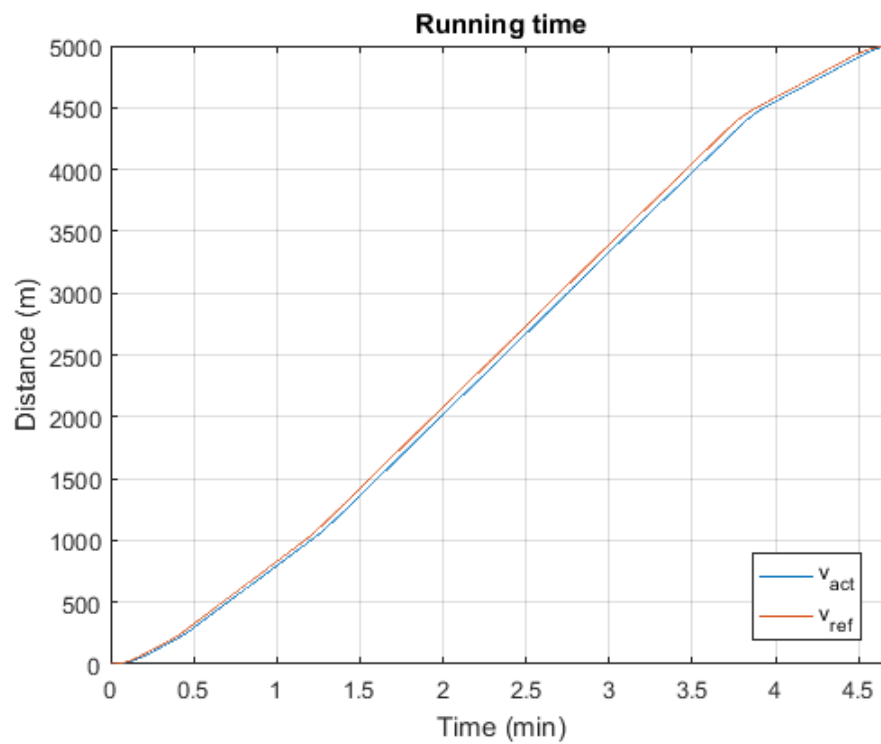


Figure 66 – Running time of PD control in full-power trajectory (Author, 2018)

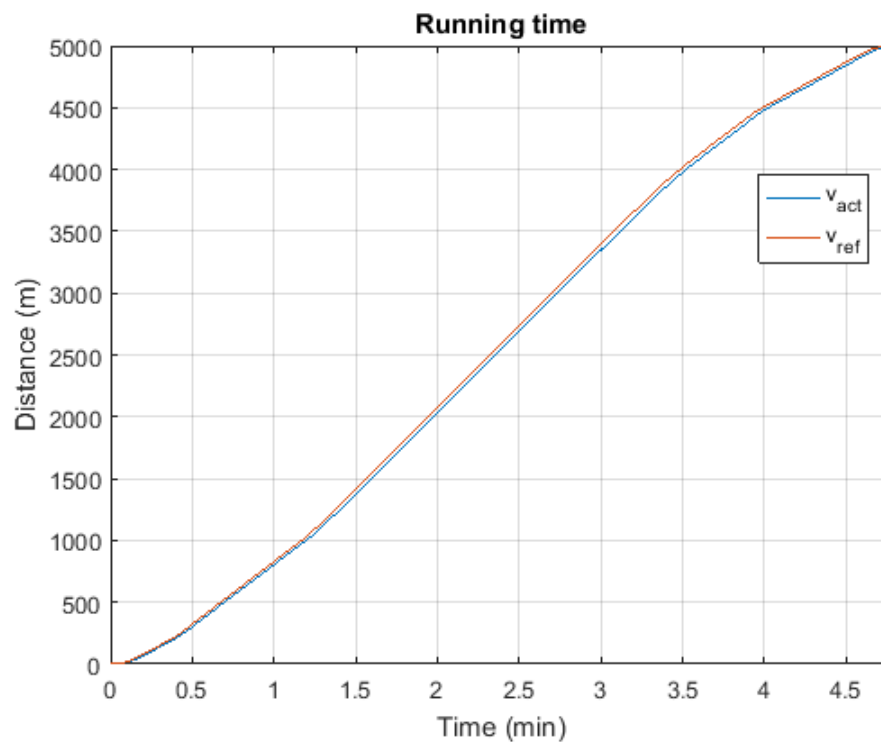


Figure 67 – Running time of PD control in trajectory with coasting (Author, 2018)

3. Assessing Fuzzy Gain Scheduling Based PD Controller

In this test of the Fuzzy gain scheduling of the PD, all parameters used for the PD test in the previous section are also employed here. The procedure before the test is the same as in 4.4.2 for Fuzzy gain scheduling of the PD control. Here, the γ value used is also the same, i.e. 0.6.

The error deviations of the Fuzzy-PD for both the full-power trajectory and the trajectory with a coasting strategy are denoted in Figure 68 and Figure 69, respectively. One can see that the Fuzzy-PD shows satisfactory results without any error deviation of significantly more than the $\pm 3\%$ error limit.

Afterwards, for the running time, for the full power trajectory, as denoted in Figure 70, the Fuzzy-PD spends a maximum time of 280.6447 seconds, or 4.6774 minutes, which is 0.13825 seconds later than the reference speed. Therefore, the time constraint is satisfied. In trajectory with coasting, as shown in Figure 71, the maximum time of actual speed is 287.1798 seconds, or 4.7863 minutes, or 0.14696 seconds later than the reference speed. Therefore, this time constraint is also satisfied.

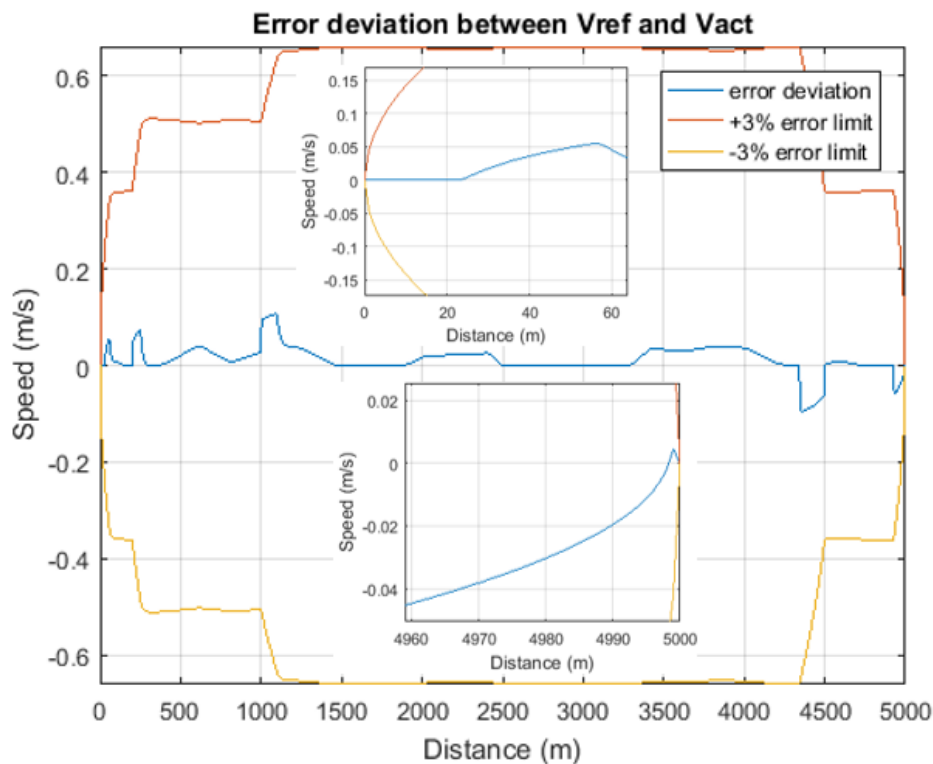


Figure 68 – Error deviation of Fuzzy-PD in full-power trajectory (Author, 2018)

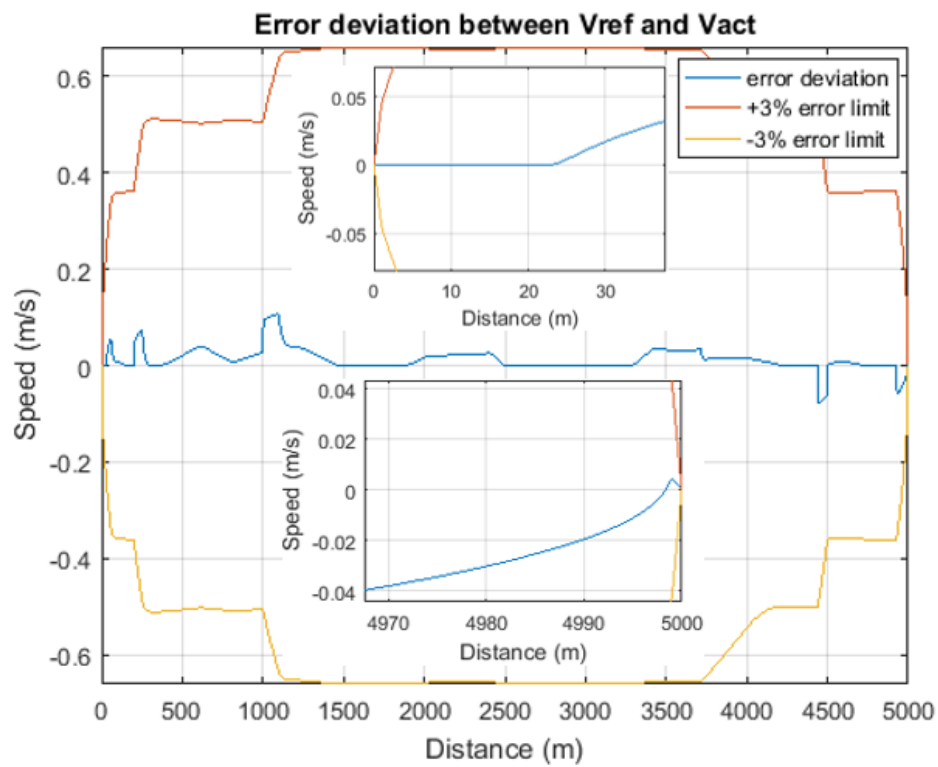


Figure 69 – Error deviation of Fuzzy-PD in trajectory with coasting (Author, 2018)

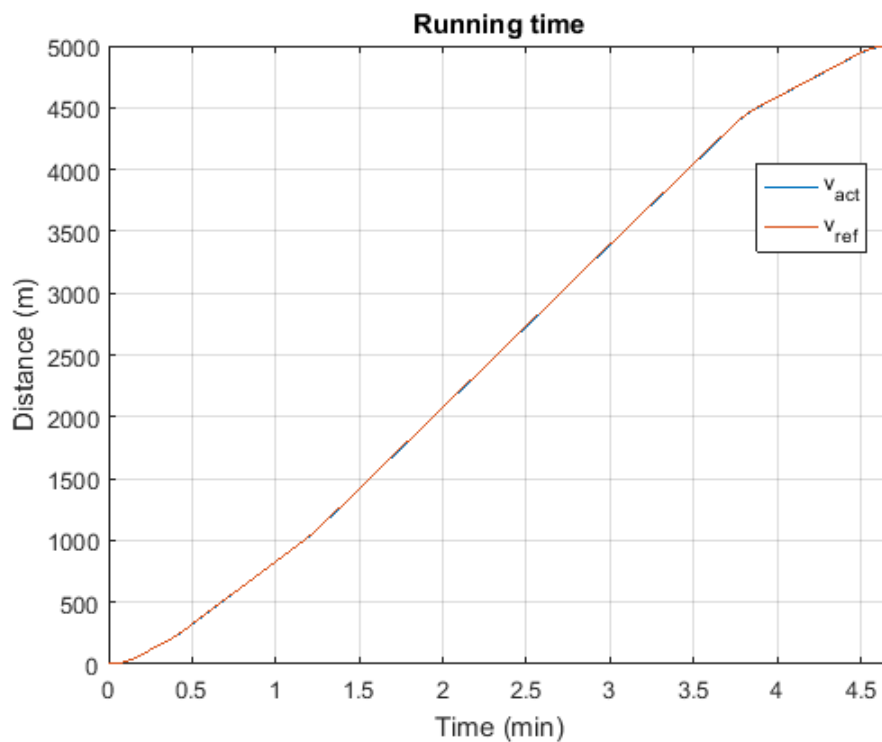


Figure 70 – Running time of Fuzzy-PD in full-power trajectory (Author, 2018)

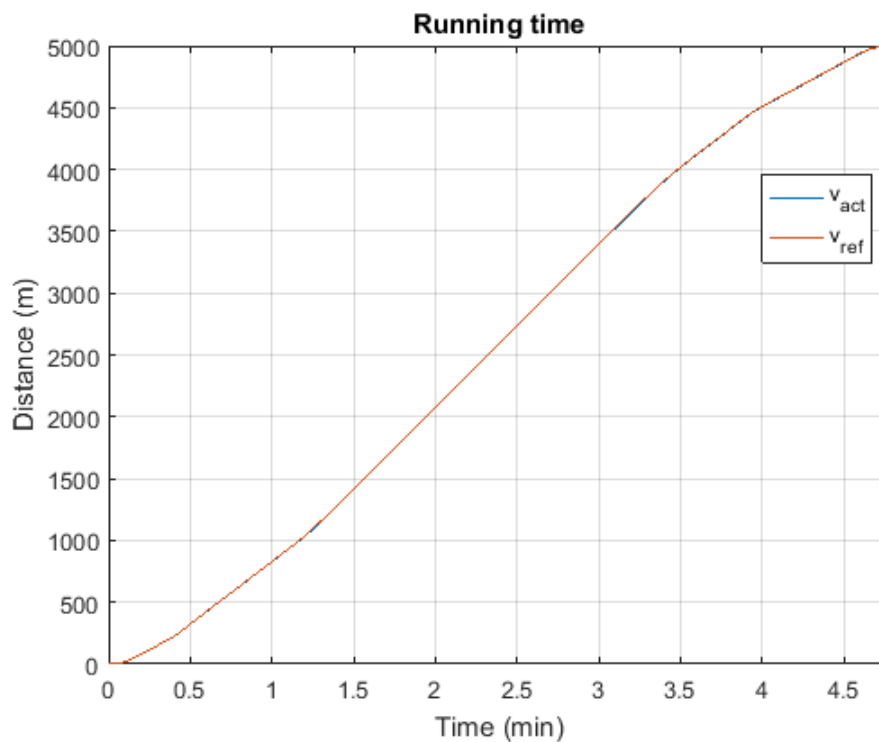


Figure 71 – Running time of Fuzzy-PD in trajectory with coasting (Author, 2018)

Finally, in regard to its IAE and ISE performance, these are 11.8668 and 3.3069, respectively, on the full-power trajectory, and 10.5027 and 3.1779, respectively, on the trajectory with a coasting strategy.

4. Implementing Measurement Errors

As described in 4.3.1, measurement noise is introduced to the system output in this test, and after implementing the noise, the error deviation is illustrated to demonstrate that, indeed, the measurement error ruins the system output, and even the controllers are unable to cope with this issue. Here, the controller used is Fuzzy gain scheduling of the PD control.

Figure 72 and Figure 73 show the error deviations for the process output on the full-power trajectory and the trajectory with a coasting strategy when corrupted by measurement noise. Even the Fuzzy-PD, which can follow the given trajectories satisfactorily, is unable to deal with such a noisy environment.

Next, the running time of the noisy system on both the full-power trajectory and the trajectory with coasting are shown in Figure 74 and Figure 75, where the maximum times of both are 286.9139 seconds, or 4.7819 minutes, or 6.4074 seconds later than reference speed so that time constraint is satisfied, and 289.6539 seconds, or 4.8276 minutes, 2.6211 seconds later than the reference speed so that the time constraint is satisfied, respectively.

The performance of the IAE and ISE for the noisy system are not calculated since it is obvious that they will produce exceptionally high errors.

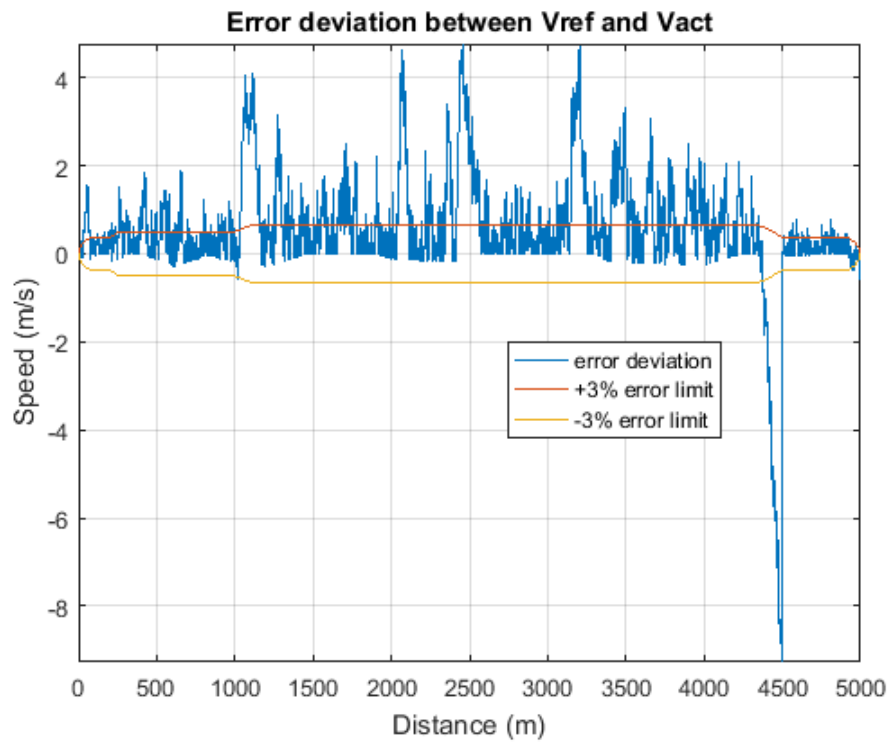


Figure 72 – Error deviation of noisy Fuzzy-PD in full-power trajectory (Author, 2018)

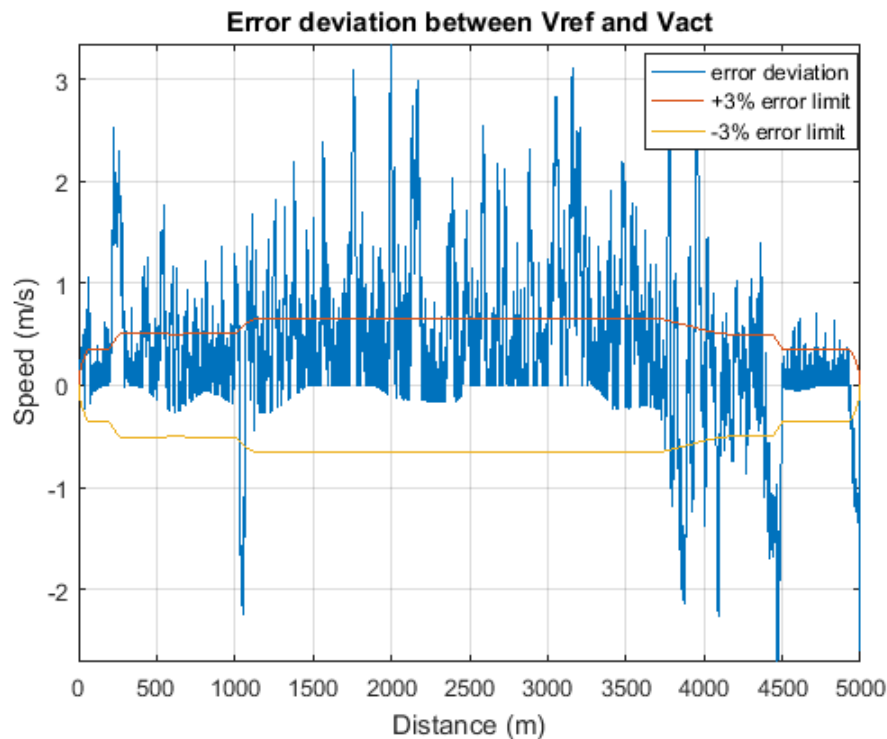


Figure 73 – Error deviation of noisy Fuzzy-PD in trajectory with coasting (Author, 2018)

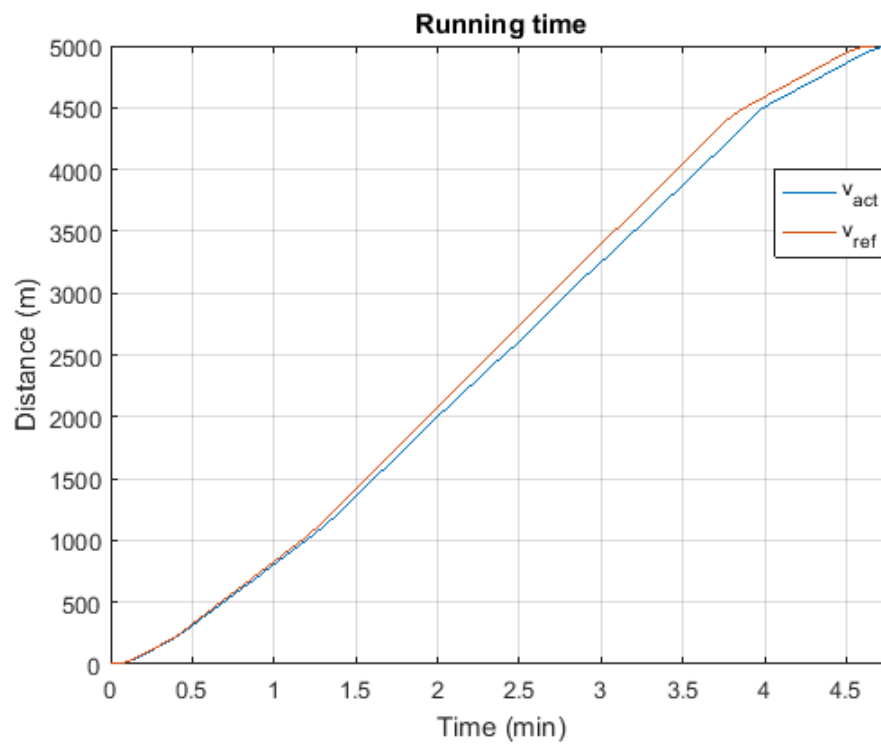


Figure 74 – Running time of noisy Fuzzy-PD in full-power trajectory (Author, 2018)

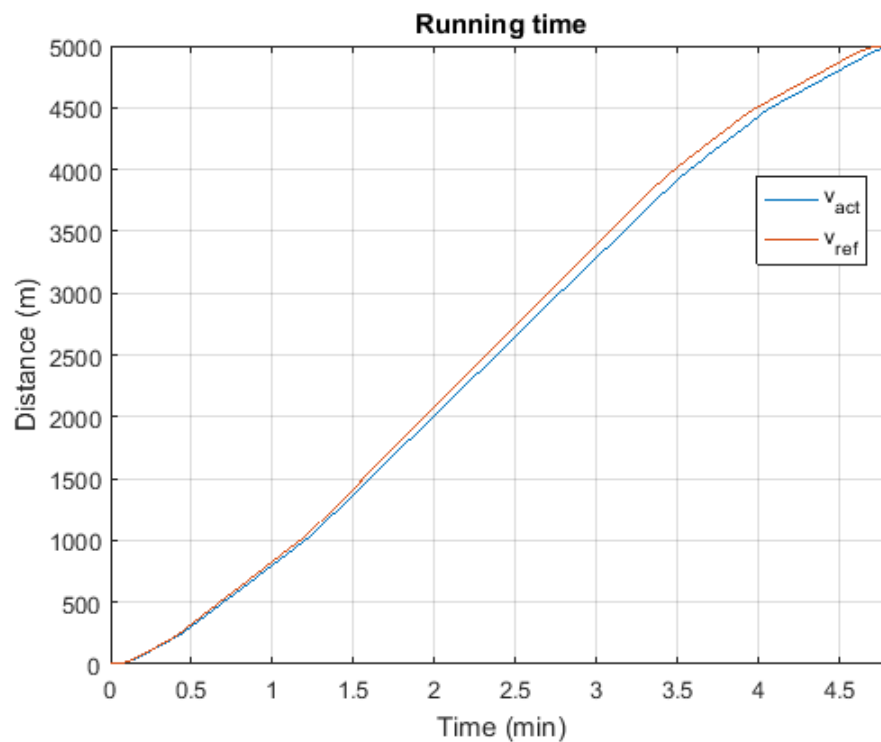


Figure 75 – Running time of noisy Fuzzy-PD in trajectory with coasting (Author, 2018)

5. Applying Kalman Filter

As proven in the previous test, the measurement noise devastates the system, it is therefore necessary to improve the controllers, as mentioned in 4.3.2, so that a Kalman filter is utilised. To implement the filter, one has to arrange its parameters as defined in 4.3.2.

In Figure 76 and Figure 77, one can see that the Kalman filter is capable of improving the results with the noisy environment, as seen in Figure 72 and Figure 73, so that the process output has an error lower than the error limit. Figure 76 shows the error deviation for the full-power trajectory, whereas Figure 77 shows the trajectory with coasting.

Figure 78 shows the journey time for the full-power trajectory, whereas Figure 79 shows that for the trajectory with coasting. Their maximum times respectively are 280.5297 seconds, or 4.6755 minutes, or 0.023255 seconds later than reference speed, so the time constraint is satisfied, and 287.0311 seconds, or 4.7839 minutes, or 0.0016816 seconds earlier than the reference speed, so the time constraint is again satisfied.

Finally, the performance of the IAE and ISE for both the full-power trajectory and the trajectory with a coasting strategy are, respectively, 9.1911 and 2.853, and 9.0569 and 2.8062.

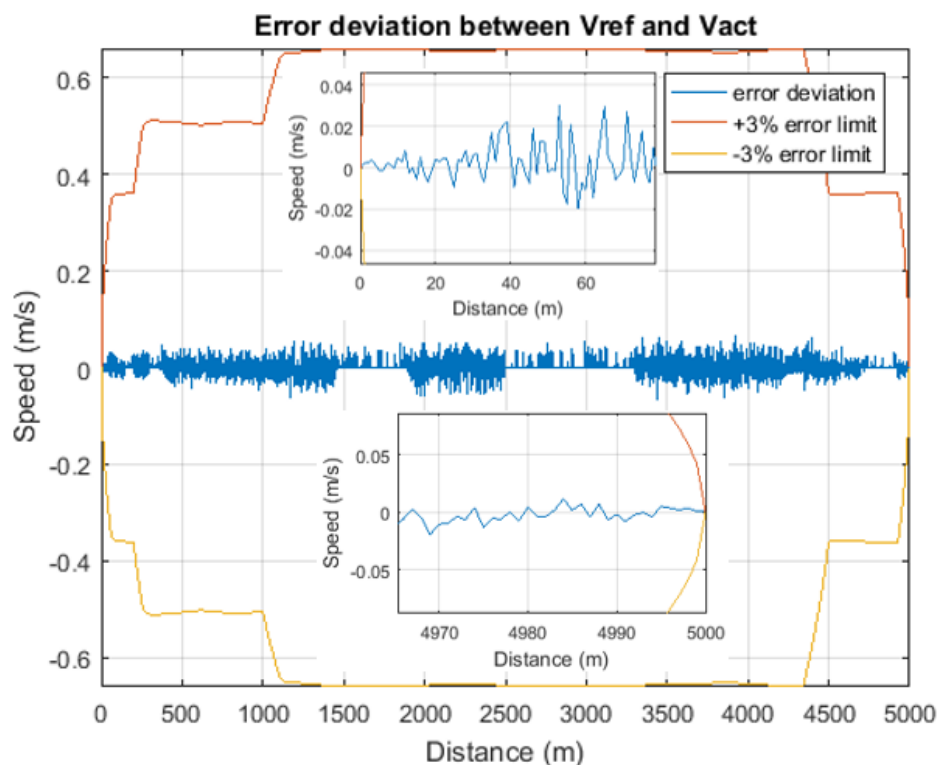


Figure 76 – Error deviation of noisy Fuzzy-PD with KF in full-power trajectory (Author, 2018)

6. Comparisons

The summary and comparisons of all tests in 4.4.3 are presented in Table 3 where $e_{3\%}$ and e_{Time} are the indices of the 3% error limit and the time deviation. First, only the Fuzzy-PD and Fuzzy-PD with the Kalman filter satisfy the $\pm 3\%$ error limit. However, remember that not only does the Fuzzy-PD with the Kalman filter comply with the index of the 3% error limit, but it also improves the results in a noisy environment. Secondly, all tests meet the time deviation index. '+' notation means later, while '-' notation means earlier. Thirdly, for the IAE and ISE, the PD yields an enormous number, especially for the full-power trajectory, whereas the Fuzzy-PD and Fuzzy-PD with the Kalman filter are almost the same, although the latter indicates superior results. Eventually, based on these results, only the Fuzzy-PD controller and the one with the Kalman filter are employed for the next chapter in the Case Study.

Table 3 – Comparison indices of artificial trajectory test

| Indices | Full-power Trajectory | | | |
|------------|--------------------------|-----------|----------------|------------------------|
| | PD | Fuzzy-PD | Noisy Fuzzy-PD | Noisy Fuzzy-PD with KF |
| $e_{3\%}$ | Unsatisfied | Satisfied | Unsatisfied | Satisfied |
| e_{Time} | -1.6375 | +0.13825 | +6.4074 | +0.023255 |
| IAE | 80.2453 | 11.8668 | Poor | 9.1911 |
| ISE | 80.6098 | 3.3069 | Poor | 2.853 |
| Indices | Trajectory with Coasting | | | |
| | PD | Fuzzy-PD | Noisy Fuzzy-PD | Noisy Fuzzy-PD with KF |
| $e_{3\%}$ | Unsatisfied | Satisfied | Unsatisfied | Satisfied |
| e_{Time} | -0.95353 | +0.14696 | +2.6211 | -0.0016816 |
| IAE | 49.7983 | 10.5027 | Poor | 9.0569 |
| ISE | 40.8824 | 3.1779 | Poor | 2.8062 |

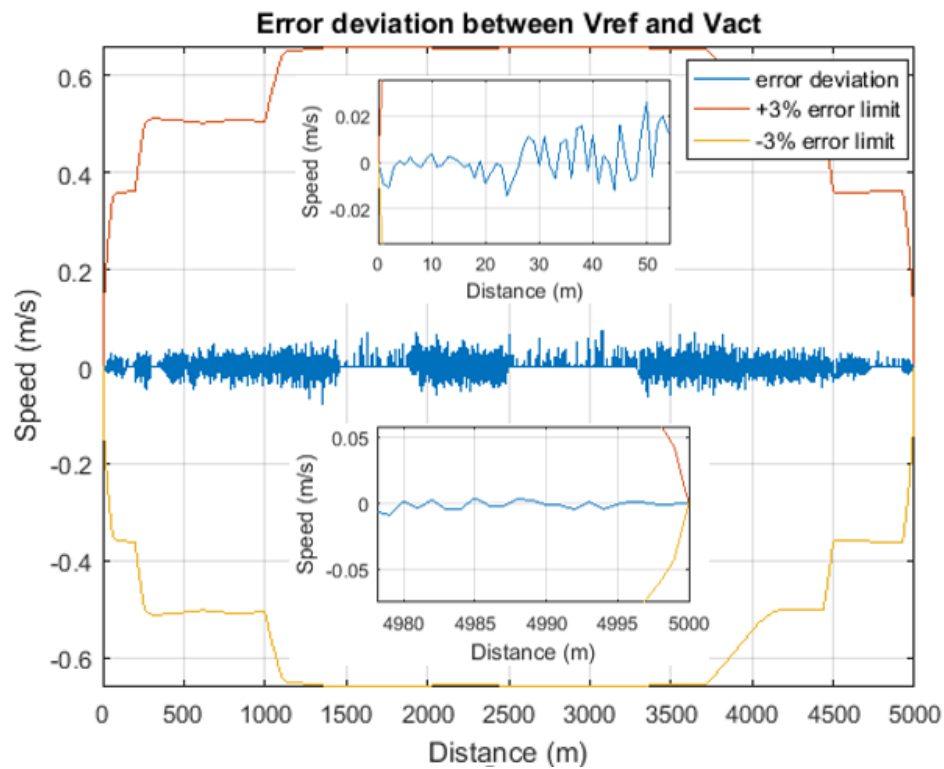


Figure 77 – Error deviation of noisy Fuzzy-PD with KF in trajectory with coasting (Author, 2018)

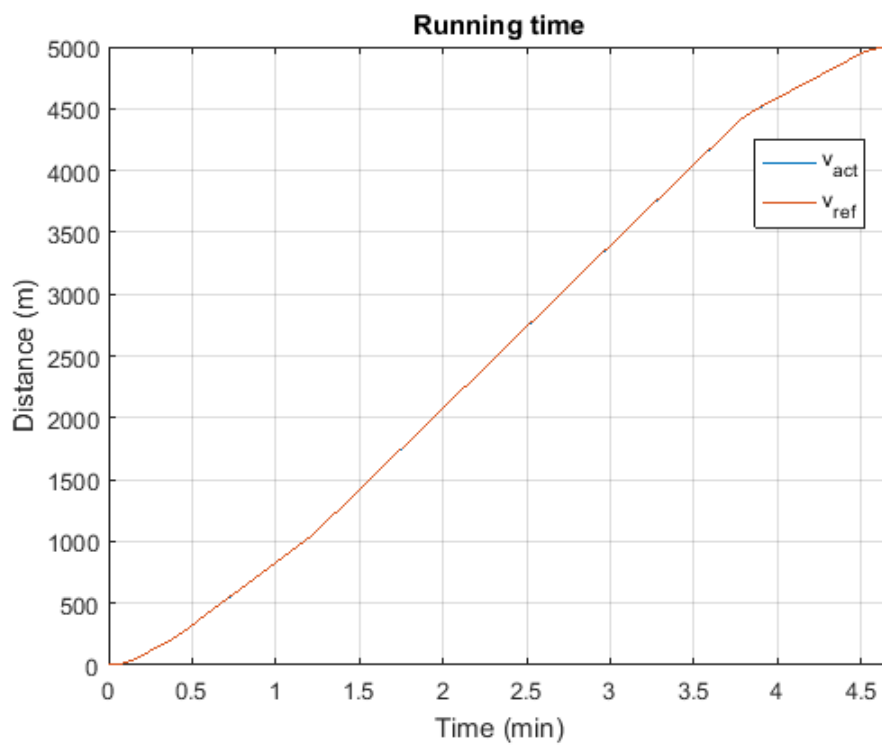


Figure 78 – Running time of noisy Fuzzy-PD with KF in full-power trajectory (Author, 2018)

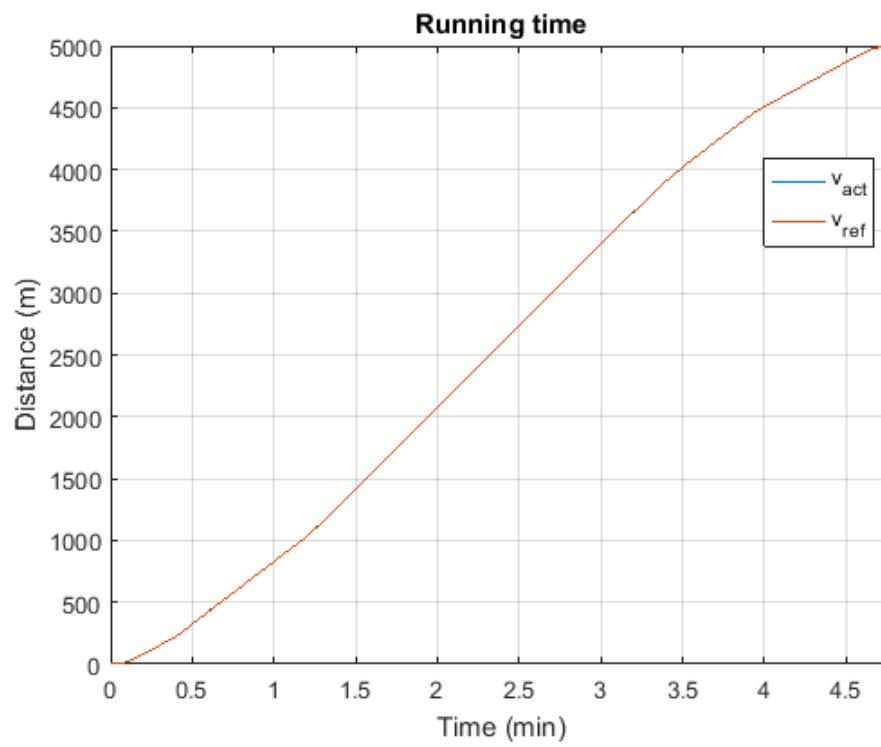


Figure 79 – Running time of noisy Fuzzy-PD with KF in trajectory with coasting (Author, 2018)

5 Case Study

In addition to examining the methods for an artificial train trajectory, a real case study is performed as well. Based on the actual data of the DLR directly from Transport for London (TfL), in this chapter, a DLR rolling stock and route are adopted to investigate the controller since the DLR operates at GoA3 (Keevill, 2016) which indeed consists of the ATP and ATO systems. The DLR rolling stock and its route are described. Based on the approach demonstrated in Chapter 4, the control design is executed to cope with the case study. Moreover, the results are shown and discussed based on the control objectives, as illustrated in subchapter 1.2.

5.1 Docklands Light Railway

Besides the DLR service, on the rail transport systems in Greater London provided by TfL, the Central Line, Jubilee Line, Northern Line and Victoria Line of London Underground also apply ATP and ATO systems, but these lines still require the driver to open and close the train doors and to initiate the motion of the train (Connor, 2015). In other words, these lines operate at GoA2 (Keevill, 2016). On the other hand, DLR implements a more sophisticated signalling system, resulting in it being the only line of TfL which has applied driverless train technology (GoA3 which requires a staff member to be on board, as shown in Figure 80) since it was first introduced to the public in 1987 (Pearce, Hardy, & Stannard, 2006).



Figure 80 – An on-board staff on DLR train (Author, 2017)

The DLR line is employed to evaluate the proposed control design. Figure 81 shows a DLR train preparing to depart from Stratford station. In the following subchapters, the information regarding DLR is described.



Figure 81 – DLR rolling stock (Author, 2017)

5.1.1 Rolling Stock Parameters

As the latest version of DLR rolling stock, B2007 Stock is selected for the case study. Figure 82 shows this type of stock physically in duty. The rolling stock parameters needed for the simulation are presented in Table 4.

Table 4 – B2007 Stock Information

| Parameters | Value | Parameters | Value |
|-----------------------------|------------------------------------------|--------------------------------|----------------------------|
| Total length of a car | 28.8 metres coupler face to coupler face | Maximum traction force | 65 kN |
| Total tare mass per car | 38.2 tonnes | Maximum/permitted acceleration | 1.4 m/s ² |
| Overload train mass per car | 57.3 tonnes | Maximum braking force | 206.3 kN (Emergency Brake) |
| Maximum speed | 80 km/h (22.2 m/s) | Service braking rate | −0.8 m/s ² |
| Maximum power per car | 4×130 kW | Emergency braking rate | −1.4 m/s ² |



Figure 82 – B2007 rolling stock (Rail Technology Magazine, 2017)

Exclusively for the maximum traction force parameter, the tractive effort and running resistance curve, approximate values are obtained from Kemp (1987). Figure 83 shows the tractive effort/speed curve of the DLR rolling stock. This shows two curves of traction connected to each other in the middle, caused by the fact that the DLR vehicle operates with two motors.

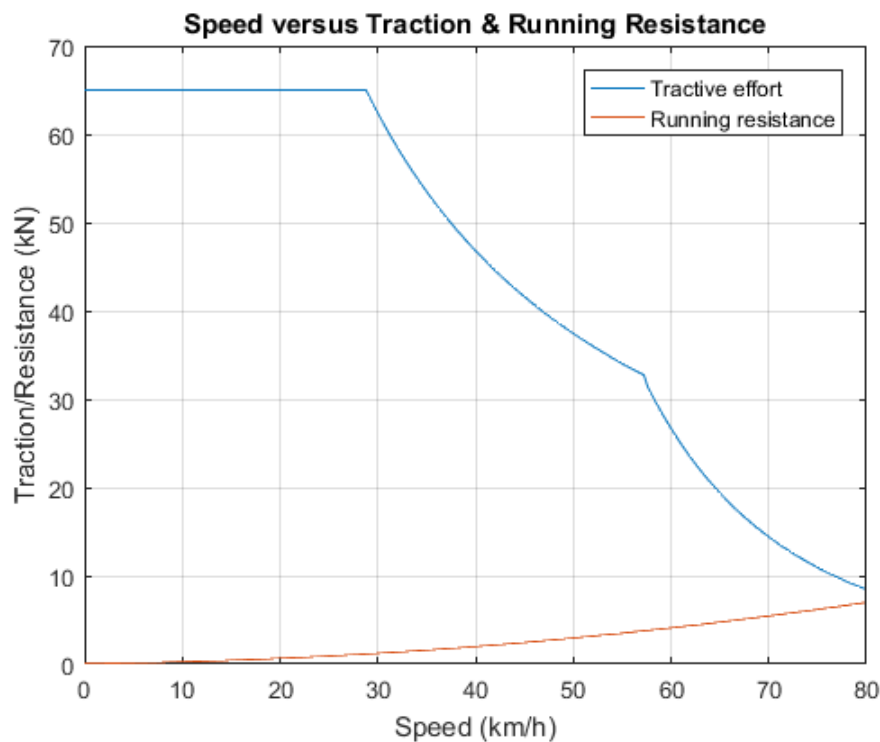


Figure 83 – Traction curve and running resistance of DLR rolling stock (Kemp, 1987)

5.1.2 Route Characteristics

As of December 2017, the DLR network serves five different two-way routes surrounding the Docklands area. Moreover, its primary depot is situated in Beckton, close to the Beckton DLR station. These routes are the following (TfL, 2015b)²⁶:

- Bank – Lewisham,
- Bank – Woolwich Arsenal,
- Stratford – Lewisham,
- Stratford International – Woolwich Arsenal,
- Tower Gateway – Beckton.

²⁶ The total number of stations located in each route can be seen in Figure 106 in Appendix B – DLR Route Map.

The route from Stratford International to Woolwich Arsenal²⁷ is utilised in this study. Figure 84 shows the platform at Stratford International station, whereas the platform at Woolwich Arsenal station is shown in Figure 85. Figure 86 shows the Google Map of the route. The route is located in east London and crosses the River Thames. Figure 87 illustrates the position of each station from Stratford International.



Figure 84 – Platform at Stratford International station (Author, 2017)

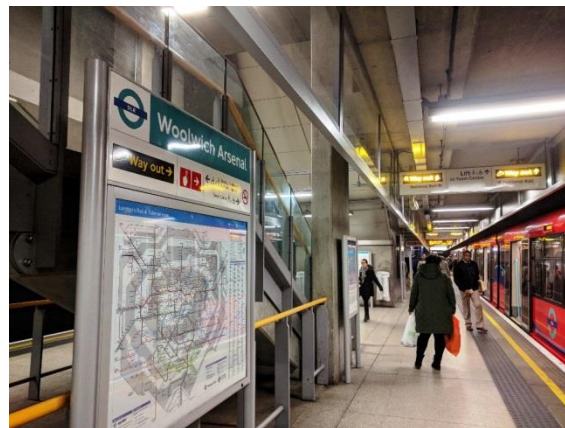


Figure 85 – Platform at Woolwich Arsenal station (Author, 2017)

²⁷ Its total length is 11.671 km with 12 stations counted from Stratford International to Woolwich Arsenal. The distance of each station from the station of Stratford International is the following: Stratford (1330 metres), Stratford High Street (1770 metres), Abbey Road (2408 metres), West Ham (3000 metres), Star Lane (3788 metres), Canning Town (4577 metres), West Silvertown (6274 metres), Pontonn Dock (7052 metres), London City Airport (8151 metres), King George V (9199 metres) and Woolwich Arsenal (11,671 metres).

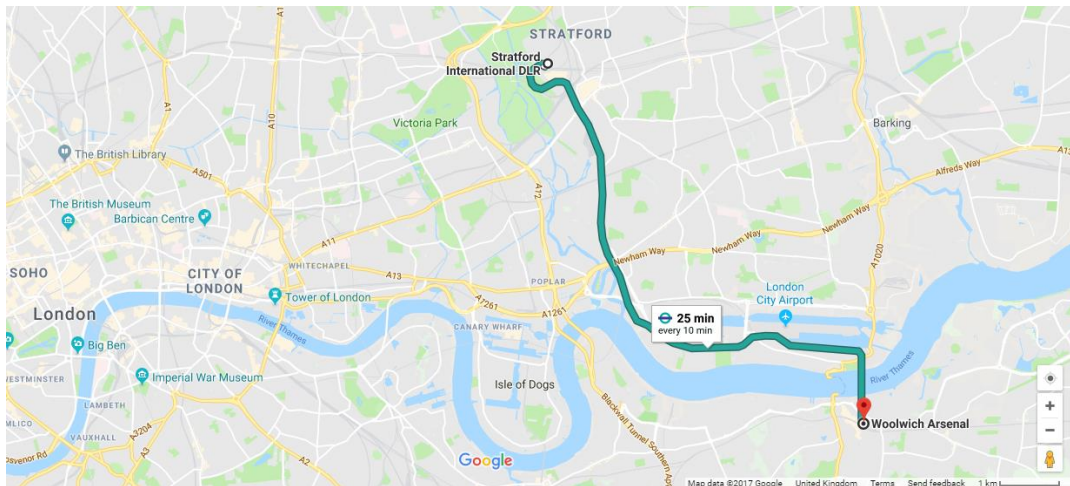


Figure 86 – Map of the route from Stratford Int'l to Woolwich Arsenal (Google Inc., n.d.)

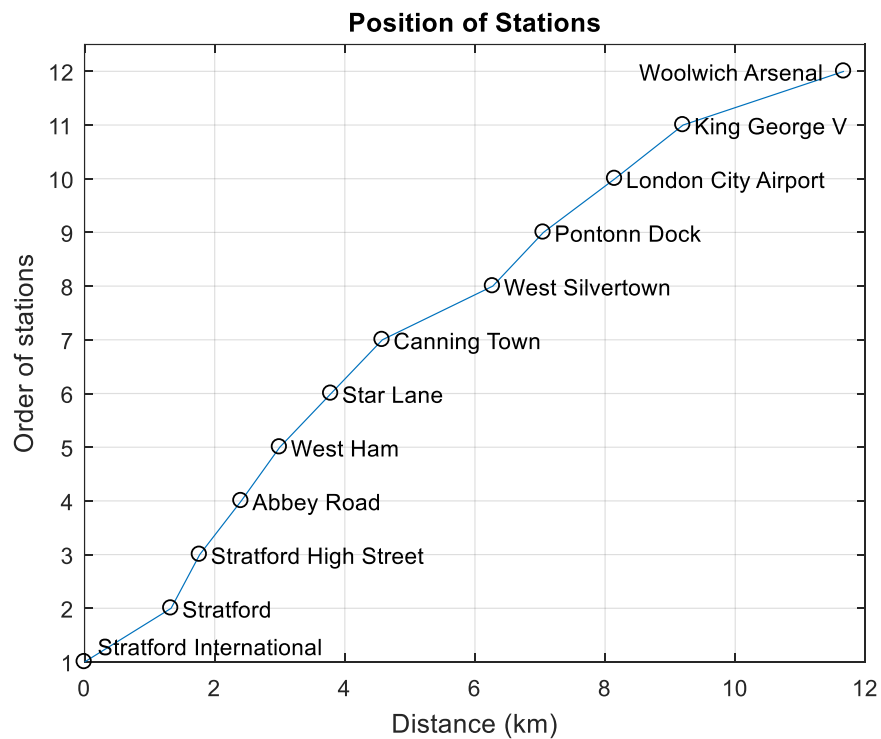


Figure 87 – Position of stations in the route from Stratford Int'l to Woolwich Arsenal (Author, 2017)

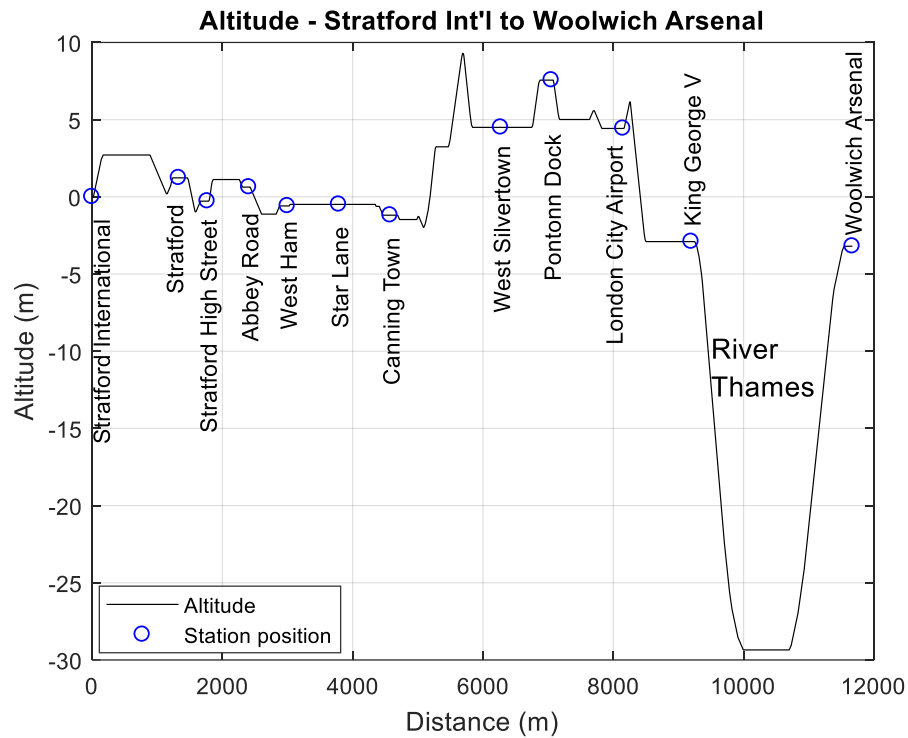


Figure 88 – Altitude of the route from Stratford International to Woolwich Arsenal (Author, 2017)

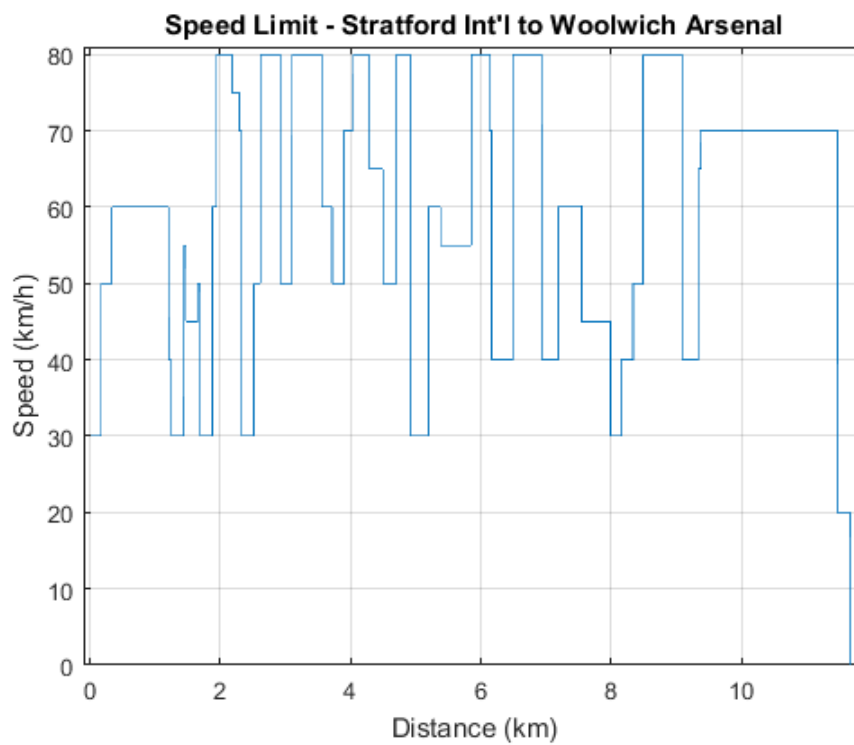


Figure 89 – Speed limit of the route from Stratford International to Woolwich Arsenal (Author, 2017)

In addition, the altitude of the route is shown in Figure 88. This shows that the DLR route has significant slopes, especially the major slope at a distance of around 10 km due to the tunnel under the River Thames. Using this figure, one could determine the gradient²⁸ of the route for every 1 metre and then calculate the gradient resistances.

The speed limit²⁹ applied by TfL to DLR on the route from Stratford International to Woolwich Arsenal is denoted by the black dashed line in Figure 89. Based on this line, one could generate the optimised train trajectory.

5.2 Controller Design

In this subchapter, the author defines the controller design used to comply with the route from Stratford International to Woolwich Arsenal. As analysed and discussed in 4.4, Fuzzy-PD gain scheduling is proven to be superior to the other controllers, in this case study therefore, only the Fuzzy-PD and that with the Kalman filter are employed to examine whether they are able to yield good resulting using real data.

5.2.1 Modification of Fuzzy Gain Scheduling of PD Controller

In general, for this case study, the way to design the controller is the same as in 4.2 and 4.3, except for some parameters, i.e. K_u , T_u , K_p , T_i and T_d . However, due to the complexity of the case study route, the author modifies the Fuzzy-PD gain scheduling to deal with the trajectories. Compared with the previous block diagram in Figure 28, the modified controllers, as shown in Figure 90, consider the train model as an integrated subsystem, i.e. traction, braking and train dynamics, although the model itself is not changed at all. This is merely for ease of the modified controllers.

²⁸ The figure regarding the gradient of the route in more detail can be seen in Figure 107 in Appendix C – Gradient and Speed Limit.

²⁹ The figure regarding the speed limit of the route in more detail can be seen in Figure 108 in Appendix C – Gradient and Speed Limit.

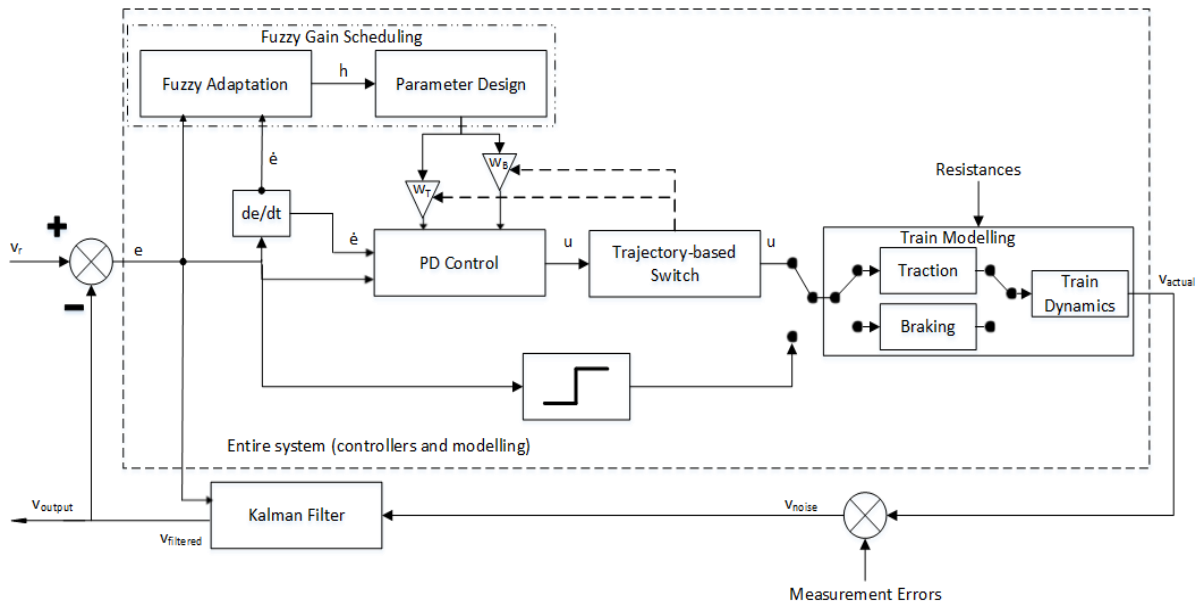


Figure 90 – Block diagram of train modelling and modified controllers (Author, 2017)

A new block, called the trajectory-based switch, is added. This component has two crucial functions, namely, first to switch the appropriate control signal from PD control to either traction or braking based on the behaviour of the trajectory used at that moment. For example, at the time when the trajectory is generated before being used by the ATO control system, besides the speed profiles, the trajectory also produces the combination of the forward and backward accelerations, as explained in 4.4.3. Then, the acceleration profiles can be utilised to decide when the PD control has to release either a positive or negative signal, as defined in Equation 54, where a_f and a_b are the forward and backward accelerations, respectively. This technique is more advantageous than leaving the PD to decide the signals itself, as it is usually poorly managed, because the acceleration profiles contain valuable data that can be used as a guide. Second, the switch continuously updates the weight blocks, i.e. w_T (traction weight) and w_B (braking weight) as defined in Equation 55, according to the acceleration profiles of the optimised trajectory. Therefore, the trigger for activating either w_T or w_B also takes place at the same time as the switch's first function, as formulated in Equation 56 which uses Equation 45.

Equation 54 – Trajectory-based switch (first function)

$$u(s) = \begin{cases} +; & a_f(s) \geq 0 \\ -; & a_b(s) > 0 \end{cases}$$

Remember that K_p in Equation 56 is applied only at $s \neq 0$ since at zero distance $s = 0$, $\alpha(0) = 0.5$ so that the equation uses its initial form as described in Equation 3. Moreover, when both a_f and a_b are zero, w_B is inactive, and then w_T is active with a value of 2.

Equation 55 – Definitions of traction and braking weights

$$w_T(s) = 2 + a_f(s)$$

$$w_B(s) = 1 + a_b(s)$$

Equation 56 - K_p in Equation 45 with traction and braking weights (second function)

$$K_p(s+1) = \begin{cases} 1.2 \cdot \alpha(s+1) \cdot K_u \cdot w_T(s); & a_f(s) \geq 0 \\ 1.2 \cdot \alpha(s+1) \cdot K_u \cdot w_B(s); & a_b(s) > 0 \end{cases}$$

5.2.2 Initial Parameters

Subsequently, before using the modified controllers, as usual, relay-based auto-tuning is employed. The step input, this time, is adjusted to 3, not 1, since in this case study, different parameters also lead to different system behaviours from that in 4.1.4. Then, based on Figure 91, parameters K_u , T_u , K_p , T_i and T_d are found to be 2.3, 0.95, 1.38, 0.477 and 0.12, respectively.

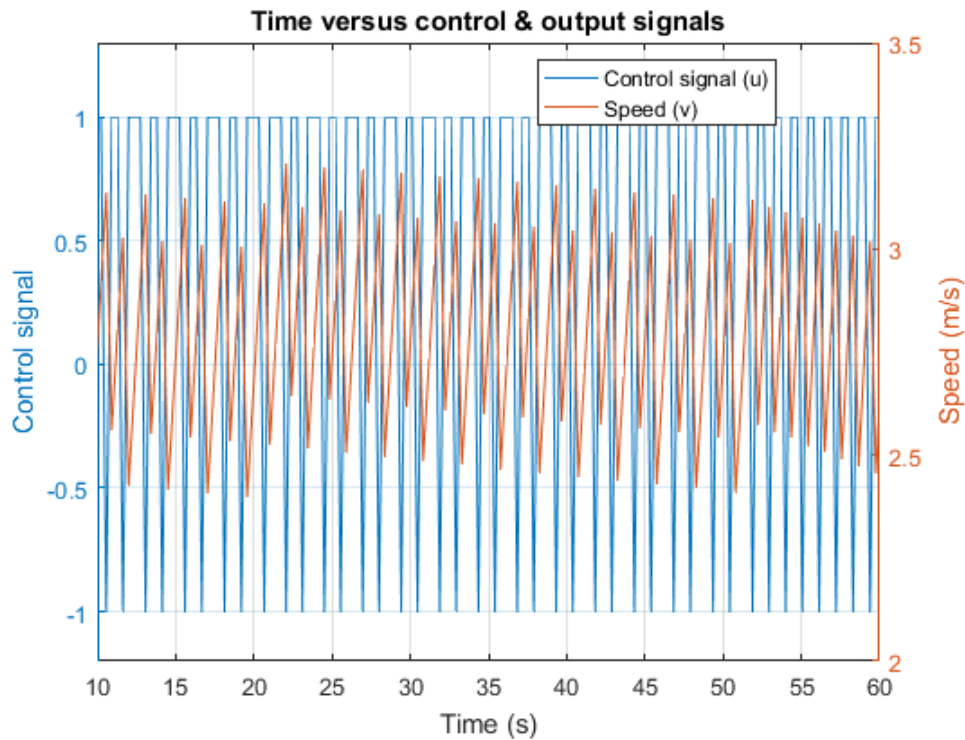


*Figure 91 – Plot chart of control and output signals with respect to time – case study
(Author, 2018)*

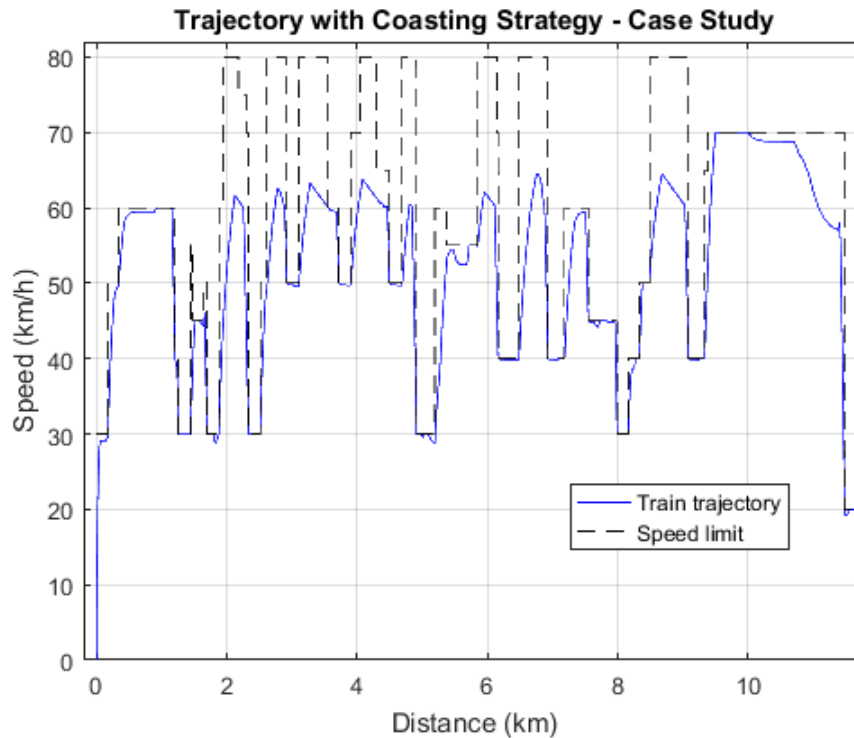


Figure 93 – Train trajectory with Coasting Strategy – case study (Author, 2018)

5.3.2 Results and Discussion

- Assessing Fuzzy Gain Scheduling Based PD Controller

The parameters used have been determined in 5.2. Figure 94 and Figure 95 denote the results for the full-power trajectory and the trajectory with coasting. In both figures, the modified controllers can cope with the error limit, even in a complex environment.

Figure 96 and Figure 97, show the running times for the full-power trajectory and the trajectory with coasting. Their maximum time of actual speed respectively are 879.6034 seconds, or 14.6601 minutes, or 2.0009 seconds later than the reference speed, so that time constraint is satisfied, and 884.6196 seconds, or 14.7437 minutes, or 1.232 seconds later than reference speed, so that the time constraint is satisfied.

Subsequently, the IAE and ISE performance for the full-power trajectory are 48.0497 and 7.3507, and they are 33.0713 and 5.4352, for the trajectory with coasting.

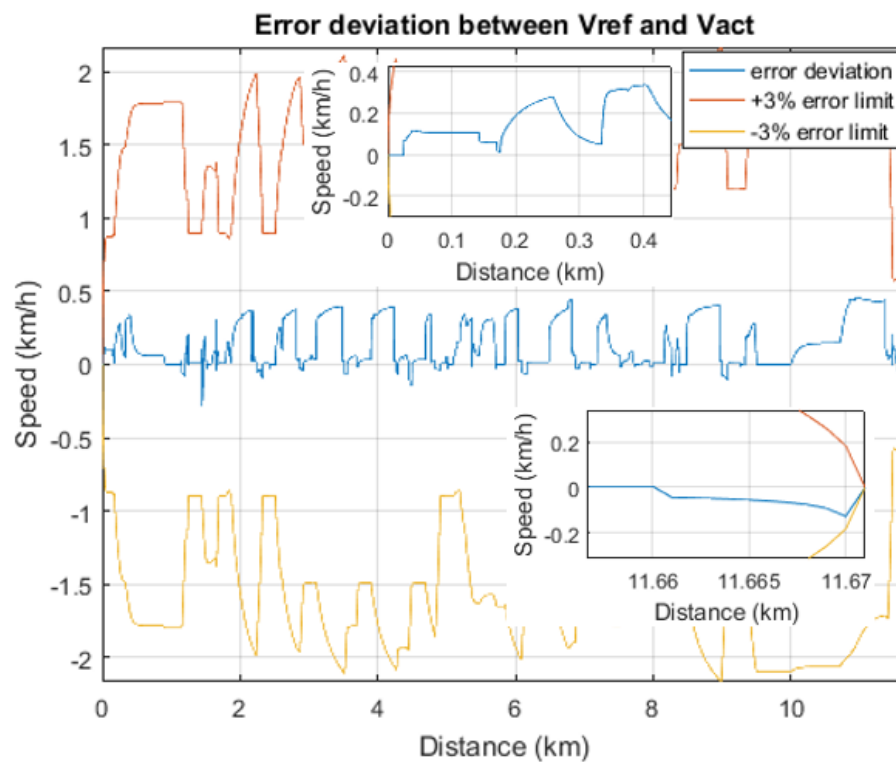


Figure 94 – Error deviation of Fuzzy-PD in full-power trajectory – case study (Author, 2018)

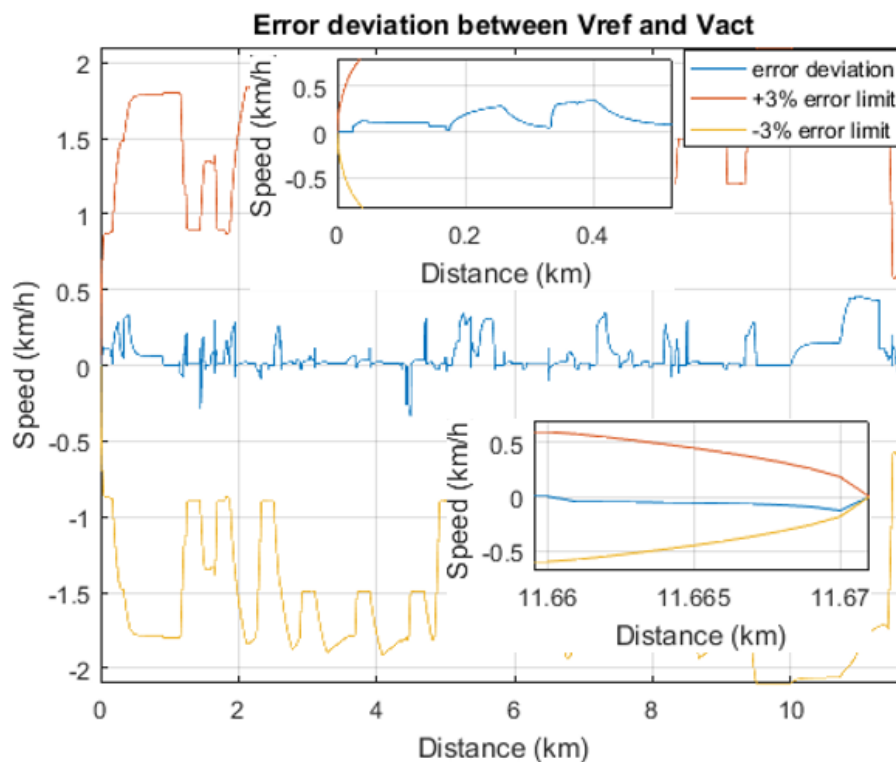


Figure 95 – Error deviation of Fuzzy-PD in trajectory with coasting – case study (Author, 2018)

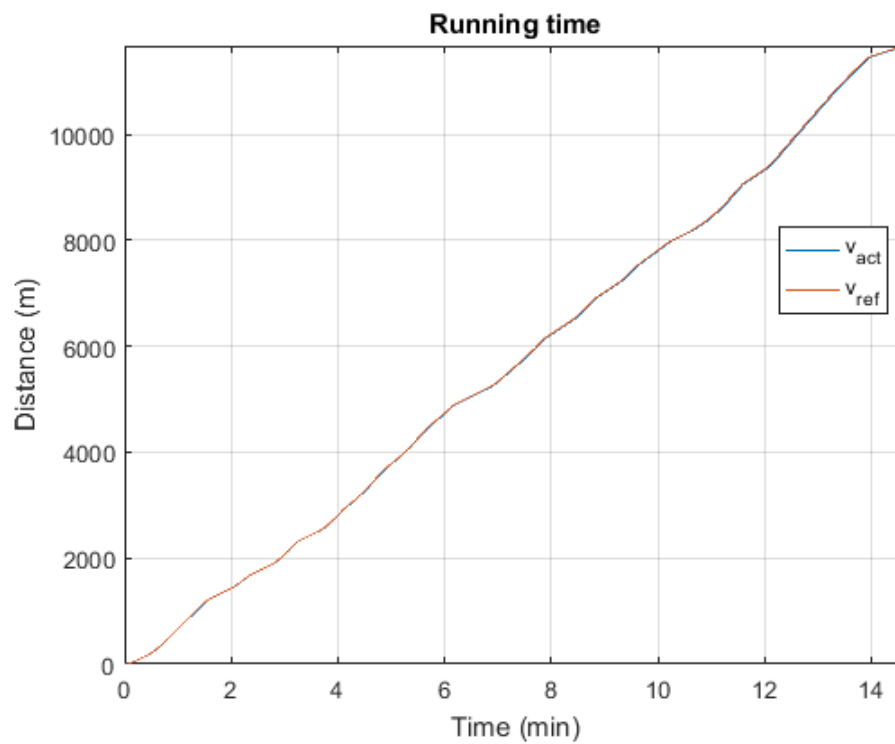


Figure 96 – Running time of Fuzzy-PD in full-power trajectory – case study (Author, 2018)

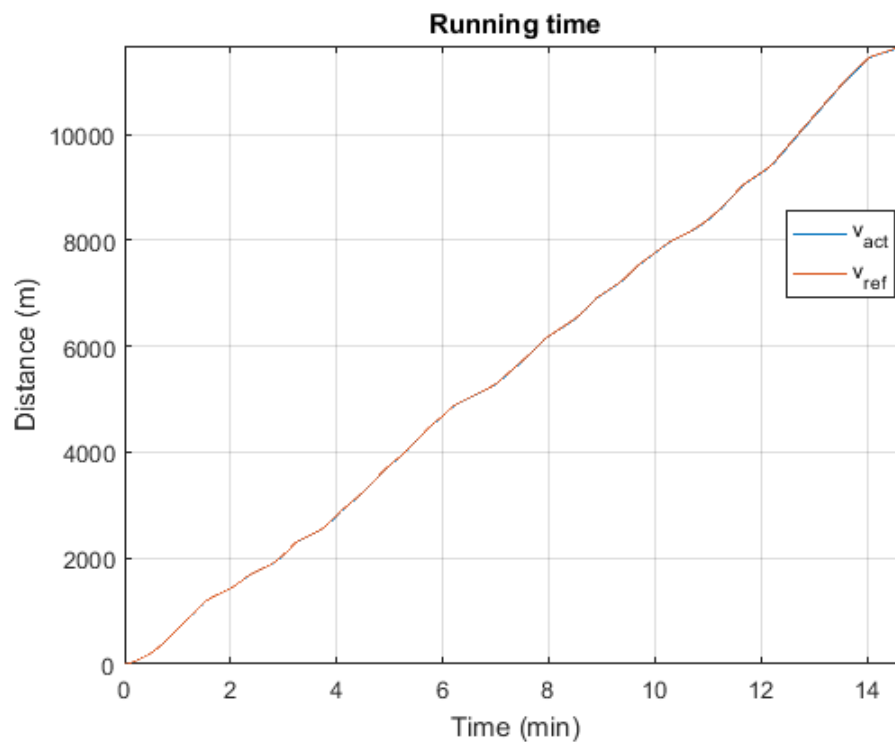


Figure 97 - Running time of Fuzzy-PD in trajectory with coasting – case study (Author, 2018)

- Implementing Measurement Errors and Kalman Filter

In this part, both adding measurement errors and implementing of the Kalman filter are presented in order to analyse their differences immediately. Moreover, as described previously, measurement noise and the Kalman filter are applied based on the same conditions as in 3.4.3, 3.4.4 and 4.3.

For error deviation both for the full-power trajectory and the trajectory with coasting, one can see, in Figure 98 and Figure 99, that naturally measurement noise devastates the actual data of the process output from which the controller is supplied to data with huge deviations. This condition, consequently, causes misinformation continuously and in loops. Fortunately, thanks to the Kalman filter, the noise can be significantly improved as shown in Figure 100 and Figure 101. The filtered output can facilitate the feedback of the controllers so that inaccurate information can be minimised. The noisy and filtered outputs are not presented in one figure since, when mixed, due to noise attenuation visually interrupting the display of the figure, the line of the filtered output is unable to be clearly seen, so that it is more convenient to see them separately.

Then, for the running time both for the full-power trajectory and the trajectory with coasting, the punctuality of the noisy system deviates far from that of the reference speed, namely 25.6829 seconds later (maximum time 903.2853 seconds or 15.0548 minutes) and 14.3324 seconds later (maximum time 897.7199 seconds or 14.962 minutes), respectively. This condition is one of the effects of the misinformation, as discussed earlier. However, as the time constraint is no later and no earlier than 30 seconds, the noisy system can still be classified as satisfying the time index. Subsequently, again, by implementing the Kalman filter, the system can be saved from the noisy environment so that not only is the time performance index satisfied, but also the running time can be reduced to a more acceptable time deviation value. The maximum times of actual speed both for the full-power trajectory and the trajectory with coasting are 877.6723 seconds, or 14.6279 minutes, or 0.069856 seconds later than the reference speed and 883.4535 seconds, or 14.7242 minutes, or 0.065964 seconds later than the reference speed, respectively.

Lastly, for the IAE and ISE performance of the noisy system, for both trajectories, these are not calculated because, again, their values are doubtless very large. The IAE and ISE performance of the filtered system for both trajectories are, respectively, 23.5872 and 4.0589, and 23.0153 and 4.0453.

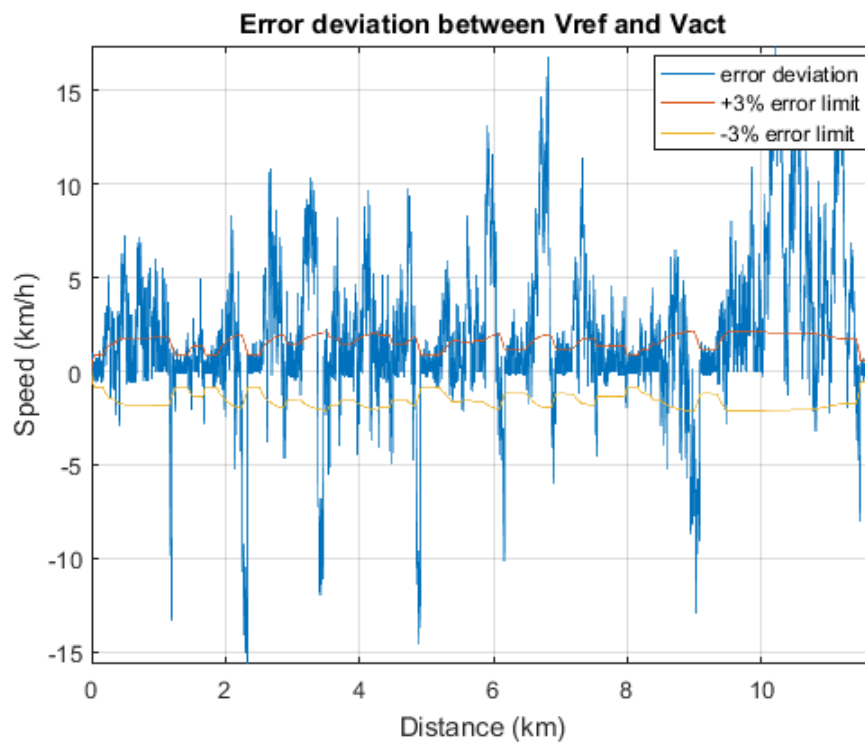


Figure 98 – Error deviation of noisy Fuzzy-PD in full-power trajectory – case study (Author, 2018)

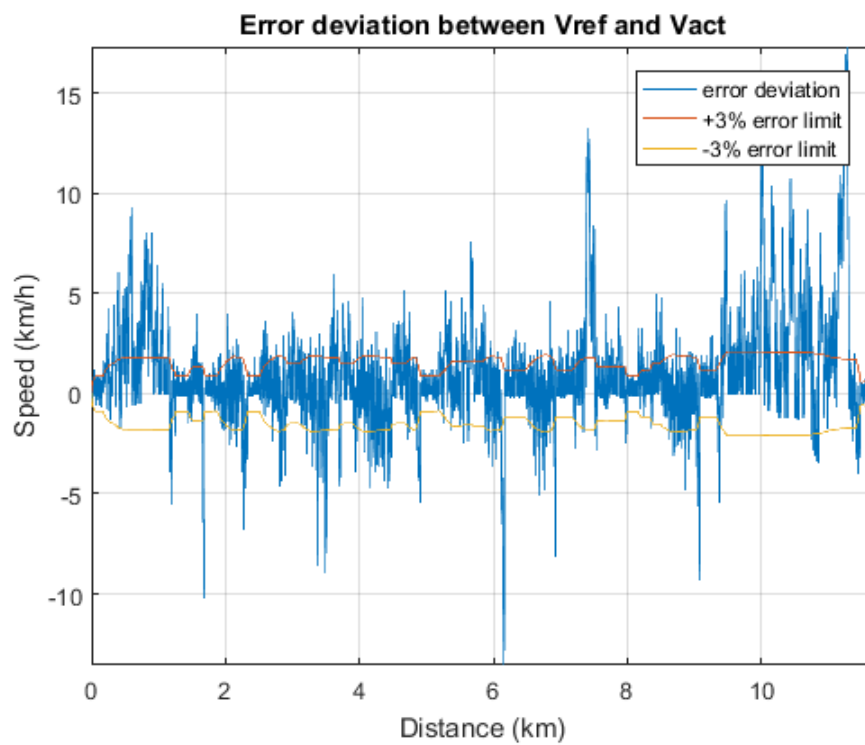


Figure 99 – Error deviation of noisy Fuzzy-PD in trajectory with coasting – case study (Author, 2018)

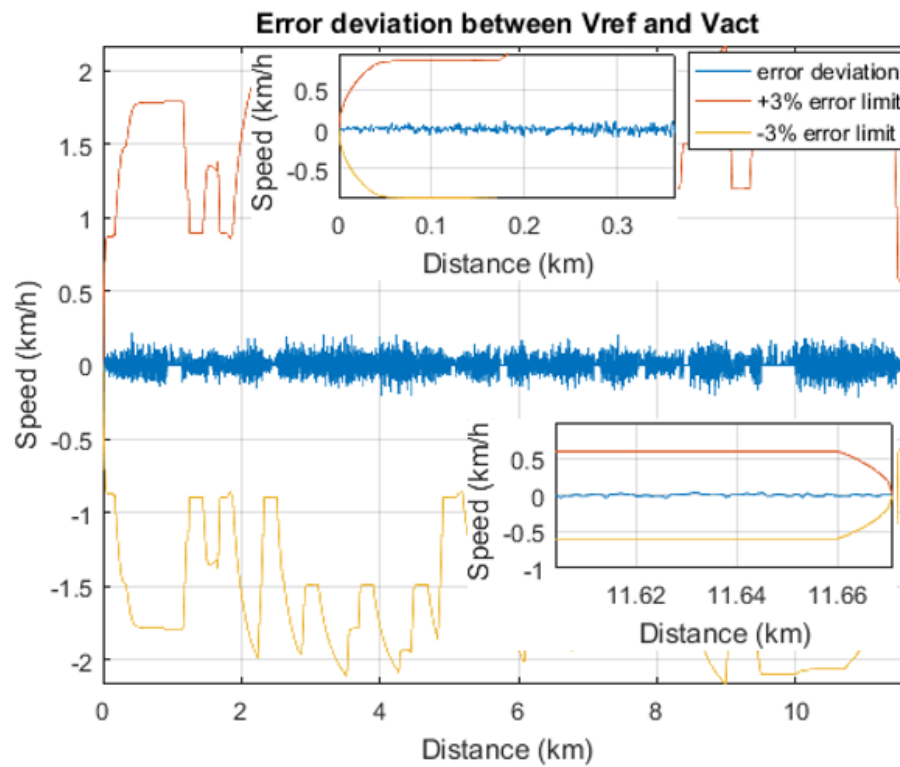


Figure 100 – Error deviation of noisy Fuzzy-PD with KF in full-power trajectory – case study
(Author, 2018)

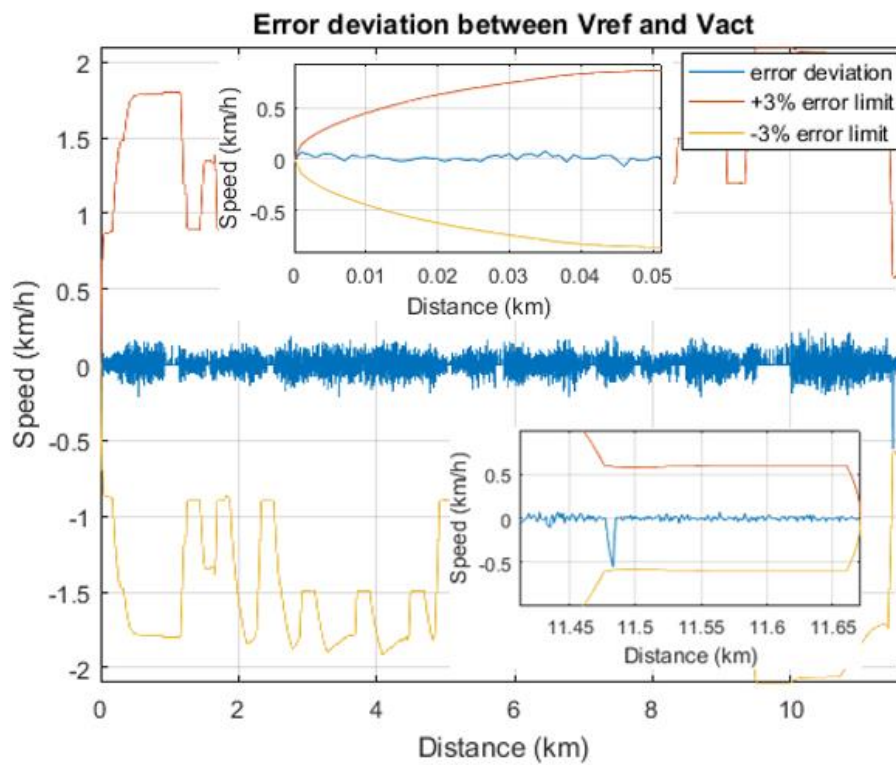


Figure 101 - Error deviation of noisy Fuzzy-PD with KF in trajectory with coasting – case study
(Author, 2018)

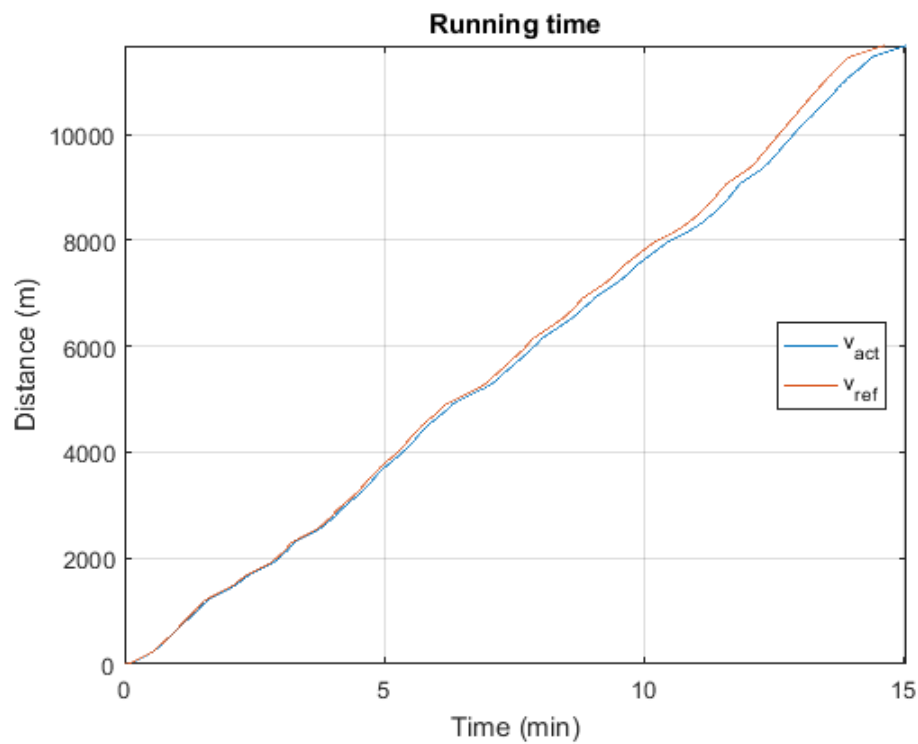


Figure 102 – Running time of noisy Fuzzy-PD in full-power trajectory – case study (Author, 2018)

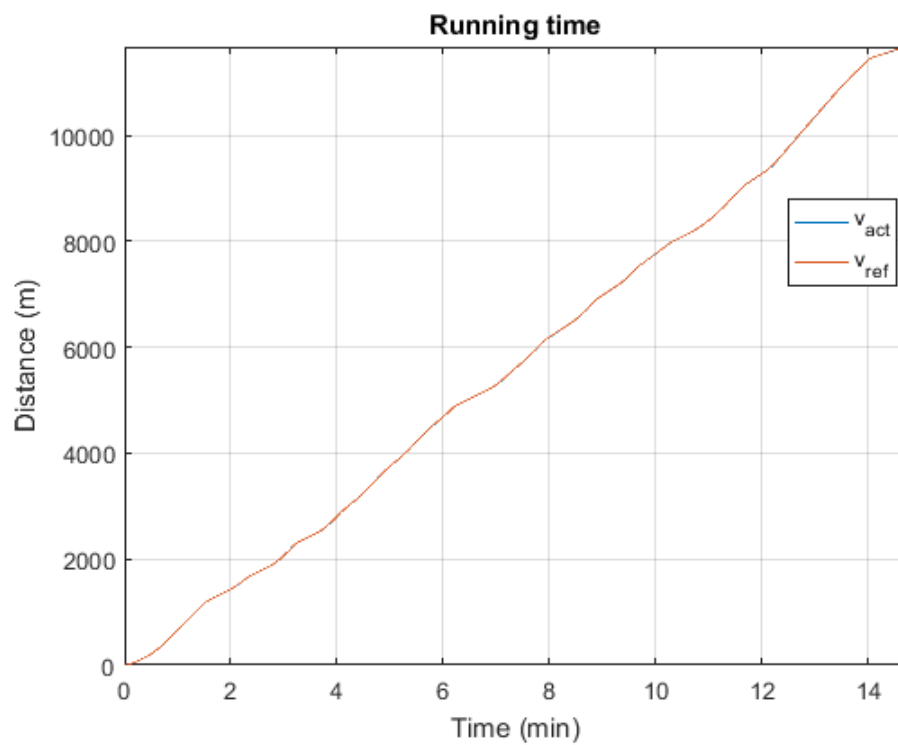


Figure 103 – Running time of noisy Fuzzy-PD with KF in full-power trajectory – case study (Author, 2018)

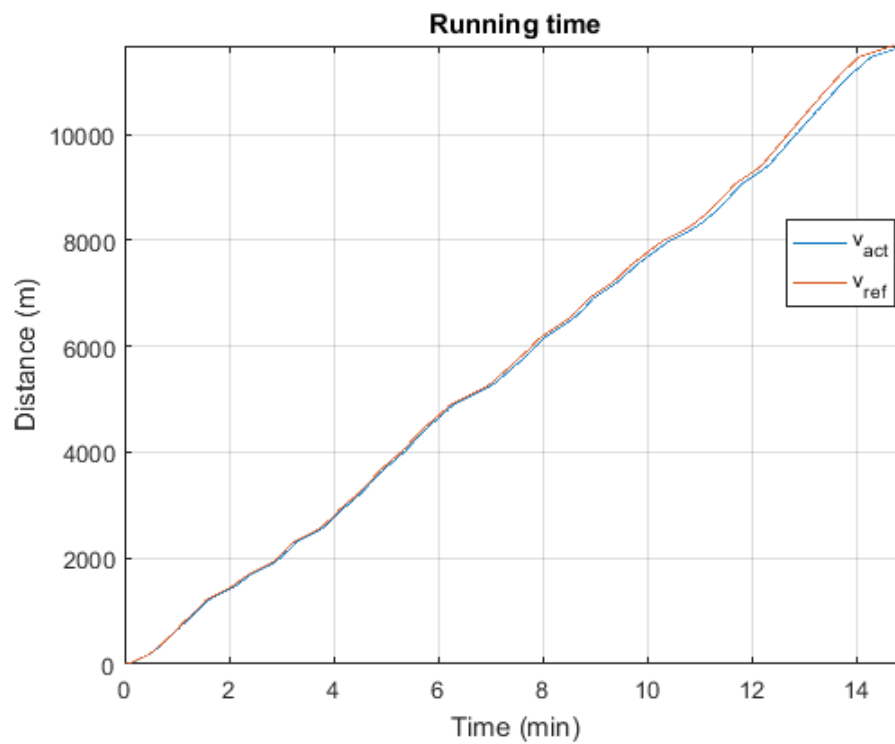


Figure 104 – Running time of noisy Fuzzy-PD in trajectory with coasting – case study (Author, 2018)

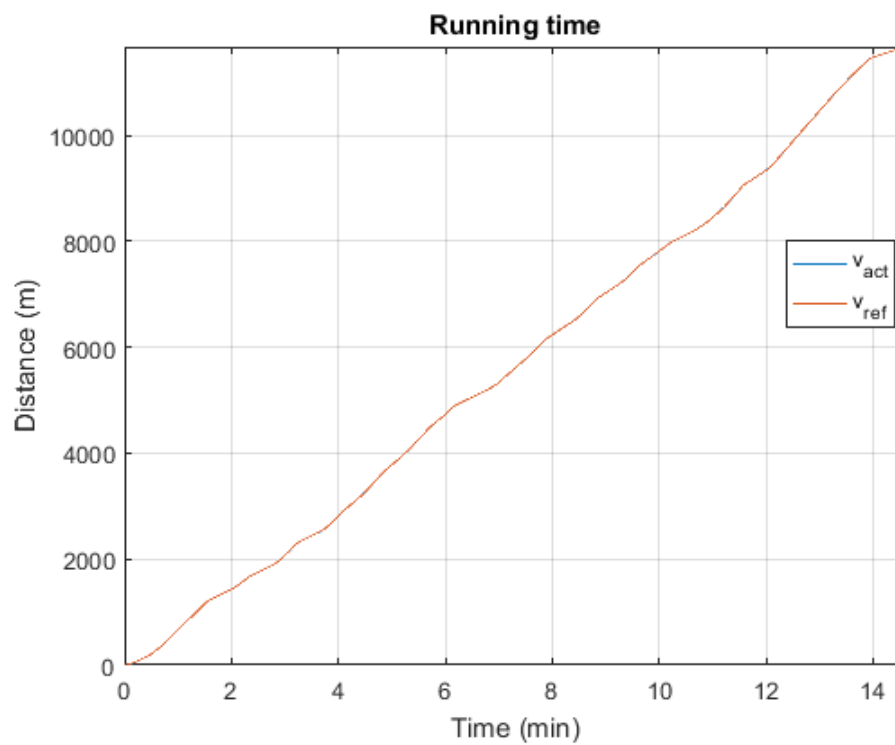


Figure 105 – Running time of noisy Fuzzy-PD with KF in trajectory with coasting – case study (Author, 2018)

- Comparisons

All four performance indices are used to evaluate the performance of each method. As with the results from 4.4.3, doubtless the noisy system indicates poor results, and in this case study, one can see that, due to the noise, it shows the worst results in regard to all indices and trajectories. Meanwhile, the Fuzzy-PD can cope with all indices with satisfactory performance. However, the Fuzzy-PD with the Kalman filter, on the other hand, is slightly superior to the Fuzzy-PD, especially in the indices of time deviation and IAE.

Table 5 – Comparison indices of case study

| Indices | Full-power Trajectory | | |
|------------|--------------------------|----------------|------------------------|
| | Fuzzy-PD | Noisy Fuzzy-PD | Noisy Fuzzy-PD with KF |
| $e_{3\%}$ | Satisfied | Unsatisfied | Satisfied |
| e_{Time} | +2.0009 | +25.6829 | +0.069856 |
| IAE | 48.0497 | Poor | 23.5872 |
| ISE | 7.3507 | Poor | 4.0589 |
| Indices | Trajectory with Coasting | | |
| | Fuzzy-PD | Noisy Fuzzy-PD | Noisy Fuzzy-PD with KF |
| $e_{3\%}$ | Satisfied | Unsatisfied | Satisfied |
| e_{Time} | +1.232 | +14.3324 | +0.065964 |
| IAE | 33.0713 | Poor | 23.0153 |
| ISE | 5.4352 | Poor | 4.0453 |

6 Conclusions

To summarise this thesis, the conclusions are divided into two parts: findings and recommendations. Findings include the summary of research contributions in order to respond to the aim and objectives and to answer the research questions. Subsequently, in recommendations, all improvements that can be undertaken to enhance the quality of this thesis and for future works are listed.

6.1 Findings

- Measurement error is scarcely considered in ATO control systems in previous works;
- The mathematical model of the train has been modelled and implemented.
- The Fuzzy-PD gain scheduling assisted by the Kalman filter can meet: (1) following the predefined trajectory, (2) satisfying a speed tracking error of less than 3%, (3) complying a punctuality of no less more 30 seconds early and no more than 30 seconds late from the trajectory running time, and (4) showing superior IAE and ISE performances compared to conventional controllers.
- The Gaussian white noise of 5% measurement errors has been added to the system output to resemble noisy environments of an instrumentation device.
- The Kalman filter has been introduced to improve the controllers to cope with noisy speed profile.
- The DLR route from Stratford International to Woolwich Arsenal and B2007 Stock have been implemented as a real case study.
- After assisted by the Fuzzy gain scheduling, PD control can cope with all tests in normal conditions, but not in noisy situations.
- By implementing the Kalman filter, an algorithmic estimator, Fuzzy-PD can be improved to overcome all tests in normal and noisy conditions. The design method of the Kalman filter in order to assist Fuzzy-PD has also been presented in 3.4.4 and 4.3.2.
- The DLR is selected to represent real train environments in order to assess the control design since it is considered to have a GoA3 system which implements the ATO system.

6.2 Recommendations

- An anti-windup controller should be designed to overcome actuator saturation.
- The error constraint should be restricted tighter.

- The controller should consider other factors, such as the TASC system and other inputs, e.g. running resistance, gradient, tunnel resistance, curvature resistance and so on.
- The implemented fuzzy controller should be improved, for example, by applying type-2 Fuzzy sets and ANFIS.
- The implemented Kalman filter should be improved, possibly by applying the unscented Kalman filter approach or by improving the controller to deal with such noise directly without any filter.
- The future research may be combined with the research of ATO speed profile optimisation, particularly moving block or CBTC system, to achieve more criteria, e.g. energy efficiency and passenger comfort.
- The future research should consider multi-point mass or cascade mass point of the train for train modelling and the cases in which each carriage has a variable load mass.
- Position tracking should also be considered.
- In order to examine the proposed idea, the future research should be applied not only to a simulation-based case study but also to a real application.

7 List of References

- Ahn, K. K., & Truong, D. Q. (2009). Online tuning fuzzy PID controller using robust extended Kalman filter. *Journal of Process Control*, 19(6), 1011-1023. doi:<https://doi.org/10.1016/j.procont.2009.01.005>
- Ahrens, J. H., & Khalil, H. K. (2009). High-gain observers in the presence of measurement noise: A switched-gain approach. *Automatica*, 45(4), 936-943. doi:<https://doi.org/10.1016/j.automatica.2008.11.012>
- Allotta, B., Colla, V., & Malvezzi, M. (2002). Train position and speed estimation using wheel velocity measurements. *Proceedings of the Institution of Mechanical Engineers, Part F: Journal of Rail and Rapid Transit*, 216(3), 207-225. doi:10.1243/095440902760213639
- Alstom. (2012). Urbalis™ CBTC Solution - Performance You Can Rely on. In Alstom (Ed.): Alstom.
- Astrom, K. J., & Hagglund, T. (1984, 12-14 Dec. 1984). *A frequency domain method for automatic tuning of simple feedback loops*. Paper presented at the The 23rd IEEE Conference on Decision and Control, Las Vegas.
- Åström, K. J., & Häggglund, T. (1984a). Automatic Tuning of Simple Regulators. *IFAC Proceedings Volumes*, 17(2), 1867-1872. doi:[https://doi.org/10.1016/S1474-6670\(17\)61248-5](https://doi.org/10.1016/S1474-6670(17)61248-5)
- Åström, K. J., & Häggglund, T. (1984b). Automatic tuning of simple regulators with specifications on phase and amplitude margins. *Automatica*, 20(5), 645-651. doi:[https://doi.org/10.1016/0005-1098\(84\)90014-1](https://doi.org/10.1016/0005-1098(84)90014-1)
- Åström, K. J., & Häggglund, T. (1995). *PID Controllers: Theory, Design, and Tuning* (Vol. 2). Research Triangle Park, NC: Instrument Society of America.
- Åström, K. J., & Häggglund, T. (2006). *Advanced PID Control*: ISA-The Instrumentation, Systems, and Automation Society.
- Åström, K. J., & Murray, R. M. (2008). *Feedback Systems: An Introduction for Scientists and Engineers*. Woodstock: Princeton University Press.
- Ball, A. A., & Khalil, H. K. (2008, 9-11 Dec. 2008). *High-gain observers in the presence of measurement noise: A nonlinear gain approach*. Paper presented at the 2008 47th IEEE Conference on Decision and Control.
- Bavdekar, V. A., Deshpande, A. P., & Patwardhan, S. C. (2011). Identification of process and measurement noise covariance for state and parameter estimation using extended Kalman filter. *Journal of Process Control*, 21(4), 585-601. doi:<https://doi.org/10.1016/j.procont.2011.01.001>
- Bing, G., Hairong, D., & Yanxin, Z. (2009, 14-16 Aug. 2009). *Speed Adjustment Braking of Automatic Train Operation System Based on Fuzzy-PID Switching Control*. Paper presented at the 2009 Sixth International Conference on Fuzzy Systems and Knowledge Discovery.
- Bombardier. (2017). INNOVIA APM 200 – London Heathrow Airport, UK. Retrieved from <http://uk.bombardier.com/en/transportation/presence-in-country/projects/project.innovia-london-uk.html>
- Britannica Educational Publishing. (2012). *The Complete History of Railroads: Trade, Transport, and Expansion* (R. Curley Ed. First ed.): Britannica Educational Publishing.

- Bryc, W. (1995). *The Normal Distribution*. In *Lecture Notes in Statistics*, Vol. 100. *Characterizations with Applications* (pp. VIII, 139). Retrieved from <http://www.springer.com/gb/book/9780387979908>
- Buonaccorsi, J. P. (2010). *Measurement Error: Models, Methods, and Applications*. In *Chapman & Hall/CRC Interdisciplinary Statistics*, (pp. 464). Retrieved from <https://www.taylorfrancis.com/books/9781420066586>
- Carvajal-Carreño, W. (2017). *Efficient Driving of CBTC ATO Operated Trains*. (Doctor), Comillas Pontifical University, Delft University of Technology, KTH Royal Institute of Technology, Madrid. Retrieved from <https://repository.tudelft.nl/islandora/object/uuid%3A9c1f1489-84fc-47cf-b889-ddbe3b87862f>
- Carvajal-Carreño, W., Cucala, A. P., & Fernández-Cardador, A. (2014). Optimal design of energy-efficient ATO CBTC driving for metro lines based on NSGA-II with fuzzy parameters. *Engineering Applications of Artificial Intelligence*, 36, 164-177. doi:10.1016/j.engappai.2014.07.019
- Carvajal-Carreño, W., García, A. P. C., Fernández-Cardador, A., & Söder, L. (2015, 3-5 June 2015). *Efficient driving algorithms for non-disturbed and disturbed trains with the CBTC signalling system*. Paper presented at the 2015 International Conference on Models and Technologies for Intelligent Transportation Systems (MT-ITS).
- Chang, C., Jia, L., Xu, N., & Zhang, X. (1996). The Application of Fuzzy Control To Automatic Train Operation. *IFAC Proceedings Volumes*, 29(1), 7674-7679. doi:[http://dx.doi.org/10.1016/S1474-6670\(17\)58925-9](http://dx.doi.org/10.1016/S1474-6670(17)58925-9)
- Chang, C. S., & Sim, S. S. (1997). Optimising train movements through coast control using genetic algorithms. *IEE Proc.: Electr. Power Appl.*, 144, 65.
- Chen, G., & Pham, T. T. (2000). *Introduction to Fuzzy Sets, Fuzzy Logic, and Fuzzy Control Systems*. In (pp. 328). Retrieved from <https://www.taylorfrancis.com/books/9781420039818>
- Chen, L. (2017). *Railway Automation 1: Driver Assist and ATP Systems*. Lecture slides. Birmingham Centre for Railway Research and Education. University of Birmingham.
- Colla, V., Vannucci, M., Allottay, B., & Malvezziy, M. (2003). Estimation of train speed via neuro-fuzzy techniques. In J. Mira & J. R. Álvarez (Eds.), *Artificial Neural Nets Problem Solving Methods: 7th International Work-Conference on Artificial and Natural Neural Networks, IWANN2003 Maó, Menorca, Spain, June 3–6, 2003 Proceedings, Part II* (pp. 497-503). Berlin, Heidelberg: Springer Berlin Heidelberg.
- Connor, P. (2015). *The London Underground Electric Train*. Marlborough, UK: The Crowood Press Ltd.
- Cui, K., & Dong, D. (2018). Train Speed Measurement and Position Identification Approach Based on Confidence Interval. *Cictp 2017*. doi:doi:10.1061/9780784480915.217
- Daiss, A., & Kiencke, U. (1995, 28-29 Sep 1995). *Estimation of vehicle speed fuzzy-estimation in comparison with Kalman-filtering*. Paper presented at the Proceedings of International Conference on Control Applications.
- Davies, S. D. (2000). *Automatic Train Protection for the Railway Network in Britain - A Study* (ISBN 1 871634 88 1). Retrieved from London: http://www.railwaysarchive.co.uk/documents/RAE_ATP2000.pdf

- Dequan, S., Guili, G., Zhiwei, G., & Peng, X. (2012). Application of Expert Fuzzy PID Method for Temperature Control of Heating Furnace. *Procedia Engineering*, 29(Supplement C), 257-261. doi:<https://doi.org/10.1016/j.proeng.2011.12.703>
- Domínguez, M., Fernández-Cardador, A., Cucala, A. P., Gonsalves, T., & Fernández, A. (2014). Multi objective particle swarm optimization algorithm for the design of efficient ATO speed profiles in metro lines. *Engineering Applications of Artificial Intelligence*, 29, 43-53. doi:10.1016/j.engappai.2013.12.015
- Dong, H., Gao, S., Ning, B., & Li, L. (2011a). Extended fuzzy logic controller for high speed train. *Neural Computing and Applications*, 22(2), 321-328. doi:10.1007/s00521-011-0681-8
- Dong, H., Gao, S., Ning, B., & Li, L. (2011b, 22-24 July 2011). *Modeling and simulation of automatic train operation system based on self-regulating fuzzy algorithm*. Paper presented at the Proceedings of the 30th Chinese Control Conference.
- Dong, H., Li, L., & Ning, B. (2010, 20-23 June 2010). *Fuzzy switch of high-speed ATO systems based on running conditions*. Paper presented at the The 2010 IEEE International Conference on Information and Automation.
- Dong, H., Li, L., Ning, B., & Hou, Z. (2010, 29-31 July 2010). *Fuzzy tuning of ATO system in train speed control with multiple working conditions*. Paper presented at the Proceedings of the 29th Chinese Control Conference.
- Dong, H., Lin, X., Yao, X., Bai, W., & Ning, B. (2017). Composite Disturbance-Observer-Based Control and \mathcal{H}^∞ Control for High Speed Trains with Actuator Faults. *Asian Journal of Control*, n/a-n/a. doi:10.1002/asjc.1590
- Dong, H., Ning, B., Cai, B., & Hou, Z. (2010). Automatic Train Control System Development and Simulation for High-Speed Railways. *IEEE Circuits and Systems Magazine*, 10(2), 6-18. doi:10.1109/mcas.2010.936782
- Dounis, A. I., Kofinas, P., Alafodimos, C., & Tseles, D. (2013). Adaptive fuzzy gain scheduling PID controller for maximum power point tracking of photovoltaic system. *Renewable Energy*, 60, 202-214. doi:<http://dx.doi.org/10.1016/j.renene.2013.04.014>
- Faieghi, M., Jalali, A., & Mashhadi, S. K.-e.-d. M. (2014). Robust adaptive cruise control of high speed trains. *ISA Transactions*, 53(2), 533-541. doi:<https://doi.org/10.1016/j.isatra.2013.12.007>
- Fangjun, J., & Zhiqiang, G. (2000, 2000). *An adaptive nonlinear filter approach to the vehicle velocity estimation for ABS*. Paper presented at the Proceedings of the 2000. IEEE International Conference on Control Applications. Conference Proceedings (Cat. No.00CH37162).
- Faragher, R. (2012). Understanding the Basis of the Kalman Filter Via a Simple and Intuitive Derivation [Lecture Notes]. *IEEE Signal Processing Magazine*, 29(5), 128-132. doi:10.1109/MSP.2012.2203621
- Fenner, D. (2002). Train protection. *IEE Review*, 48(5), 29-33. doi:10.1049/ir:20020504
- Franke, R., Terwiesch, P., & Meyer, M. (2000, 2000). *An algorithm for the optimal control of the driving of trains*. Paper presented at the Proceedings of the 39th IEEE Conference on Decision and Control (Cat. No.00CH37187).
- Fu, Y., Yang, H., & Wang, D. (2017a). Real-time optimal control of tracking running for high-speed electric multiple unit. *Information Sciences*, 376(Supplement C), 202-215. doi:<https://doi.org/10.1016/j.ins.2016.10.024>

- Fu, Y., Yang, H., & Wang, D. (2017b). Real-time optimal control of tracking running for high-speed electric multiple unit. *Information Sciences*, 376, 202-215. doi:<https://doi.org/10.1016/j.ins.2016.10.024>
- Gao, S., Dong, H., Chen, Y., Ning, B., & Chen, G. (2013). Adaptive and robust automatic train control systems with input saturation. *Control and Intelligent Systems*, 41(2), 103-111. doi:10.2316/Journal.201.2013.2.201-2451
- Gao, S., Dong, H., Ning, B., Roberts, C., & Chen, L. (2016). Neural adaptive coordination control of multiple trains under bidirectional communication topology. *Neural Computing and Applications*, 27(8), 2497-2507. doi:10.1007/s00521-015-2020-y
- Geistler, A., & Bohringer, F. (2004, 14-17 June 2004). *Robust velocity measurement for railway applications by fusing eddy current sensor signals*. Paper presented at the IEEE Intelligent Vehicles Symposium, 2004.
- Gibbs, K. (2013). *The Steam Locomotive: An Engineering History*. Stroud: Amberley Publishing.
- Goddard, E. (2012, 5-8 Nov. 2012). *IET vacation school electric traction systems overview of signalling and train control systems*. Paper presented at the IET Professional Development Course on Electric Traction Systems (2012).
- Google Inc. (n.d.). [Google Maps directions from Stratford International DLR, London E15 2ER to Woolwich Arsenal, Woolwich, London SE18 6JY by Docklands Light Railway]. Retrieved from <https://goo.gl/JggJqE>
- Gou, J. (2014). Multimode Speed Control Based on Fuzzy Decision-Making for Automatic Train Operation. *Indonesian Journal of Electrical Engineering and Computer Science*, 12(9), 6764-6770.
- Hamid, H. A., Nicholson, G. L., Douglas, H., Zhao, N., & Roberts, C. (2016, 23-25 Aug. 2016). *Investigation into train positioning systems for saving energy with optimised train trajectories*. Paper presented at the 2016 IEEE International Conference on Intelligent Rail Transportation (ICIRT).
- He, S.-Z., Tan, S., Xu, F.-L., & Wang, P.-Z. (1993). Fuzzy self-tuning of PID controllers. *Fuzzy Sets and Systems*, 56(1), 37-46. doi:[https://doi.org/10.1016/0165-0114\(93\)90183-I](https://doi.org/10.1016/0165-0114(93)90183-I)
- Hitachi Rail. (2013). ATO (Automatic Train Operation) System. Retrieved from <http://www.hitachi-rail.com/products/signalling/ato/index.html>
- Howlett, P. G., & Pudney, P. J. (1995). *Energy-Efficient Train Control* (1 ed.): Springer-Verlag London.
- Huang, S.-J., & Her, S.-L. (1997). Fuzzy Control Of Automatic Train Operation System. *International Journal of Modelling and Simulation*, 17(2), 143-150. doi:10.1080/02286203.1997.11760323
- Hwang, H.-S. (1998). Control strategy for optimal compromise between trip time and energy consumption in a high-speed railway. *IEEE Transactions on Systems, Man, and Cybernetics - Part A: Systems and Humans*, 28(6), 791-802. doi:10.1109/3468.725350
- Institute of Electrical and Electronics Engineers [IEEE]. (2004). IEEE Standard for Communications-Based Train Control (CBTC) Performance and Functional Requirements. In *IEEE Std 1474.1-2004 (Revision of IEEE Std 1474.1-1999)* (pp. 0_1-45).
- institution of Railway Signal Engineers [IRSE]. (1982). *Railway Signalling: a Treatise on the Recent Practice of British Railways* (O. S. Nock Ed.). London: A & C Black.

- Institution of Railway Signal Engineers [IRSE]. (1993). *Railway Control Systems* (M. Leach Ed.). London: A & C Black.
- Institution of Railway Signal Engineers [IRSE]. (2008). *European Railway Signalling* (C. Bailey Ed.). London: A & C Black.
- Institution of Railway Signal Engineers [IRSE]. (2009). *Metro Railway Signalling* (E. Goddard Ed.). London: Institution of Railway Signal Engineers.
- International Association of Public Transport [UITP]. (2014). Metro Automation: Facts, Figures and Trends. Retrieved from <http://www.uitp.org/metro-automation-facts-figures-and-trends>
- International Association of Public Transport [UITP]. (2015). World Metro Figures Statistics Brief. Retrieved from <http://www.uitp.org/world-metro-and-automated-metro-latest-figures>
- Jang, J. S. R., Sun, C. T., & Mizutani, E. (1997). *Neuro-Fuzzy and Soft Computing - A Computational Approach to Learning and Machine Intelligence* (T. Robbins & J. Scordato Eds.). Upper Saddle River, NJ: Prentice-Hall.
- Jones, E. G., Franca, D., Zhou, Y., & Forsberg, M. (2009). *Estimating train speeds for train preemption using multiple sensor data*.
- Juang, C. F., & Tsao, Y. W. (2008). A Self-Evolving Interval Type-2 Fuzzy Neural Network With Online Structure and Parameter Learning. *IEEE Transactions on Fuzzy Systems*, 16(6), 1411-1424. doi:10.1109/TFUZZ.2008.925907
- Kalman, R. E. (1960). A New Approach to Linear Filtering and Prediction Problems. *Journal of Basic Engineering*, 82(1), 35-45. doi:10.1115/1.3662552
- Kalman, R. E., & Bucy, R. S. (1961). New Results in Linear Filtering and Prediction Theory. *Journal of Basic Engineering*, 83(1), 95-108. doi:10.1115/1.3658902
- Karasakal, O., Guzelkaya, M., Eksin, I., Yesil, E., & Kumbasar, T. (2013). Online tuning of fuzzy PID controllers via rule weighing based on normalized acceleration. *Engineering Applications of Artificial Intelligence*, 26(1), 184-197. doi:<http://dx.doi.org/10.1016/j.engappai.2012.06.005>
- Ke, B. R., Chen, M. C., & Lin, C. L. (2009). Block-Layout Design Using MAX-MIN Ant System for Saving Energy on Mass Rapid Transit Systems. *IEEE Transactions on Intelligent Transportation Systems*, 10(2), 226-235. doi:10.1109/TITS.2009.2018324
- Ke, B. R., & Chen, N. (2005). Signalling blocklayout and strategy of train operation for saving energy in mass rapid transit systems. *IEE Proceedings - Electric Power Applications*, 152(2), 129-140. doi:10.1049/ip-epa:20045188
- Ke, B. R., & Chen, N. (2007, 13–16 March 2007). *Optimization of Train-Speed Trajectory of Mass Rapid Transit Systems*. Paper presented at the ASME/IEEE 2007 Joint Rail Conference and Internal Combustion Engine Division Spring Technical Conference, Pueblo.
- Ke, B. R., Lin, C.-L., & Lai, C.-W. (2011). Optimization of train-speed trajectory and control for mass rapid transit systems. *Control Engineering Practice*, 19(7), 675-687. doi:<http://dx.doi.org/10.1016/j.conengprac.2011.03.003>
- Keevill, D. (Producer). (2016, 16 January 2018). Increasing Levels of Automation with CBTC: IRSE Seminar 2016 – CBTC and Beyond. [Seminar slideshow presentation] Retrieved from

- <http://www.irse.org/knowledge/publicdocuments/IRSE%20CBTC%20Conference%20%20-%202016%20Toronto%20-%20%20Dave%20Keevill%20Increasing%20GoA%20rev2.pdf>
- Kemp, R. J. (1987). Docklands light railway. *IEE Proceedings B - Electric Power Applications*, 134(3), 127-133. doi:10.1049/ip-b:19870019
- Kiam Heong, A., Chong, G., & Yun, L. (2005). PID control system analysis, design, and technology. *IEEE Transactions on Control Systems Technology*, 13(4), 559-576. doi:10.1109/TCST.2005.847331
- Kobayashi, K., Cheok, K. C., & Watanabe, K. (1995, 21-23 Jun 1995). *Estimation of absolute vehicle speed using fuzzy logic rule-based Kalman filter*. Paper presented at the American Control Conference, Proceedings of the 1995.
- Li, S., Yang, L., & Gao, Z. (2015). Coordinated cruise control for high-speed train movements based on a multi-agent model. *Transportation Research Part C: Emerging Technologies*, 56(Supplement C), 281-292. doi:<https://doi.org/10.1016/j.trc.2015.04.016>
- Li, Y., Chen, B., Zheng, V. W., Temple, W. G., Kalbarczyk, Z., & Wu, Y. (2017, 26-29 June 2017). *Enhancing Anomaly Diagnosis of Automatic Train Supervision System Based on Operation Log*. Paper presented at the 2017 47th Annual IEEE/IFIP International Conference on Dependable Systems and Networks Workshops (DSN-W).
- Li, Z., & Hou, Z. (2015). Adaptive Iterative Learning Control Based High Speed Train Operation Tracking Under Iteration-Varying Parameter and Measurement Noise. *Asian Journal of Control*, 17(5), 1779-1788. doi:10.1002/asjc.1093
- Li, Z., Hou, Z., & Yin, C. (2015). Iterative learning control for train trajectory tracking under speed constraints with iteration-varying parameter. *Transactions of the Institute of Measurement and Control*, 37(4), 485-493. doi:10.1177/0142331214543095
- Liang, C., Yanru, S., Yongsheng, Z., Hongwei, L., & Mingfa, X. (2010, 20-22 Aug. 2010). *Vehicle lateral and longitudinal velocity estimation based on Adaptive Kalman Filter*. Paper presented at the 2010 3rd International Conference on Advanced Computer Theory and Engineering(ICAETE).
- Lin, X., Dong, H., Yao, X., & Bai, W. (2017). Neural adaptive fault-tolerant control for high-speed trains with input saturation and unknown disturbance. *Neurocomputing*, 260(Supplement C), 32-42. doi:<https://doi.org/10.1016/j.neucom.2017.02.083>
- Liu, H., Zhang, X., & Chang, W. (2009, 24-25 April 2009). *PID Control to Maglev Train System*. Paper presented at the 2009 International Conference on Industrial and Information Systems.
- Liu, J., Cai, B. g., & Wang, J. (2016, 19-22 June 2016). *Track-constrained GNSS/odometer-based train localization using a particle filter*. Paper presented at the 2016 IEEE Intelligent Vehicles Symposium (IV).
- Malvezzi, M., Allotta, B., & Rinchi, M. (2011). Odometric estimation for automatic train protection and control systems. *Vehicle System Dynamics*, 49(5), 723-739. doi:10.1080/00423111003721291
- Malvezzi, M., Vettori, G., Allotta, B., Pugi, L., Ridolfi, A., & Rindi, A. (2014). A localization algorithm for railway vehicles based on sensor fusion between tachometers and inertial measurement units. *Proceedings of the Institution of Mechanical Engineers, Part F: Journal of Rail and Rapid Transit*, 228(4), 431-448. doi:10.1177/0954409713481769

- Mamdani, E. H., & Assilian, S. (1975). An experiment in linguistic synthesis with a fuzzy logic controller. *International Journal of Man-Machine Studies*, 7(1), 1-13. doi:[https://doi.org/10.1016/S0020-7373\(75\)80002-2](https://doi.org/10.1016/S0020-7373(75)80002-2)
- Mao, Z., Tao, G., Jiang, B., Yan, X.-G., & Zhong, M. (2017). Adaptive Position Tracking Compensation for High-Speed Trains with Actuator Failures. *IFAC-PapersOnLine*, 50(1), 14266-14271. doi:<https://doi.org/10.1016/j.ifacol.2017.08.1835>
- Mendel, J., Hagrass, H., Tan, W.-W., Melek, W. W., & Ying, H. (2014). *Introduction to Type-2 Fuzzy Logic Control: Theory and Applications*. In I. P. E. Board (Ed.), (pp. 376). Retrieved from <http://onlinelibrary.wiley.com/book/10.1002/9781118886540> doi:10.1002/9781118886540
- Narayan, K., Mahesh, B., & Andreas, S. (2013). *An Introduction to Kalman Filtering with MATLAB Examples*: Morgan & Claypool.
- Pearce, A., Hardy, B., & Stannard, C. (2006). *Docklands Light Railway Official Handbook* (Fifth Edition ed.). Harrow, UK: Capital Transport Publishing.
- Pichlík, P., & Zděnek, J. (2017). Train velocity estimation method based on an adaptive filter with fuzzy logic. *Journal of Electrical Engineering*, 68(2), 125. doi:10.1515/jee-2017-0017
- Ponton, J. W. (2007). Closed Loop Tuning. Retrieved from <http://homepages.ed.ac.uk/jwp/control06/controlcourse/course/map/ZN/closednotes.html>
- Rail Accident Investigation Branch [RAIB]. (2008). *Rail Accident Report Signal passed at danger and subsequent near miss at Didcot North junction 22 August 2007* (Report 23/2008). Retrieved from Derby: https://assets.publishing.service.gov.uk/media/547c902a40f0b60241000195/R232008_081120_Didcot.pdf
- Rail Safety and Standards Board [RSSB]. (2004). Requirements for the Train Protection and Warning System (TPWS) In. London: Rail Safety and Standards Board.
- Rail Safety and Standards Board [RSSB]. (2015a). *AWS and TPWS Handbook*. In Vol. RS/522 Issue 3. (pp. 24). Retrieved from <https://www.rssb.co.uk/rgs/rulebooks/RS522%20Iss%203.pdf>
- Rail Safety and Standards Board [RSSB]. (2015b). Guidance on AWS and TPWS Interface Requirements. In *Issue Two*. London: Rail Safety and Standards Board.
- Rail Technology Magazine. (2017). TfL opens bidding for 43 new DLR trains. In DLR_-_Copy (Ed.), (Vol. 306 KB, pp. DLR B2007 stock). Manchester: Cognitive Publishing Ltd.
- Rochard, B. P., & Schmid, F. (2000). A review of methods to measure and calculate train resistances. *Proceedings of the Institution of Mechanical Engineers, Part F: Journal of Rail and Rapid Transit*, 214(4), 185-199. doi:doi:10.1243/0954409001531306
- Schmid, F. (Producer). (2015, 18/01/2018). Human Factors, Systems and Safety. [Seminar presentation slides] Retrieved from <https://www.birmingham.ac.uk/Documents/college-eps/railway/RSEI-event/SCHMID-Felix-Human-Factors-Systems-and-Safety.pdf>
- Sekine, S., Imasaki, N., & Endo, T. (1995, 20-24 Mar 1995). *Application of fuzzy neural network control to automatic train operation and tuning of its control rules*. Paper presented at the Proceedings of 1995 IEEE International Conference on Fuzzy Systems.

- Sekine, S., & Nishimura, M. (1995, 20-24 Mar 1995). *Application of fuzzy neural network control to automatic train operation*. Paper presented at the Proceedings of 1995 IEEE International Conference on Fuzzy Systems.
- Seong Ho, H., Yun Sub, B., Jong Hyen, B., Tae Ki, A., Su Gil, L., & Hyun Jun, P. (1999, 1999). *An optimal automatic train operation (ATO) control using genetic algorithms (GA)*. Paper presented at the TENCON 99. Proceedings of the IEEE Region 10 Conference.
- Siebler, B., Heirich, O., & Sand, S. (2018, 23-26 April 2018). *Relative train localization with magnetic field measurements*. Paper presented at the 2018 IEEE/ION Position, Location and Navigation Symposium (PLANS).
- Siemens (Producer). (2016, 17 December 2016). Automated Driving by Rail: Positive Impact of Rail Market Transformation. [PowerPoint slides] Retrieved from <https://www.siemens.com/press/pool/de/events/2016/mobility/2016-09-innotrans/presentation-automated-driving-e.pdf>
- Sinthipsomboon, K., Hunsacharoonroj, I., Khedari, J., Pongaen, W., & Pratumswan, P. (2011). *A hybrid of fuzzy and fuzzy self-tuning PID controller for servo electro-hydraulic system*.
- Sivanandam, S. N., Sumathi, S., & Deepa, S. N. (2007). *Introduction to Fuzzy Logic using MATLAB*. In (pp. XIV, 430). Retrieved from <https://link.springer.com/book/10.1007/978-3-540-35781-0> doi:10.1007/978-3-540-35781-0
- Song, Q., Song, Y. d., Tang, T., & Ning, B. (2011). Computationally Inexpensive Tracking Control of High-Speed Trains With Traction/Braking Saturation. *IEEE Transactions on Intelligent Transportation Systems*, 12(4), 1116-1125. doi:10.1109/TITS.2011.2143409
- Song, Q., & Sun, T. (2017). Neuroadaptive PID-like Fault-Tolerant Control of High Speed Trains with Uncertain Model and Unknown Tracking/Braking Actuation Characteristics. In F. Cong, A. Leung, & Q. Wei (Eds.), *Advances in Neural Networks - ISNN 2017: 14th International Symposium, ISNN 2017, Sapporo, Hakodate, and Muroran, Hokkaido, Japan, June 21–26, 2017, Proceedings, Part II* (pp. 318-325). Cham: Springer International Publishing.
- Su, S., Tang, T., Chen, L., & Liu, B. (2014). Energy-efficient train control in urban rail transit systems. *Proceedings of the Institution of Mechanical Engineers, Part F: Journal of Rail and Rapid Transit*, 229(4), 446-454. doi:10.1177/0954409713515648
- Su, S., Tang, T., & Wang, Y. (2016). Evaluation of Strategies to Reducing Traction Energy Consumption of Metro Systems Using an Optimal Train Control Simulation Model. *Energies*, 9(2).
- Sun, H., Hou, Z., & Tang, T. (2011). An Iterative Learning Approach for Train Trajectory Tracking Control. *IFAC Proceedings Volumes*, 44(1), 14916-14921. doi:<https://doi.org/10.3182/20110828-6-IT-1002.01270>
- Talvitie, J., Levanen, T., Koivisto, M., Pajukoski, K., Renfors, M., & Valkama, M. (2018, 15-18 April 2018). *Positioning of high-speed trains using 5G new radio synchronization signals*. Paper presented at the 2018 IEEE Wireless Communications and Networking Conference (WCNC).
- Transport for London. (2015a, 13 June 2017). DLR - Transport for London. Retrieved from <https://tfl.gov.uk/maps/track/dlr>
- Transport for London. (2015b, 9 February 2017). DLR route - Transport for London. Retrieved from <https://tfl.gov.uk/dlr/route/dlr/>
-

- Ulusoy, M. (Producer). (2017, 25/01/2018). Understanding Kalman Filters, Part 3: An Optimal State Estimator. [Video] Retrieved from <https://uk.mathworks.com/videos/understanding-kalman-filters-part-3-optimal-state-estimator--1490710645421.html>
- Utomo, R. D., Sumardi, & Widiyanto, E. D. (2015, 16-18 Oct. 2015). *Control system of train speed based on fuzzy logic controller*. Paper presented at the 2015 2nd International Conference on Information Technology, Computer, and Electrical Engineering (ICITACEE), Semarang.
- Wang, L., Wang, X., Sun, D., & Hao, H. (2017). Multi-objective Optimization Improved GA Algorithm and Fuzzy PID Control of ATO System for Train Operation. In D. Yue, C. Peng, D. Du, T. Zhang, M. Zheng, & Q. Han (Eds.), *Intelligent Computing, Networked Control, and Their Engineering Applications: International Conference on Life System Modeling and Simulation, LSMS 2017 and International Conference on Intelligent Computing for Sustainable Energy and Environment, ICSEE 2017, Nanjing, China, September 22-24, 2017, Proceedings, Part II* (pp. 13-22). Singapore: Springer Singapore.
- Wang, Q. Y., Wu, P., Liang, Z. C., & Feng, X. Y. (2014, 24-26 June 2014). *The Hierarchical Real-time Control Of High Speed Trains For Automatic Train Operation*. Paper presented at the The International conference on Railway Engineering Design and Optimization (COMPRAIL 2014), Rome.
- Wang, X., & Tang, T. (2017). Optimal operation of high-speed train based on fuzzy model predictive control. *Advances in Mechanical Engineering*, 9(3), 1687814017693192. doi:10.1177/1687814017693192
- Wang, Y., Ning, B., Boom, T. v. d., & Schutter, B. D. (2016). *Optimal Trajectory Planning and Train Scheduling for Urban Rail Transit Systems* (1 ed.): Springer International Publishing.
- Woodland, D. (2004). *Optimisation of Automatic Train Protection Systems*. (PhD), University of Sheffield, Sheffield. Retrieved from <http://etheses.whiterose.ac.uk/14543/1/531116.pdf>
- Xiangxian, C., Yue, Z., & Hai, H. (2010, 16-17 Dec. 2010). *Train Speed Control Algorithm Based on PID Controller and Single-Neuron PID Controller*. Paper presented at the 2010 Second WRI Global Congress on Intelligent Systems.
- Xiaojuan, L., Baofeng, M., & Haiying, D. (2015). Optimization Control of ATO-S Based on Implicit Generalized Predictive of Chaotic Particle Swarm Algorithm. *International Journal of Control and Automation*, 8(5), 199-208.
- Xu, X., Li, K., & Li, X. (2016). A multi-objective subway timetable optimization approach with minimum passenger time and energy consumption. *Journal of Advanced Transportation*, 50(1), 69-95. doi:10.1002/atr.1317
- Yang, H., Fu, Y., & Zhang, K. (2012, July 31 2012-Aug. 2 2012). *Generalized Predictive Control Based on Neurofuzzy Model for Electric Multiple Unit*. Paper presented at the 2012 Third International Conference on Digital Manufacturing & Automation.
- Yang, J., Jia, L., Fu, Y., & Lu, S. (2017). Speed Tracking Based Energy-Efficient Freight Train Control Through Multi-Algorithms Combination. *IEEE Intelligent Transportation Systems Magazine*, 9(2), 76-90. doi:10.1109/MITS.2017.2666580

- Yasunobu, S., Miyamoto, S., & Ihara, H. (1983). *Fuzzy Control for Automatic Train Operation System*. Paper presented at the IFAC/IFIP/IFORS Conference on Control in Transportation Systems (4th), New York.
- Yin, J., Chen, D., & Li, Y. (2016). Smart train operation algorithms based on expert knowledge and ensemble CART for the electric locomotive. *Knowledge-Based Systems*, 92(Supplement C), 78-91. doi:<https://doi.org/10.1016/j.knosys.2015.10.016>
- Yu, C. C. (2006). *Autotuning of PID Controllers: Relay Feedback Approach* (2 ed.). London: Springer London.
- Yuan, L., Zhao, W., Li, C., & Zhou, D. (2013, 6-8 March 2013). *Error correction method for train speed measurement using Doppler radar in train control system*. Paper presented at the 2013 IEEE Eleventh International Symposium on Autonomous Decentralized Systems (ISADS).
- Zadeh, L. A. (1965). Fuzzy sets. *Information and Control*, 8(3), 338-353. doi:[https://doi.org/10.1016/S0019-9958\(65\)90241-X](https://doi.org/10.1016/S0019-9958(65)90241-X)
- Zhang, M., Chen, Y., Sun, X., Hou, X., & Cai, H. (2014, 9-10 Oct. 2014). *Particle-optimized control for automatic train operation based on sliding mode observer*. Paper presented at the Proceedings 2014 International Conference on Informative and Cybernetics for Computational Social Systems (ICCSS).
- Zhao, N., Roberts, C., & Hillmansen, S. (2012). The application of an enhanced Brute Force algorithm to minimise energy costs and train delays for differing railway train control systems. *Proceedings of the Institution of Mechanical Engineers, Part F: Journal of Rail and Rapid Transit*, 228(2), 158-168. doi:10.1177/0954409712468231
- Zhao, Z.-Y., Tomizuka, M., & Isaka, S. (1992, 13-16 Sep 1992). *Fuzzy gain scheduling of PID controllers*. Paper presented at the [Proceedings 1992] The First IEEE Conference on Control Applications.
- Zhao, Z.-Y., Tomizuka, M., & Isaka, S. (1993). Fuzzy gain scheduling of PID controllers. *IEEE Transactions on Systems, Man, and Cybernetics*, 23(5), 1392-1398. doi:10.1109/21.260670
- Zhou, Y. W. (2012) Research of multi-sensor integration system for train speed and position measurement. In: *Vol. 105-107* (pp. 1920-1925).
- Zhuan, X., & Xia, X. (2010). Fault-tolerant control of heavy-haul trains. *Vehicle System Dynamics*, 48(6), 705-735. doi:10.1080/00423110902974100
- Ziegler, J. G., & Nichols, N. B. (1942). Optimum Settings for Automatic Controllers. *Transactions of the A.S.M.E.*, 759-768.

8 Appendix A – Table of Difference among GoAs

Table 6 – Grades of Automation in more detail (Keevill, 2016). ‘Ops’ stands for operator.

| | | Increasing GoA | | | | |
|---------------------------------------------------------|-----------------------------------------------------------------------------------------------------------------------------------|------------------------------|---------------|----------------|------------|-----------------------------|
| | | On-sight | Non-automated | Semi-automated | Driverless | Unattended |
| Basic functions of train operation | | GoA0 | GoA1 | GoA2 | GoA3 | GoA4 |
| Ensure safe movement of trains | Ensure safe route | Ops Staff (route by systems) | Systems | Systems | Systems | Systems |
| | Ensure safe separation of trains | Ops Staff | Systems | Systems | Systems | Systems |
| | Ensure safe speed | Ops Staff | Ops Staff | Systems | Systems | Systems |
| Drive train | Control acceleration and braking | Ops Staff | Ops Staff | Systems | Systems | Systems |
| Supervise guideway | Prevent collision with obstacles | Ops Staff | Ops Staff | Ops Staff | Systems | Systems |
| | Prevent collision with persons on tracks | Ops Staff | Ops Staff | Ops Staff | Systems | Systems |
| | Control passengers doors | Ops Staff | Ops Staff | Ops Staff | Ops Staff | Systems |
| Supervise passenger transfer | Prevent injuries to persons between cars or between platform and train | Ops Staff | Ops Staff | Ops Staff | Ops Staff | Systems |
| | Ensure safe starting conditions | Ops Staff | Ops Staff | Ops Staff | Ops Staff | Systems |
| Operate a train | Put in or take out of operation | Ops Staff | Ops Staff | Ops Staff | Ops Staff | Systems |
| | Supervise the status of the train | Ops Staff | Ops Staff | Ops Staff | Ops Staff | Systems |
| Ensure detection and management of emergency situations | Detect fire/smoke and detect derailment, detect loss of train integrity, manage passenger requests (call/evacuation, supervision) | Ops Staff | Ops Staff | Ops Staff | Ops Staff | Systems and/or staff in OCC |

Ability for more functions

9 Appendix B – DLR Route Map

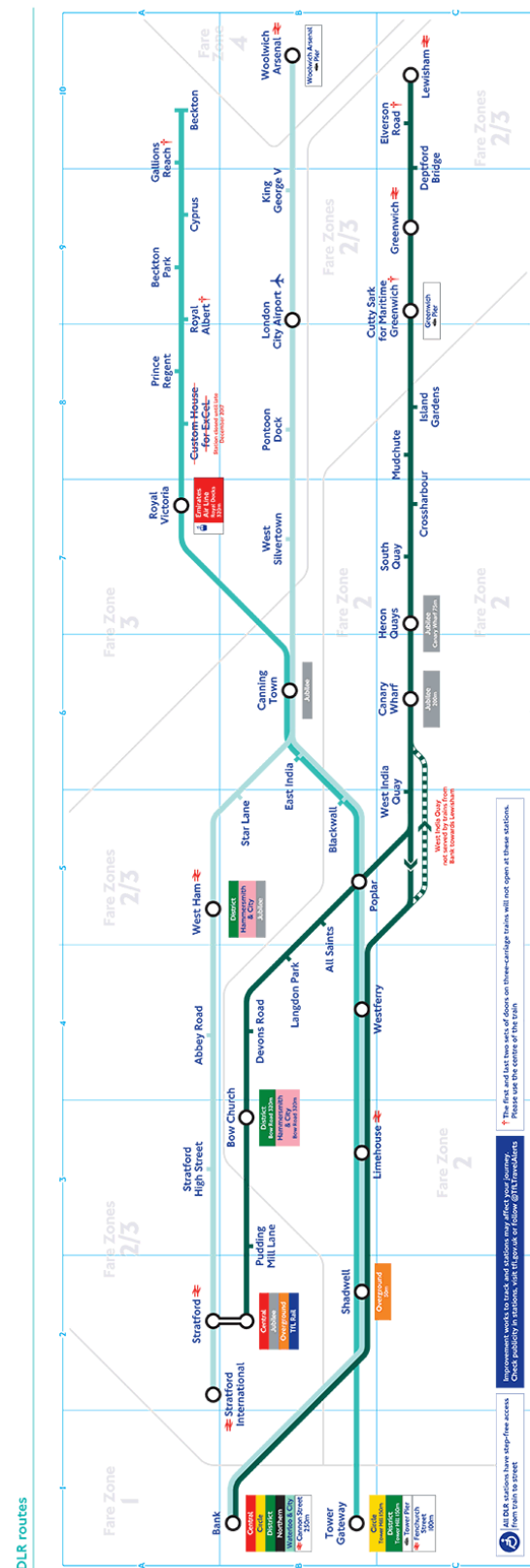


Figure 106 – Map of DLR routes (TfL, 2015a)

10 Appendix C – Gradient and Speed Limit

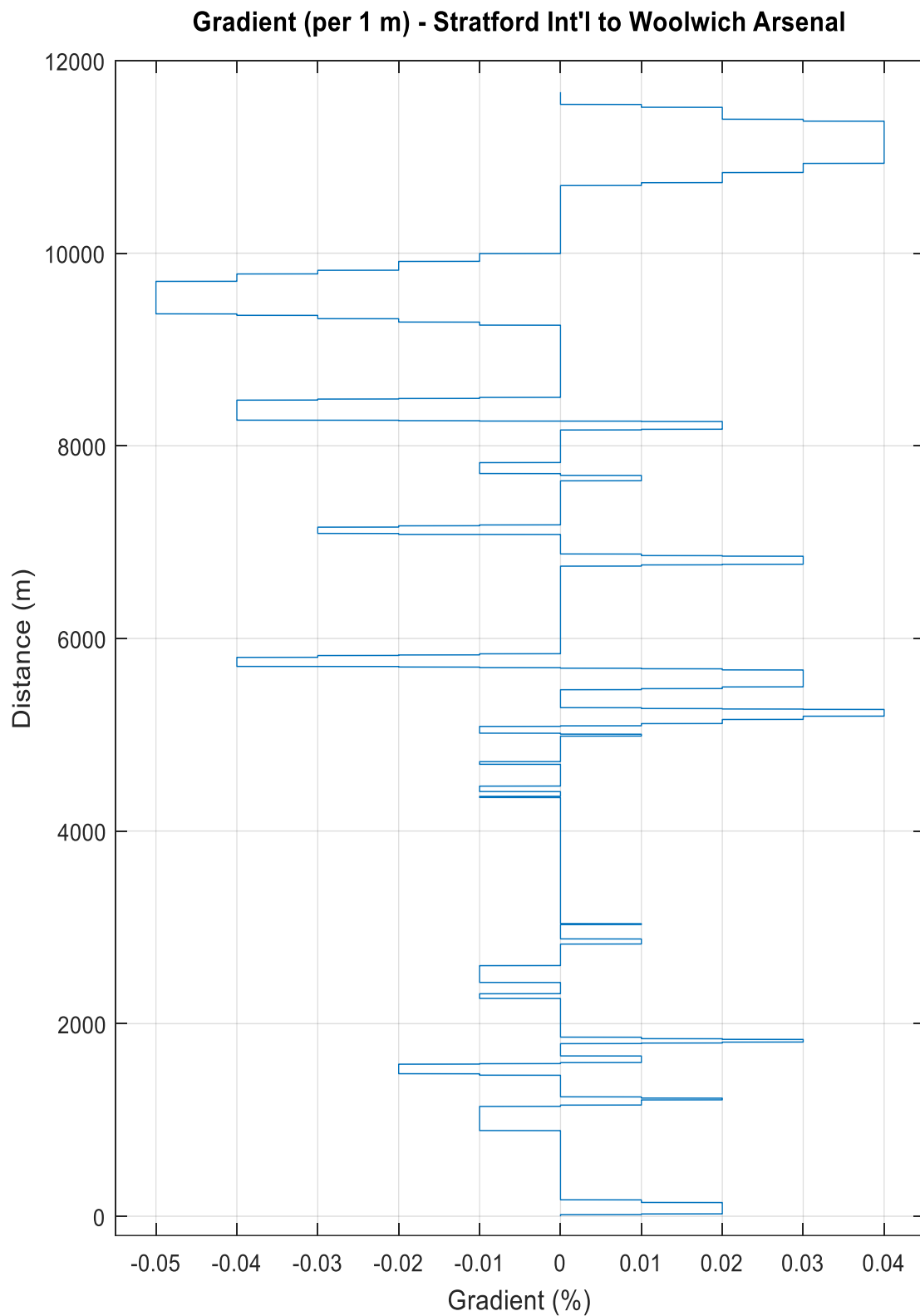


Figure 107 - Gradient of the route from Stratford International to Woolwich Arsenal (Author, 2017)

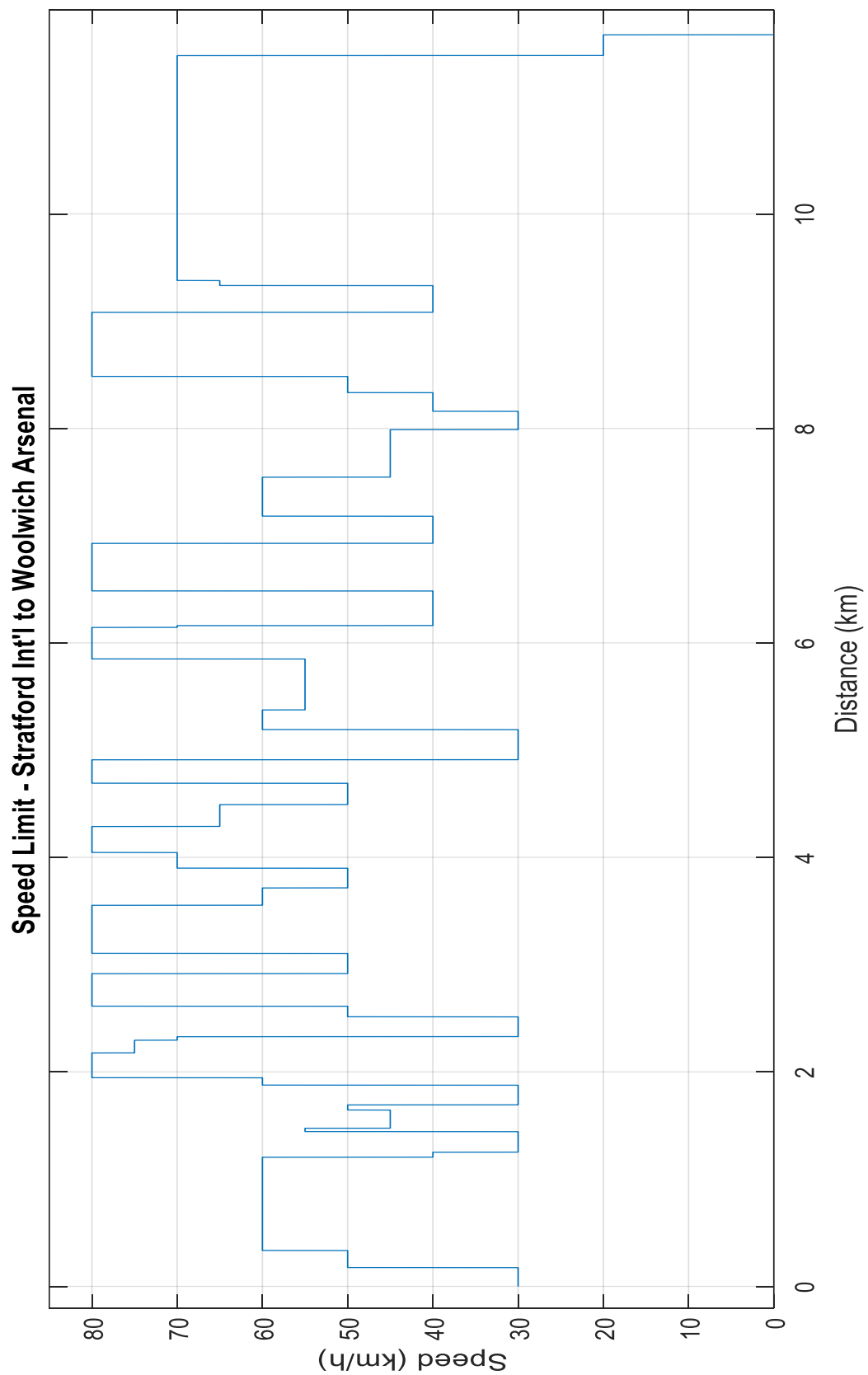


Figure 108 – Speed limit of the route from Stratford International to Woolwich Arsenal
(Author, 2017)